Proceedings of Lunar and Planetary Science, Volume 21, pp. 229-289
Lunar and Planetary Institute, Houston, 1991

Geochemical Stratigraphy of Two Regolith Cores from the Central Highlands of the Moon

R. L. Korotev

Department of Earth and Planetary Sciences and the McDonnell Center for the Space Sciences, Washington University, St. Louis, MO 63130

Concentrations of 20-22 chemical elements were determined by instrumental neutron activation analysis in 121 samples of <1-mm fines from double drive tube 60009/10 (0.6 m length) and 353 samples of <1-mm fines from deep drill core 60001-7 (2.2 m length). Approximately 40 >1-mm regolith particles from each core were also studied. These two cores were taken 35-40 m apart at the LM/ALSEP site during the Apollo 16 mission to the Central Highlands of the Moon. Compositional variation with depth in the <1-mm fines is large. For elements associated with major mineral phases (Na, Ca, Sc, Cr, Fe, and Eu), the variations in concentration in both cores exceed that observed in approximately 40 samples of surface and trench soils taken over a lateral distance of 8 km at the site. Most of the variation in lithophile element concentrations results from two-component mixing. The two components are (1) soil that is relatively mafic and rich in incompatible trace elements (ITEs), e.g., Sm and Th, as a result of a significant component of mafic, ITE-rich, impact-melt breccias and (2) coarse-grained anorthosite. As a result of this binary mixing, concentrations of ITEs generally correlate with those of elements associated with mafic minerals (Sc, Fe) in soil from both cores because anorthosite contains low concentrations of both sets of elements. The anorthosite component responsible for most of the compositional variation in the fines is identified as "ferroan anorthosite" consisting of approximately 99% plagioclase and not some more mafic variety. This argues that the numerous hand specimens of nearly monomineralic anorthosite found at the Apollo 16 site are not sampling anomalies, but are typical of the source of the anorthosite. The mafic, ITE-rich soil component is identified as the "Cayley soil component" because its composition is similar to that inferred for the average surface of the Cayley Plains west of the landing site based on orbital data. The Cayley soil component is a complex mixture of many lithologies, and samples with the characteristic composition are usually relatively mature and fine grained. Lack of perfect correlation among element pairs on two-element concentration plots occurs because of variation in the relative proportions of the various subcomponents of the Cayley soil component (impact-melt breccias, metamorphosed breccias, and mare basalt and glass) and variation in the composition of the plagioclase in the anorthosite component (anorthite content). These variations are evident in two ways, one trivial and one of stratigraphic significance: (1) Some individual small subsamples of <1-mm fines are anomalous because they contain one or a few large particles of distinct composition. (2) An entire stratigraphic unit of soil may be enriched or depleted in some particular lithologic component. The 60009/10 core shows more variation in composition with depth than any lunar core yet studied. It varies from 0% anorthosite component at about 20 cm depth (100% Cayley soil component) to 75% anorthosite component (25% Cayley soil component) at 54 cm depth. A second anorthosite-rich layer occurs at 43 cm depth. Magnetic separates of soil from this core made in earlier studies preferentially contained metal-bearing, mafic impact-melt breccias that accounted for the enrichment of these separates in Sc, Cr, and ITEs. The 60001-7 core is more uniform in composition with depth (5-10% anorthosite component through most of the lower half). However, an anorthosite-rich layer (45% anorthosite component) occurs at about 20 cm depth, which may be related to the anorthosite-rich layers in 60009/10. No other stratigraphic unit in 60001-7 can be identified with any of those occurring in 60009/10, although the surface material in both cores is similar. Data presented here show that the contents of the 60006 section of the core have been mixed and disturbed, and retain no stratigraphic information. A unit of soil between 103 and 187 cm depth (60003 and 60004 sections) contains 0.5% to 1.5% mare material (basalt and/or glass), similar to the unit between 26 and 48 cm depth in the Station 4 core, 64001; no soil similarly enriched in mare material was sampled among the surface and trench soils from Apollo 16. Siderophile-element concentrations are also slightly higher in this unit of soil. At the bottom of this unit is a 10-cm-wide zone that is particularly rich in siderophile elements (177-187 cm depth). Relative siderophile-element and Cr concentrations in this zone are generally consistent with debris from an ordinary chondrite in which the ratio of metal to silicate phases is unusually high, ~40/60. At the maximum enrichment, this zone of soil contains 3% meteoritic material in excess of the approximately 1.5% present throughout the rest of the core. Some individual samples above the 10-cm-wide zone of siderophile-element enrichment have anomalously high concentrations of Au compared with other siderophile elements, possibly as a result of vapor-phase condensation. Below 187 cm depth (60001 and 60002) the soil is compositionally distinct, most notably in containing a higher concentration of Na. This soil cannot be modeled as a mixture of components that adequately accounts for compositions of soils above this layer or the soils from 60009/10. This unit of soil appears to be of different provenance than the surface (Cayley) soils and may be related to trench soil 61221. It is similar in composition to particles of regolith breccia found in this unit and probably derives primarily from disaggregation of regolith breccia boulders. Two >1-mm particles from this unit are unusual in being nearly pure plagioclase with An_{90-91} compositions. Although the lithology from which they derive is unknown, rare-earth-element concentrations in these particle are intermediate to those of ferroan anorthosite and alkali anorthosite.

1. INTRODUCTION

Three core samples were taken in the vicinity of the lunar module by astronauts Charles Duke and John Young during the Apollo 16 mission to the Central Highlands of the Moon (Fig. 1). One of these was the "deep drill core," a rotary-percussion drill string consisting of seven sections designated sequentially 60001 through 60007 (hereafter, 60001-7). The deep drill core was 2 cm in inside diameter and penetrated to a depth of 2.2 m. The other two cores were drive tubes that were pushed or hammered into the regolith. Both were "double drive tubes" in that they consisted of two sections each 42 cm long and 4 cm inside diameter. Core sections 60009 and 60010 constituted one double drive tube (designated 60009/10) and sections 60013 and 60014 constituted the other (60013/14). Both double drive tubes returned columns of soil about 60 cm long. The sampling locations of these three cores form a triangular array about 40-50 m on a side (Fig. 1). This is the only such array of cores taken on the Moon and, consequently, these cores are the only samples we can use to seek stratigraphically contiguous subsurface units that might occur on this scale.

This work presents high-resolution concentration profiles (~5-mm sampling intervals) for 20-22 chemical elements in the <1-mm grain-size fractions of 60001-7 and 60009/10, which were taken about 35-40 m apart (Fig. 1). Both cores were intensely studied in the mid 1970s. At this writing, 60013/14 has not yet been opened, although gross structural features are known from X-radiographs (*Fruland and Reimold*, 1981). I have restudied 60001-7 and 60009/10 for several

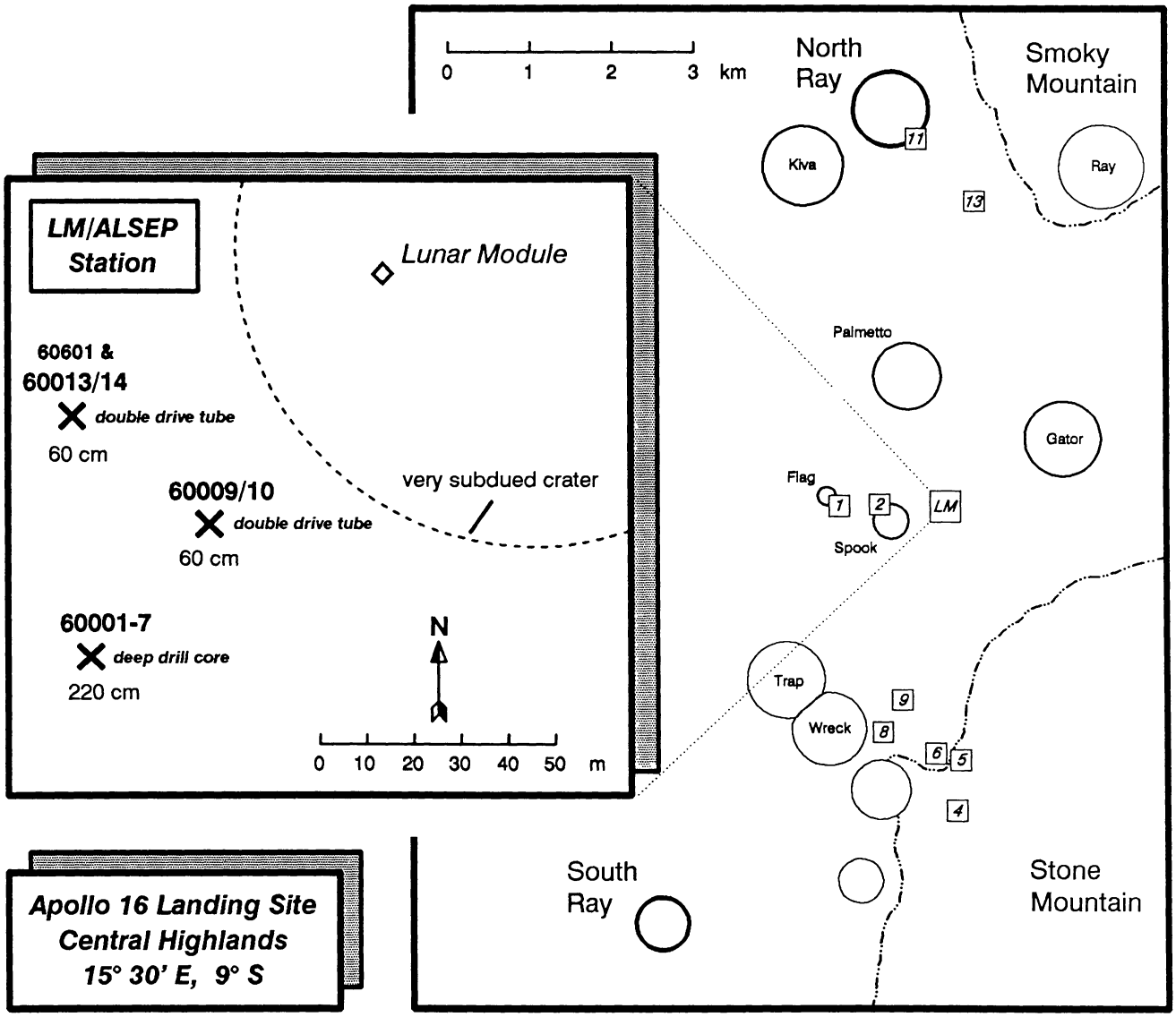

Fig. 1. Schematic map of the Apollo 16 landing site with an insert of the LM/ALSEP Station showing the location of the three cores taken at this station. Squares with enclosed numbers indicate sampling stations (main map); Xs indicate core locations (insert). Maps are based on Fig. 5 of *Muehlberger* (1981) and Fig. 1 of *Schaber* (1981).

reasons. First, samples from the 60013/14 core are scheduled to be available within the next year and it will be useful to have a self-consistent dataset for comparison of this unique set of three cores. Second, our studies of two other lunar cores at high resolution (*Korotev et al.,* 1984; *Morris et al.,* 1989) have revealed stratigraphic features that would not have been observed with the more widely spaced sampling intervals typical of earlier studies of other cores. Third, earlier studies of 60009/10 and 60001-7 left some problems unresolved and posed questions that were left unanswered. Considering the advances that have been made in the understanding of lunar geology and geochemistry in the 13 years since the cores were last studied, it seemed likely that the high-resolution studies would provide answers to some of these questions and yield some new insights. Finally, the 24 core strings returned by the Apollo missions provide the only data on variation with depth of parameters such as grain size, composition, mineralogy, and exposure effects for the upper 1-2 m of the lunar regolith. If we intend to interpret wisely the results of the forthcoming Lunar Observer mission, which will only provide information about the upper few micrometers to centimeters, it is imperative that we learn as much about these variations as the Apollo cores have to offer.

In this paper I will emphasize the stratigraphic features of the cores and compare the new results with those of previous works, particularly earlier petrographic and geochemical studies. Detailed comparison of the core soils with other Apollo 16 regolith samples and discussion of the relationship of Apollo 16 regolith to the local site geology are deferred to a subsequent paper. It is impossible, however, to separate discussion of compositional variations with depth from discussion of the lithologies responsible for the variations, which in turn are related to site geology. Thus, I will sometimes address soil-rock relationships without discussing the source of the rocks. Compositional trends in the core soils, when compared with those for rocks, provide certain constraints on the evolution of the Apollo 16 regolith (*Korotev,* 1990b), but as they do not relate directly to stratigraphy, those ideas will be developed more fully in a subsequent paper.

2. SAMPLES AND ANALYSIS

2.1. Samples Studied

For this investigation I have studied a total of 623 individual samples. These fall into two categories: (1) <1-mm fines with nominal masses of 50 mg and (2) individual particles mostly 1-2 mm in diameter (1-10 mg in mass). The two cores were processed at the Johnson Space Center (JSC) in Houston; details of the processing are given by *Duke and Nagle* (1976) and *Fruland et al.* (1982). Additional documentation and curatorial information is given by *Fruland and Reimold* (1981). At JSC, both cores were sampled at depth intervals of approximately 0.5 cm, except for the 60005 section of 60001-7, which was sampled at 1-cm intervals. One subsample (rarely two) of <1-mm fines from nearly every sampling interval of each core was analyzed.

2.1.1. 60009/10. The analyzed subsamples (n = 121) were unsieved (but generally <1 mm) fines from the fourth dissection column of 60009 and sieved fines (<1 mm) from the third dissection column of 60010. At approximately 52 cm deep in the core, a diagonal contact cuts across two consecutive sampling intervals, with dark, more mafic material above and light, more feldspathic material below. A "dark" and "light" split was made of each of these sampling intervals at JSC, thus two points occur at these depths in subsequent figures. Analytical results for these samples are presented in Table A1.

Results for the <1-mm fines indicated compositional extremes at 20, 54, and 58 cm depth. To help identify the lithologies responsible for these extremes, I also studied a suite of 40 individual >1-mm particles selected by the JSC curatorial staff to be representative of those found at each of these three depths. Allocation details are presented in Table 1. After chemical analysis, thin sections of most of the particles were prepared. For 60009/10, particle designations are coded according to the nominal depth from which they came, e.g., "20-A" is particle A from 20 cm (nominal) depth. Analytical results for these samples are presented in Table A2.

TABLE 1. Allocation data for >1-mm particles from 60009/10 and 60001-7.

Sample Number		Depth	Nominal	Number of Particles		Fraction
Specific	Parent	Interval (cm)	Depth (cm)	Total	Studied	Studied (%)
60010,478	,90	20.0-20.5	20	49	20	41
60009,618	,214	53.8-54.3	54	19	10	53
60009,1270	,1154	57.8-58.3	58	28	10	36
60002,736	,95	193.2-193.8	193	~100	6	<10
60002,732	,124	199.9-200.4	200	>100	3	<5
60002,731	,126	200.4-201.0	201	>100	7	<10
60002,733	,137	203.5-204.5	204	>50	4	<10
60002,734	,139	204.0-204.5	204	~50	5	~10
60002,735	,147	205.4-205.9	205	~50	9	~20

2.1.2. 60001-7. I analyzed a total of 353 samples of <1-mm fines. For all samples from the bit of the drill, material <0.35 mm in diameter had been previously removed at JSC for a different experiment (*Duke and Nagle,* 1976), thus for the eight 60001 samples, the grain size of the analyzed material is 0.35-1.0 mm. Analytical results for <1-mm fines from 60001-7 are presented in Table A3.

While preparing the <1-mm fines samples for analysis, I encountered some particles that I removed for individual analysis. These included 12 large particles (2 exceeding 13 mg, i.e., >25% of the mass of the allocated fines sample) and 6 small spheres. Nine of the large particles were from 60001 and 60002, where the average grain size was larger than for the rest of the core; the other three were from 60004. For 60001-7, particle designations are coded according to the section of the core from which they came, e.g., "4.03" is particle 3 from 60004. Analytical results for these samples are presented in Table A4.

In addition, I have studied 34 particles from the 60002 section of the core (particles 2.01 through 2.34), which were selected by the JSC curatorial staff to be representative of the fragments present in the >1-mm grain-size fractions (allocation data are presented in Table 1). Most of these are 1-2-mm particles with masses of <10 mg; however, two particles were much larger. I broke one of these (particle 2.19, weighing 169 mg, from 60002,734) into smaller pieces and analyzed eight individual chips weighing 2-15 mg each (2.19A-2.19H). I also broke the other (particle 2.34, weighing 25 mg, from 60002,736) into smaller chips and analyzed four subsamples, three consisting of single 3-5 mg chips (2.34A-2.34C) and one consisting of all remaining residue (2.34D). Analytical results for these samples are presented in Table A5. In total, I obtained data for 49 samples of 60002 particles, 44 from >1-mm fractions and 5 removed from <1-mm fractions. After chemical analysis, thin sections of 15 of the particles were prepared.

2.1.3. Other <1-mm fines. For comparison with the core soils, I analyzed 19 samples (50-60 mg) of <1-mm fines taken at the surface or from trenches at Apollo 16. Several of these have not been well characterized previously. These samples included six replicates of 60601, which was taken at the surface near the site of the 60013/14 core (Fig. 1; Table A6); the rest are from other stations (Table A7).

2.2. Analytical Methods

I have determined the concentrations of 20-25 chemical elements by instrumental neutron activation analysis (INAA) using the following procedures. Samples and standards were encapsulated in high-purity silica tubing, usually with an outside diameter of 4 mm (5 mm for some particles) and an inside diameter of ~3 mm (T21 Suprasil, Heraeus-Amersil Inc., Buford, Georgia). Batches of about 50-70 tubes were irradiated with a thermal neutron flux of $3.9 \cdot 10^{13}$ $cm^{-2}sec^{-1}$ in the second reflector ring of the University of Missouri Research Reactor (Columbia, Missouri). All <1-mm fines samples were irradiated for 48 hours. During irradiation the sample package was rotated about its cylindrical axis at a rate of 0.1 rpm (revolutions per minute). After irradiation, the tubes were washed in 6 *M* HNO_3 for 15 min.

Samples were radioassayed by gamma-ray spectrometry in the tubes in which they were irradiated using four high-purity Ge detectors with horizontal cryostats and an ND9900 spectroscopy system (Nuclear Data Inc., now Canberra Nuclear Products Group, Schaumburg, Illinois) and associated MicroVAX II computer (Digital Equipment Corporation). During radioassay the sample tubes were spun about the cylindrical axis at a rate of 10 rpm to minimize possible geometry effects. Gamma-ray spectra were acquired at count rates of 5-12 kcounts/sec over the energy range of 30-1800 keV and accumulated digitally into 8192 channels at 0.22 keV/channel. The FWHM for the 1332-keV peak of ^{60}Co ranged from 1.75-1.90 keV under operating conditions for the four detectors, and sample-to-detector distances were typically 5-10 cm. Spectral data were reduced using new versions of the TEABAGS programs of *Lindstrom and Korotev* (1982), which Lindstrom and I have totally rewritten to take full advantage of the computing capacity of the MicroVAX. Elemental standards for the <1-mm fines are AN-G (IWG-GIT Greenland anorthosite; *Govindaraju,* 1980) for Na and Ca, synthetic multielement standards for Cr, Ni, Zr, Ir, and Au, and NBS 1633a (coal flyash) for all other elements (*Korotev,* 1987a). For the particles, fragments of synthetic glass standards were used. Blank contributions from the silica tubes, which are each typically 0.7 g in mass, are negligible for all elements when sample masses exceed 1 mg.

The <1-mm fines from 60009 and 60010 were each irradiated in a different batch with its own set of standards. The two batches were sealed in a single can for irradiation. Both batches were radioassayed simultaneously (two detectors per batch), with each sample radioassayed only once for approximately 1.3 hours between 7 and 10 days following irradiation. The <1-mm fines from 60001-7 were divided into six batches of approximately 59 stratigraphically consecutive samples each. One sample of surface soil 60601 was included in each batch, along with the standards. The 60001-7 samples were analyzed in three experiments in which two batches were irradiated together and radioassayed simultaneously. Two radioassays were done on each sample, the first between 7 and 10 days following irradiation for about 1.7 hours and the second between 3 and 4 weeks following irradiation for about 2 hours. For these samples, data for 22 elements are reported. Because the 60009/10 samples did not receive a second radioassay, analytical data for some elements determined via nuclides with long half lives (Ni, Sr, Zr, Eu, Tb, Hf, Ta, and Ir) are not as precise as those for the 60001-7 samples, which received a second radioassay. Data for Sr and Zr in 60009/10 are too imprecise to be of value and are not reported. All remaining <1-mm fines samples (surface and trench soils) were analyzed in a separate experiment and received three 2-6-hour radioassays; only for these samples are data for Cs, Ce, and Nd reported (25 elements total).

The >1-mm particles were irradiated in four different experiments with durations of 48 to 120 hours. Each particle received one or two radioassays of several hours at 6-10 days and another at 3-4 weeks following irradiation.

3. 60009/10 RESULTS

3.1. <1-mm Fines

Several layers of compositionally distinct soil are evident in the concentration profiles for 60009/10 (Fig. 2). Most of the inflections in the profiles correspond to breaks between stratigraphic units (SU) recognized by *Duke and Nagle* (1976) during processing of the core (Fig. 3). The 60009/10 core shows greater compositional variation with depth than any other lunar core yet studied. I discuss the most obvious features below.

3.1.1. Surface layer. Soil from the top 13 cm of the core (60010, SU5-7) is relatively uniform in composition. For concentrations of most elements, sample standard deviations in the 27 samples from this region of the core are only about a factor of two greater than the sample standard deviation for the six replicates of 60601 (Table A6). (For the precisely determined elements Na, Sc, Cr, Fe, Co, La, Sm, and Eu, the variations in the results for 60601 represent real compositional differences among the unground subsamples, not analytical imprecision.) The average composition of the uppermost 13 cm of soil is almost identical to that of surface soil 60601,

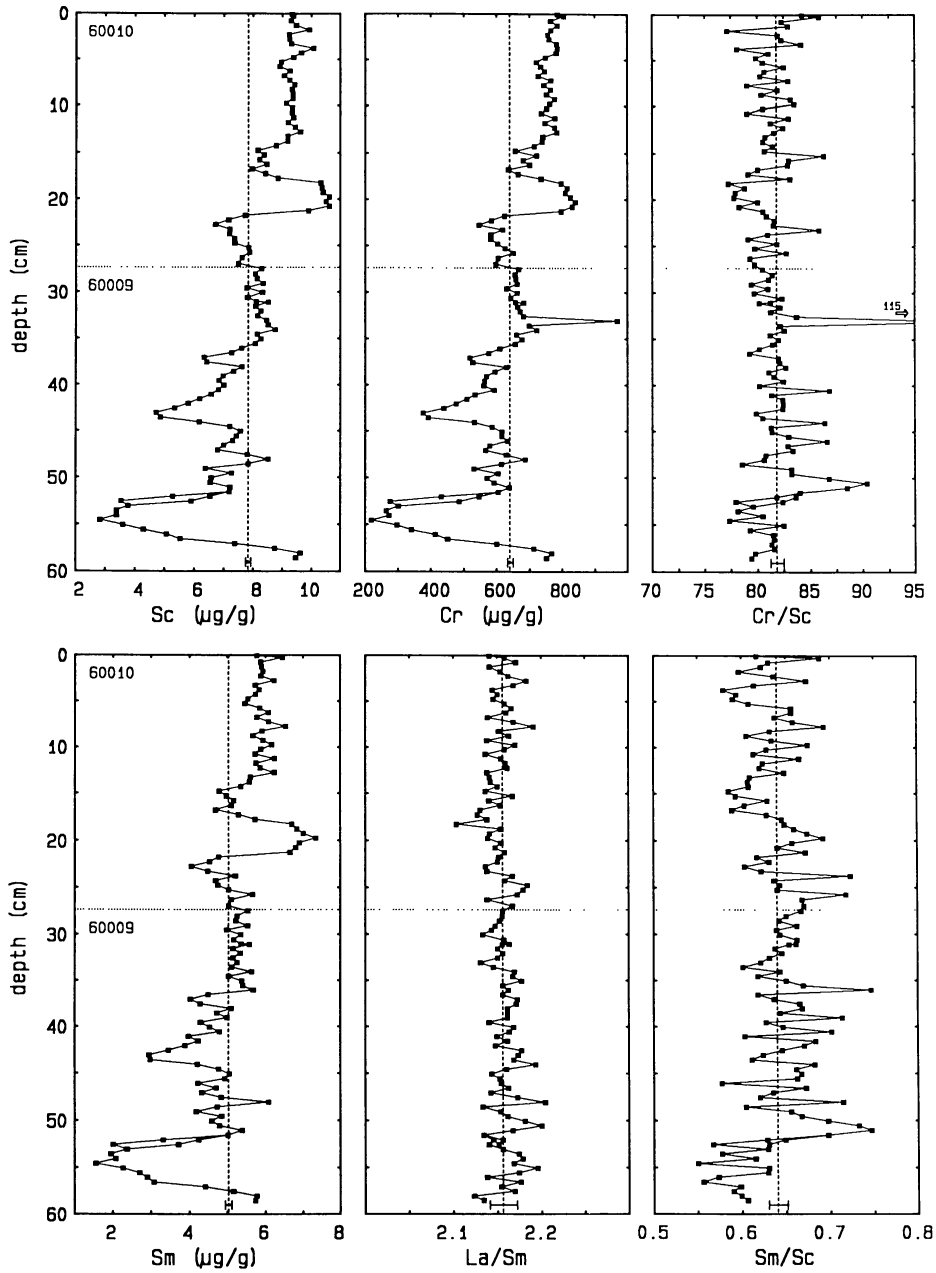

Fig. 2. Depth profiles of element concentrations and concentration ratios for <1-mm fines from 60009/10 [depth scale from Table 3.1 of *Fruland et al.* (1982); data from Table A1 of this work]. The horizontal dotted lines indicate the boundary between the 60009 and 60010 sections of the core; the vertical dashed lines indicate the mean concentration or ratio of all 121 samples. The analytical precision is indicated by the bar plotted at 59 cm depth.

which was collected near the site of the 60013/14 core, 30-40 m to the northwest of 60009/10 (Fig. 1).

3.1.2. Unit at 18-21 cm depth. In the 60010 section, the most distinctive feature is stratigraphic unit 2 (SU2) at 18-21 cm depth. The seven samples from this unit are all similar to each other in composition but are distinctly different from soils in adjacent units. SU2 contains the highest concentrations of incompatible trace elements (ITEs), e.g., Sm and Th, and elements associated with mafic mineral phases (Sc, Cr, Fe) found in the core (Fig. 2; section A1.1). The SU2 samples are slightly enriched in Sc relative to Cr (Fig. 2, Cr/Sc ratio).

3.1.3. Unit at 54 cm depth. The concentrations of all analyzed lithophile elements generally decrease with depth in the core, except for that of Ca, which increases. The most striking compositional feature of the core occurs in SU3 in 60009, a distinct layer near the bottom at about 54 cm depth in which most elements reach a minimum concentration and CaO reaches its maximum concentration, as does Al_2O_3 (*Ali and Ehmann,* 1976). This soil is whitish in color. Previous studies show that the anomaly results from a concentration of coarse-grained, nearly monomineralic plagioclase in this unit (*Duke and Nagle,* 1976; *McKay et al.,* 1976; *Blanchard et al.,*

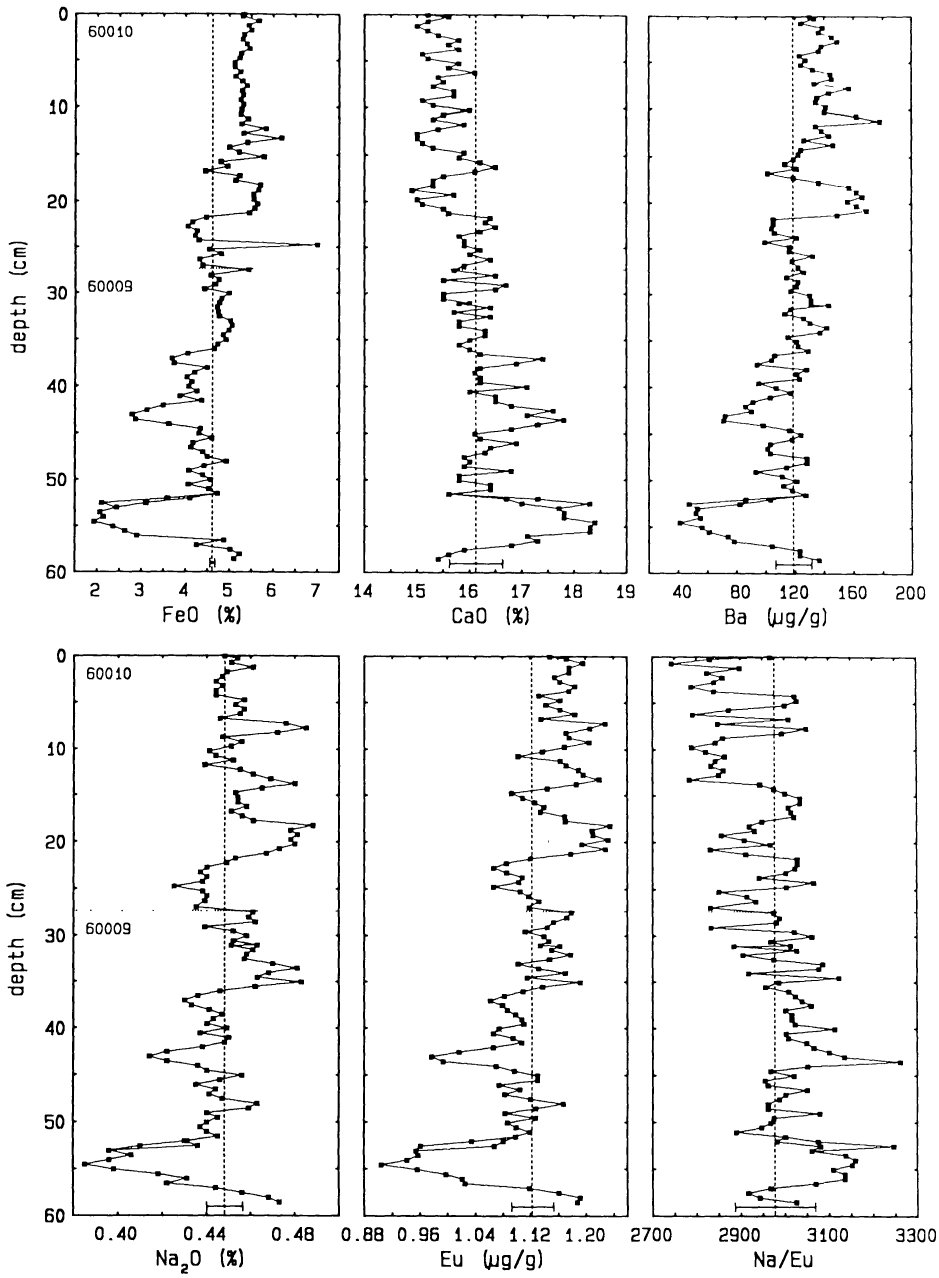

Fig. 2. (continued).

1976; *Ali and Ehmann,* 1976; *Simon et al.,* 1978). The soil at 54 cm depth in 60009 is the most feldspathic yet found among Apollo 16 regolith samples; no other Apollo 16 soil is comparably poor in Sc and other elements associated with mafic mineral phases.

There is a less extreme, but compositionally similar layer in SU7 of 60009 at 43 cm depth. This whitish layer contains anorthositic breccia fragments in addition to some plagioclase crystals (*Duke and Nagle,* 1976; *McKay et al.,* 1976). It was not so evident in previous studies that this unit is compositionally distinct because only one sample from this zone was studied.

3.1.4. Unit at 58 cm depth. Below the white layer at 54 cm depth there is an abrupt change in the concentrations of most elements. At the very bottom of the core, at 58 cm depth, is a unit (SU1 of 60009) that is similar in composition to the soil near the surface. The deepest four samples depart from the general trend of decreasing concentration with depth for most lithophile elements.

3.1.5. Siderophile elements and Fe-Ni metal. Siderophile elements show little systematic variation with depth (Fig. 2). Minima in the concentrations of Ni, Co, Au, and Ir occur at 43 and 54 cm depth as a result of dilution by the coarse-grained, feldspathic components in these units. Several

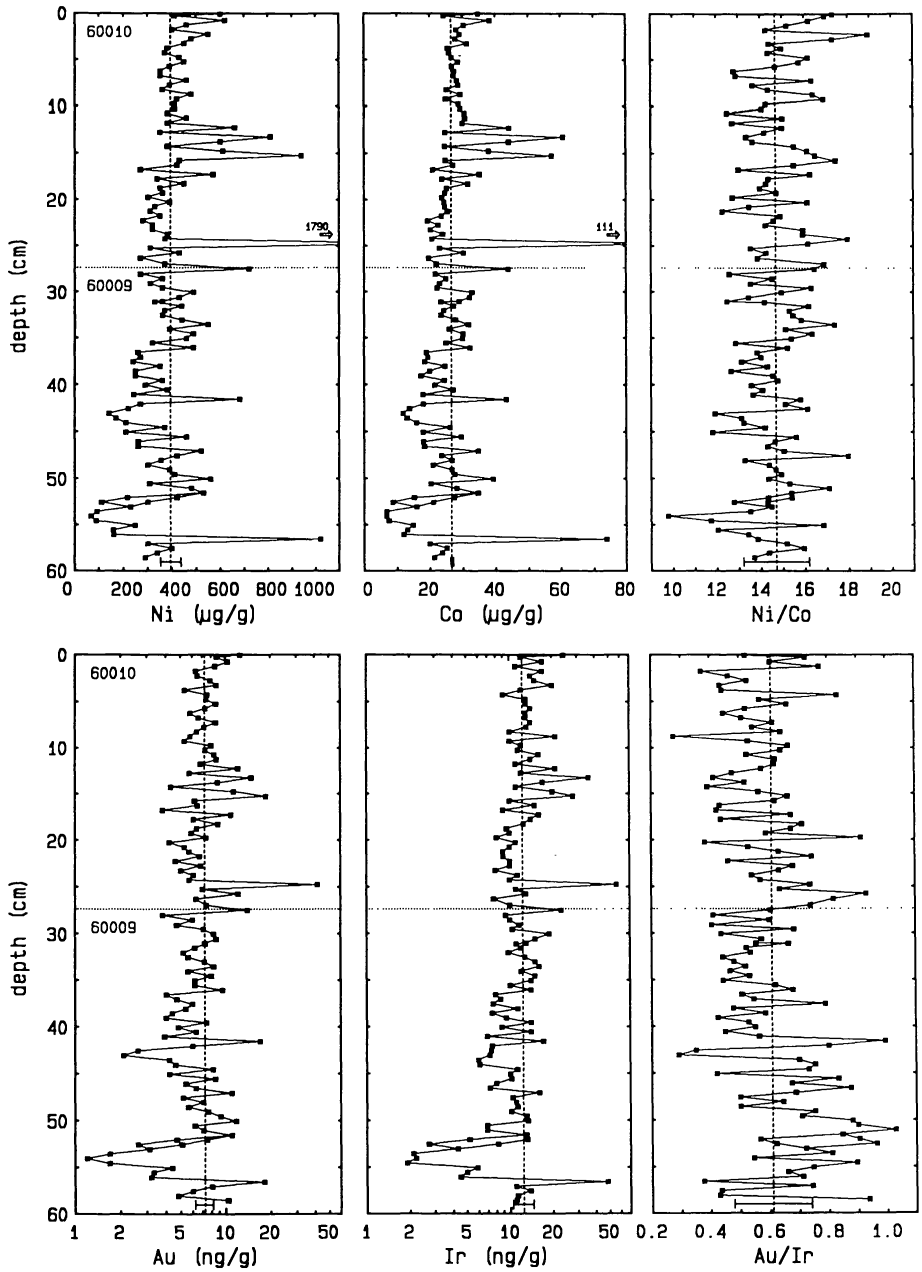

Fig. 2. (continued).

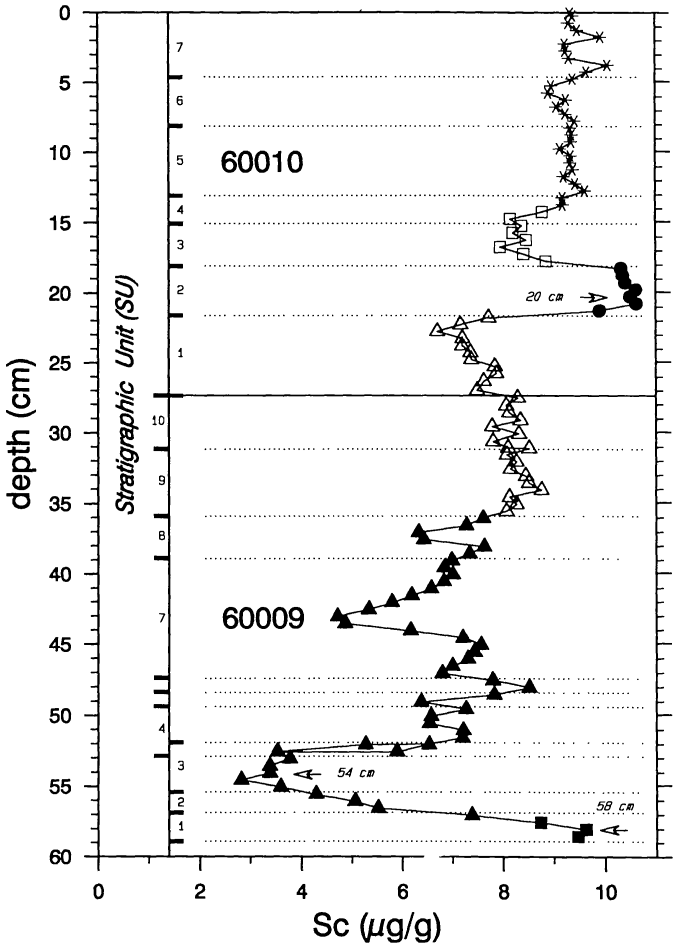

Fig. 3. The stratigraphic units (SU) of *Duke and Nagle* (1976) for 60009/10 keyed to the Sc depth profile of Fig. 2. The arrows indicate the intervals from which the >1-mm particles were obtained (Table 1).

"spikes" occur in the siderophile-element profiles, most notably at 25 and 57 cm depth. These samples have high concentrations of Ni, Co, Ir, and Au, yet stratigraphically adjacent samples are normal. Thus, the anomalies probably result from single large grains of Fe-Ni metal of meteoritic derivation in the analyzed subsample (*Korotev,* 1987b). Several of the samples between 12 and 17 cm depth are moderately enriched in siderophile elements, indicating a slight excess concentration of meteoritic material in these units (SU3 and SU4).

Ali and Ehmann (1977) report that sample 60010,40 (3-4 mm depth; section A1.B) had exceptionally large concentrations of Ni (10,600 μg/g) and Co (142 μg/g) as a result of a large grain of metal containing 93.2% Fe, 6.4% Ni, and 0.36% Co, which they recovered from the sample. This is a typical composition for metal grains in Apollo 16 soil (*Korotev,* 1987b). Both the size of the grain (~1 mm, longest dimension) and the anomalously high concentrations of Fe and Co they report for the bulk soil sample are consistent with an ~1.5-mg grain of metal of the composition they report (in a 50-mg soil sample, i.e., 3% by weight of the analyzed sample). However, there appears to be some discrepancy in the reported results because the expected Ni concentration of the bulk soil sample would be only 2400 μg/g, not 10,600 μg/g as reported.

*3.1.6. **Binary mixing.*** The concentration profiles for elements compatible with mafic mineral phases such as Fe, Sc, and Cr are similar to each other as well as to those of ITEs like Sm. Figure 4 shows that throughout the wide variation in Sc and Sm concentrations among the soils, the two elements are well correlated. As discussed in more detail below, the correlation line is a binary mixing line between the most Sc-rich (mafic), ITE-rich soils in the core and plagioclase fragments, such as those that dominate in the unit at 54 cm depth (*Blanchard et al.,* 1976). For plagioclase, the concentrations of all elements analyzed except the "plagiophile" elements Na, Ca, Sr, and Eu are very low compared with the concentrations in most of the fines. As a result, plagioclase acts as a diluent resulting in mixing trends that extrapolate toward the origin in most two-element plots such as the Sc-Sm plot of Fig. 4. For consistency, Sm will be used to represent the ITEs and Sc will be used to represent elements associated with mafic components in much of the subsequent discussion and many of the figures. Because of the mutual correlation among concentrations of those lithophile elements not associated with plagioclase in Apollo 16 fines, conclusions about mixing relationships based on Sc-Sm plots are usually valid when other lithophile elements are considered; exceptions will be noted.

3.2. >1-mm Particles

I studied individual soil particles for the purpose of identifying the lithologies responsible for the compositional variations observed in the <1-mm fines. Thin sections were prepared of many of the particles after INAA, and with the aid of B. L. Jolliff, the particles were categorized by lithologic type, e.g., impact-melt rocks, regolith breccias, etc. Detailed petrographic description of these particles is beyond the scope of this work. Petrography of the particles will be discussed in more detail in subsequent papers on 1-4-mm soil particles from Apollo 16 (B. L. Jolliff, R. L. Korotev, and L. A. Haskin, in preparation). For this report, however, I compare the compositions of the <1-mm fines and the particles with the advantage of knowing, in most cases, the rock type represented by the particles.

The >1-mm particles from 60009/10 include 20 from the Sc- and Sm-rich layer at 20 cm depth, 10 from the Sc- and Sm-poor anorthositic layer at 54 cm depth, and 10 from the Sc- and Sm-rich layer at 58 cm depth (Table 1). The particles were selected to represent the range, but not necessarily the relative distribution, of lithologies present at each depth interval. However, because a large fraction (36-53%) of all available particles in each parent split was studied (Table 1), it is unlikely that the actual distribution of large particles in each depth interval is significantly different from that of the subsets studied here. It is important to keep in mind that the relative distribution of lithologies in the >1-mm grain-size fraction may be different from that of the <1-mm fraction (*Korotev,* 1989). Analytical results for the >1-mm particles are listed in Table A2.

The compositional variation among the >1-mm particles is large and greatly exceeds that of the <1-mm fines, particularly for ITEs like Sm (Fig. 5a). This is to be expected because each analyzed sample of <1-mm fines is a mixture of many such particles. We can assume that the lithologies observed among the >1-mm particles occur as well in the <1-mm fines and that the <1-mm fines contain at least a small proportion of lithologies not represented among the 40 >1-mm particles studied here. The linear trend of <1-mm fines on Fig. 4 indicates that the mixing is systematic in some way; this topic will be discussed in more detail below.

Petrographic examination of the particles shows that they consist of a variety of lithologies (Fig. 5a). The single agglutinate (*McKay et al.,* 1972), particle 58-F, plots on the soil mixing line in the vicinity of <1-mm soils from 58 cm depth ("Aggl," Fig. 5a). This is to be expected if the particle formed from fusion of local soil during a micrometeorite impact (section 4.3.1). Three regolith-breccia particles (20-F, 20-R, 58-J) plot on the extension of the soil mixing line, at slightly greater Sc concentrations than the most Sc-rich soils. These particles are fragmental breccias consisting of lithified soil, perhaps of local derivation, that apparently contain even less plagioclase than the most mafic <1-mm fines. A fourth regolith-breccia particle (20-B) is anomalous in having the greatest concentrations of ITEs of any particle studied (Sm: 21 μg/g). It has a glassy matrix and contains a large clast of poikilitic impact-melt breccia. This particle was probably not formed from regolith such as that presently occurring at the surface of the Apollo 16 site. Impact-melt breccias span a range of compositions; ITE concentrations are particularly variable, but all particles with high Sm concentrations, except 20-B, are impact-melt breccias. Many of these have poikilitic textures

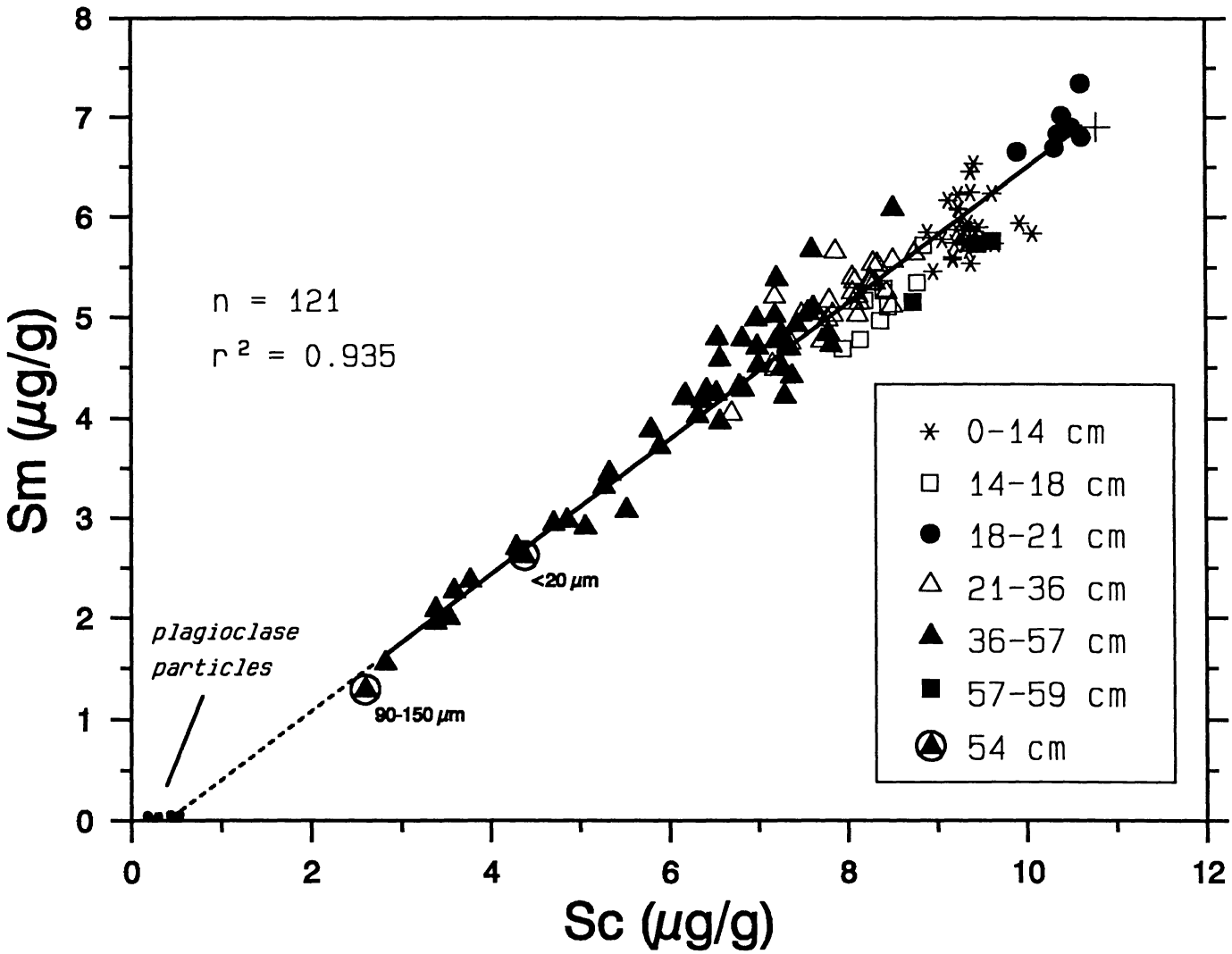

Fig. 4. Variation of Sm and Sc concentrations in <1-mm fines from 60009/10 (data from Table A1). The symbols are keyed to depth and are the same as those in Fig. 3. The solid line is the best fit to the 121 data points (excludes circled triangles; see section A2 for discussion of fitting of the line). The dotted portion of the line indicates that the trend extrapolates to plagioclase such as that found as single grains in the >1-mm grain-size fractions. This mixing line is reproduced in subsequent Sm-Sc plots. The two circled triangles are for grain-size fractions of soil at 54 cm depth (60009,457 from *Blanchard et al.,* 1976). The "+" represents the composition of the Cayley soil component used in the mixing model (Tables 3 and 4).

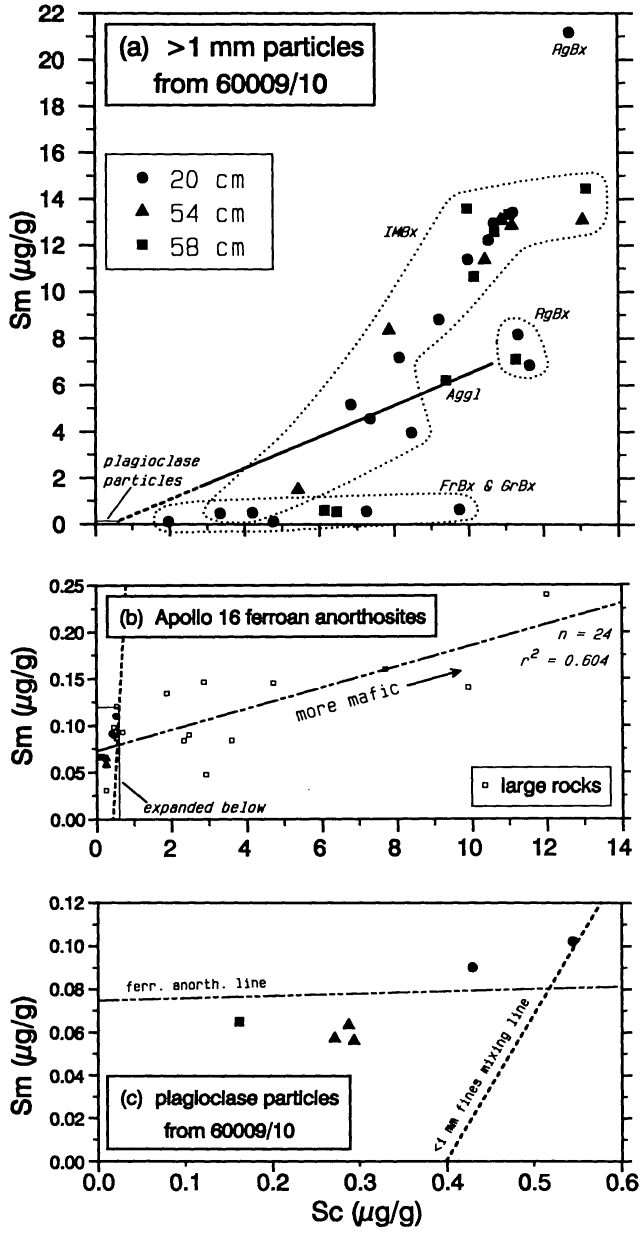

Fig. 5. Variation of Sm and Sc concentrations in >1-mm particles from three depth intervals in 60009/10 (data from Table A2). The symbols are consistent with Fig. 3 and the solid line with dashed extension is the mixing line for the <1-mm fines from Fig. 4. **(a)** The dotted lines encircle fields for petrographically similar particles: "RgBx" = regolith breccias; "IMBx" = impact-melt breccias; "Aggl" = agglutinate; "FrBx & GrBx" = fragmental breccias and granulitic breccias (some of the impact-melt breccias have granulitic textures). **(b)** Comparison of the 6 plagioclase particles to 18 samples from large ferroan anorthosites from Apollo 16 (open squares; data from compilation of *Haskin et al.*, 1981). The broken line is the simple least-squares regression to all 24 points (Sm = 0.01083 · Sc + 0.0745). **(c)** Expansion of **(a)** in the vicinity of the origin showing the plagioclase grains. The mixing line of Fig. 4 and the regression line of **(b)** are shown; their intersection provides an estimate of the composition of the ferroan-anorthosite component of the <1-mm fines at 54 cm depth in the core. (See section A2 for discussion of uncertainty in the extrapolation of the <1-mm fines mixing line.)

and probably correspond to the "poikilitic rocks" lithology that *McKay et al.* (1977) found to be most abundant at 20 cm depth in the core in their study of modal petrography of submillimeter grain-size fractions. Particles with less than 2 µg/g Sm and greater than 1 µg/g Sc are mostly feldspathic fragmental breccias, granulitic breccias, and feldspathic impact-melt breccias.

Thin sections of the remaining six particles have not been prepared. However, all are white in color and have compositions consistent with nearly pure (>99%) plagioclase feldspar (*Palme et al.*, 1984). Although at least one such particle occurs in all three depth intervals, three of the six plagioclase particles are from the immature, feldspathic unit at 54 cm depth. It is clear from the photograph provided by the curator that of the 19 >1-mm particles occurring in this depth interval (60009,214, Table 1), 8 are plagioclase grains. The three analyzed particles are virtually identical to each other in composition but are slightly different from the particles from 20 and 58 cm depth (Figs. 5b and 6). Under the binocular microscope all three are translucent and appear to be single crystals. These almost certainly correspond to the "plagioclase single crystals" lithology that dominate this immature layer in the modal petrographic studies of *McKay et al.* (1976) and *Simon et al.* (1978). The two plagioclase particles from 20 cm depth are also very similar to each other in composition and are more mafic (greater Sc, Fe, Cr), slightly more anorthitic on the average ($An_{97.1}$ vs. $An_{96.5}$, based on INAA data, Fig. 6), and have lower Eu concentrations than the other four. Under the binocular microscope these two are opaque white grains, suggesting that they are cataclastic or remelted.

Except for the abundance of plagioclase grains at 54 cm depth, there is no overwhelming evidence in the data presented here that any particular lithology is more prevalent in one depth interval than another among the >1-mm particles. For example, mafic (>8 µg/g Sc), Sm-rich (>10 µg/g), impact-melt breccias are about equally abundant in all three depth intervals.

4. 60009/10 DISCUSSION

Soil samples from the top 13 cm of the core are all similar to each other in composition as well as to most other surface soils collected in the vicinity of the lunar module (Stations LM, 1, and 2; *Korotev*, 1981; *Ali and Ehmann*, 1977). Soil in this region of the core is the most mature; among 60009/10 soils it has extreme values for most indices of surface exposure [highest fraction of agglutinate particles, small mean grain size, and the highest values for I_s/FeO (section 4.3.1); *McKay et al.*, 1977]. It is relatively rich in Sc and Sm (Figs. 2 and 4). To a first approximation, all the compositional variation in lithophile elements among the 121 samples of <1-mm fines analyzed here can be explained by addition (or subtraction) of a plagioclase-rich component, such as the plagioclase grains discussed in the previous section, to (or from) a relatively mafic soil, such as that found at the top of the core. This is essentially the conclusion of previous compositional studies (*Blanchard et al.*, 1976). I expand on the significance of that mixing relationship below.

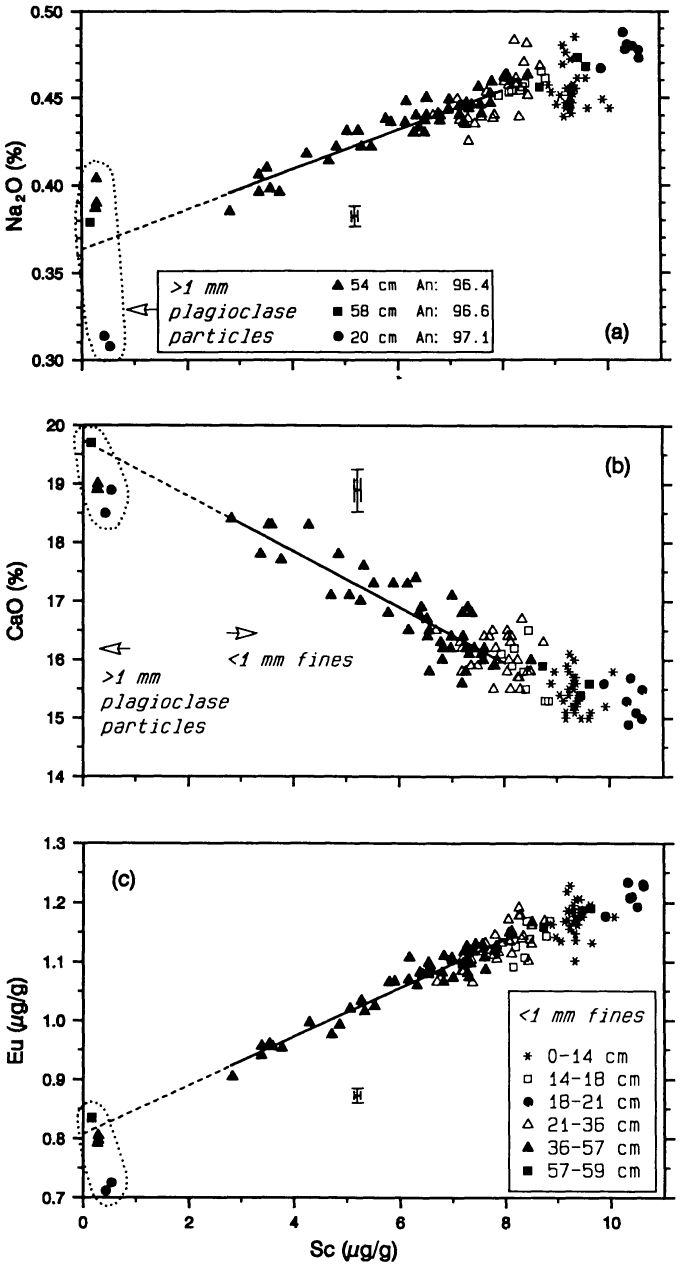

Fig. 6. Variation of Na_2O, CaO, and Eu concentrations with Sc in <1-mm fines from 60009/10 and comparison with >1-mm plagioclase particles. The lines have been fit to the data from samples in the 36-57 cm depth interval only (filled triangles). The percent anorthite concentrations of the plagioclase particles listed in **(a)** was calculated from the bulk concentrations of Na_2O and CaO.

4.1. Ferroan Anorthosite (Sc-poor) Component

4.1.1. Extrapolation of the mixing lines. The simple two-component model is demonstrated by the mixing line on the Sc-Sm plot of Fig. 4 (section A2); the same mixing relationship is indicated by any pair of lithophile elements. In this section I use mixing lines to constrain the composition of the Sc-poor component.

At one extreme the Sc-poor component may be represented by the soil with the lowest Sc concentration because any of the soils of intermediate composition can be modeled reasonably well as a mixture of soils of more extreme composition. However, the low-Sc component may be any rock type or soil of lower Sc concentration, as long as it plots along the dashed (extrapolated) portion of the mixing line on Fig. 4 and provides satisfactory mass balance for other elements as well. This excludes soils such as those found at North Ray Crater (Fig. 1; Table A7) because these do not plot on the 60009/10 mixing line (*Korotev,* 1981, 1990b). As developed below, the lithology ferroan anorthosite, however, does satisfy the requirements; thus, even if the low-Sc component is a "soil component" (section 4.2), it almost certainly is dominated by ferroan anorthosite and not more mafic anorthositic rocks such as those typical of North Ray Crater. Nonetheless, it is useful to consider this extreme. The most Sc-poor sample analyzed here, 60009,3118 from 54.3-54.8 cm depth, is similar in composition to the sample analyzed from this same depth interval by *Ali and Ehmann* (1976), who obtained data for major elements. Although these data are not precise, they constrain the Sc-poor component to contain at least 93 vol% plagioclase; thus the Sc-poor component is clearly some type of anorthosite.

Compositional data for Apollo 16 anorthosites indicate that the Sc-poor component is an anorthosite considerably richer in plagioclase than even the most Sc-poor soil. The six >1-mm plagioclase particles (section 3.2) are indistinguishable in composition from some large samples of Apollo 16 anorthosite, but several Apollo 16 anorthosites have Sc concentrations much greater than those of the plagioclase particles because they are more mafic (Fig. 5b). Samarium concentrations are very low in Apollo 16 anorthosites, averaging about 0.08 μg/g. Because the mixing trend for the <1-mm fines extrapolates directly into the range of the anorthosites and because anorthosite particles of similar composition occur in the soil, it is reasonable to assume that the Sc-poor component is an anorthosite such as those plotted in Fig. 5b. The intersection of the regression line of Fig. 5b and the mixing line of Fig. 4 represents the best estimate of average composition of the low-Sc component. The lines intersect at a point corresponding to 0.5 μg/g Sc and 0.08 μg/g Sm (Fig. 5c).

The concentration of Sc in the anorthosite component is an important parameter because it is useful for establishing the plagioclase concentration of the anorthosite. Unfortunately, the uncertainty in the Sc concentration at 0.08 μg/g Sm is relatively large, 0.5 ± 0.3 μg/g (95% confidence) because of the degree of scatter of the <1-mm fines about the mixing line and the long extrapolation (Fig. 4). Thus, within uncertainty, the three >1-mm plagioclase particles from 54 cm depth (Fig. 5c) account for the mixing trend, which is defined primarily by <1-mm fines from 36-57 cm depth (Fig. 4).

More information about the nature of the anorthosite component can be obtained from plots of the "plagiophile" elements Na, Ca, Sr, and Eu. In Fig. 6, the compositions of soils in the anorthositic zones (36-57 cm) trend toward a plagioclase composition that does not exactly match that of any of the six separated plagioclase particles, but is within the range defined by the six particles. Extrapolation of the mixing

lines in Fig. 6 to 0.5 μg/g Sc indicates that plagioclase in the soils between 36 and 57 cm depth has an average composition of $An_{96.8}$, compared with $An_{96.4}$ for the mean of the three >1-mm plagioclase grains from 54 cm depth. Electron microprobe analyses of plagioclases from this zone indicate that most have a composition of An_{96-97}, but that they range from $An_{95.5}$ to $An_{98.0}$ (*Vaniman et al.,* 1978). Thus, a portion of the scatter about the low-Sc end of the mixing lines in Fig. 6 results from variation in the mean anorthite content of the plagioclase in the analyzed samples. This variation is exacerbated by the fact that the plagioclase is coarse grained and the sample masses are small.

4.1.2. Plagioclase content of the anorthosite component. The analysis above indicates that the anorthosite component of the 60009/10 soils contains 0.5 ± 0.3 μg/g Sc and thus is very poor in Sc-bearing phases (primarily pyroxene and ilmenite). Iron-oxide concentrations for Apollo 16 anorthosites containing 0.5 μg/g Sc are typically 0.3-0.4% (*Haskin et al.,* 1981) and plagioclase from Apollo 16 anorthosites typically contains 0.1% FeO (*Hansen et al.,* 1979; *Palme et al.,* 1984). Thus, if the nonplagioclase phases in the anorthosite average at least 20% FeO, the anorthosite component responsible for the principal compositional variation in the 60009/10 soils contains at least 99% plagioclase.

4.1.3. Ferroan anorthosite and Apollo 16. The lunar crust is rich in plagioclase and a variety of plutonic and polymict anorthosites have been identified [especially if any rock containing >77.5% modal plagioclase is regarded as an "anorthosite" (*Warren et al.,* 1990)]. However, (1) the coarse grain size and high plagioclase concentration of the anorthosite, (2) the high anorthite content of the plagioclase, and (3) the ferroan nature of the associated mafic silicates (*Vaniman et al.,* 1978) identify the anorthosite component at 54 cm depth in 60009/10 as the plutonic rock type known as "ferroan anorthosite" (*Dowty et al.,* 1974). This is confirmed by the relative concentrations of rare earth elements (REE; section 5.2.4) and the low Eu concentration of 0.8 μg/g (Fig. 6), which is the typical concentration for ferroan anorthosite from the Apollo 16 site (*Korotev and Haskin,* 1988). Other types of "pristine" lunar anorthosite, e.g., alkali anorthosite and magnesian anorthosite, have higher concentrations of REE, including Eu (*Warren and Wasson,* 1981; *Warren et al.,* 1983a; *Lindstrom et al.,* 1984). [The strikingly large positive Eu anomalies of lunar ferroan anorthosites are misleading: with ~0.8 μg/g Eu, ferroan anorthosite has the lowest absolute concentration of Eu of any common lunar rock type (*Korotev and Haskin,* 1988). Only very plagioclase-poor rocks have lower Eu concentrations.]

Since the previous studies of 60009/10, ferroan anorthosite has come to represent one of the two principal "suites" of lunar plutonic rocks (*Warner et al.,* 1976; *Warren and Wasson,* 1977) and be regarded as the principal lithologic component of the earliest lunar crust (*Warren and Wasson,* 1979). An important, but unknown, parameter for models of lunar crust formation, however, is the fraction of plagioclase in the anorthosite of the early lunar crust (*Korotev and Haskin,* 1988; *Warren,* 1990). With an average Al_2O_3 concentration of 26%, the present crust averages 75-80 vol% plagioclase (*Warren,* 1985; *Korotev and Haskin,* 1988). Based on Eu mass balance for a large number of polymict samples, *Korotev and Haskin* (1988) argue that the anorthosite component of the lunar crust is, in the strict sense, a noritic anorthosite, i.e., 77.5 to 90 modal percent plagioclase (*Stöffler et al.,* 1980), and other arguments lead to a similar conclusion (*Warren,* 1990). Although samples of noritic anorthosite are common, nearly all are polymict breccias. Most samples of "pristine" ferroan anorthosite contain greater than 95% plagioclase and some well-known large specimens contain at least 99% (e.g., 15415, 60015). Perhaps the numerous hand specimens of nearly pure plagioclase found in the Apollo 16 regolith may not be representative of their source rocks, but are merely the plagioclase-rich fraction of comminuted anorthosites that are really more noritic or troctolitic, and for some reason our sampling of a finite number of discrete samples is biased in favor of the most plagioclase-rich samples (*Haskin and Lindstrom,* 1988). However, *Warren* (1990) calculates that even when only "large" samples (>10 g) of pristine ferroan anorthosite are considered, the modal fraction of mafic silicates averages 8.1 ± 8.6 wt% (93.7 vol% plagioclase). All but one (15415) of the 17 samples considered by *Warren* (1990) are from Apollo 16. Thus, even the largest anorthosite samples from Apollo 16 are much more feldspathic, on the average, than the average lunar crust.

The <1-mm fines from 60009/10 contain a large number of small mineral grains. The arguments presented above show that the ferroan anorthosite component of the <1-mm fines is ~99% plagioclase. Because of "differential comminution," i.e., the variation in mineral proportions with grain size in a comminuted rock resulting from differences in the intrinsic grain size and mechanical properties of the various minerals, the source anorthosite may be somewhat more or less mafic than the anorthosite component of the <1-mm fines (*Korotev,* 1976; *Hörz et al.,* 1984). However, there is little evidence that mafic minerals are concentrated in coarser (>1 mm) grain-size fractions of the regolith. Among more than 200 >1-mm soil particles from Apollo 16 studied in this lab, we have only encountered one particle dominated by mafic minerals (a single olivine grain, section 5.2.2). Some of the large ferroan anorthosites with >95% plagioclase from the LM/ALSEP Station, e.g., 60015, 60055, and 60215 (97-99% plagioclase; *Warren,* 1990), may derive from the same source as the 60009/10 anorthosite. However, if more mafic anorthosites such as 60025 and 60135 (90 vol% and 77 vol% plagioclase; *Warren,* 1990) also derive from the same source, then the 60009/10 data argue that either (1) these samples are atypically mafic and do not represent the source of the anorthosite or (2) the mafic minerals are preferentially excluded from the <1-mm grain-size fraction of the regolith.

Ferroan anorthosite in any form is scarce at all other sampled highland sites. None of the nonmare lunar meteorites, all of which are regolith breccias of unknown provenance, suggest that rocks containing 99% plagioclase are an important constituent in their source regions (*Korotev et al.,* 1983; *Ostertag et al.,* 1986; *Goodrich and Keil,* 1987; *Bischoff et al.,* 1987; *Takeda et al.,* 1989; *Jolliff,* 1990). Thus, the Apollo 16 region may be atypical of the lunar crust in containing such highly plagioclase-rich rocks.

4.2. Cayley Soil (Sc-rich) Component

4.2.1. A well-mixed soil component. By analogy, we might expect that extrapolation of the regolith mixing lines of Figs. 4 and 6 in the high-Sc direction might also intersect the field of some prevalent rock type. However, this would require that Apollo 16 soils are composed principally of only two lithologies, ferroan anorthosite and a single high-Sc (mafic) lithology, and this is unrealistic because petrographic studies, as well as the data for the >1-mm particles (section 3.2), indicate that Apollo 16 soils consist of many different rock types with a wide variety of compositions. Also, there is no common rock type at Apollo 16 that plots on the extrapolation of the regolith mixing lines in the high-Sc direction (other than breccias composed of regolith, e.g., Fig. 5a), thus the extrapolation has no significance other than to show the geometric effect of removing anorthosite from the most mafic soils, which probably do contain at least a small component of ferroan anorthosite.

The deceptively simple mixing trends of Figs. 4 and 6 show that the mixing event(s) represented by the trends involves two components, ferroan anorthosite and a soil composed of a previously well-mixed assortment of various lithologies. A principal conclusion of this work is that soils plotting at the high-Sc and high-Sm end of the distribution in Fig. 4 (i.e., about 10.5 μg/g Sc and 7 μg/g Sm) represent, at one level, an endmember mixing component in the same sense that the "Apennine Front soil component" is an end member at Apollo 15 (*Korotev,* 1987d). I will call this component the "Cayley soil component" because soils of this composition appear to be the dominant surface material associated with the Cayley Plains west of the landing site (below). The various more mafic subcomponents of the Cayley soil component must occur in relatively constant proportions among the various soils from 60009/10. For example, the ratio of Sm-rich impact-melt breccias to Sm-poor granulitic breccias (section 3.2; Fig. 5) must not vary greatly. If it did, then the data for the <1-mm fines would be more scattered within the area bounded by the data for the >1-mm particles in plots such as Fig. 4.

The Cayley soil component is generally finer grained than the anorthosite component that dominates at 54 cm depth. This leads to variation in composition of the soil with grain size. *Blanchard et al.* (1976) analyzed grain-size fractions of soils throughout the core. Both the 90-150-μm fraction and the <20-μm fraction of the soil from 54 cm depth (60009,457) plot on the mixing line of Fig. 4. This suggests that the variation in composition with grain size does not result from differential comminution (section 4.1.3), but from the mixing of compositionally distinct components with different grain-size distributions (*Korotev,* 1989).

Does soil with the composition of the most mafic soils in the 60009/10 core represent the Cayley soil component or is the Cayley soil component better represented by a composition plotting at higher concentrations of Sc and Sm along the mixing trend of Fig. 4? There are several pieces of evidence to suggest that soil containing significantly less plagioclase does not occur in the vicinity of the Apollo 16 site. First, the most Sc-rich soils in 60009/10 are almost identical in composition to the most Sc-rich of the surface and trench soils from Apollo 16, those from Stations 5 and 6 (*Korotev,* 1981). Second, soils plotting along the mixing trend of Fig. 4 but with higher Sc and Sm concentrations do not occur either in the Station 4 core (*Korotev et al.,* 1984) or in the deep drill core (section 5), although both cores contain samples of similar composition to the most Sc-rich soils from 60009/10. (Samples containing >10.5 μg/g Sc occur in both these cores, but they plot off the Sc-Sm mixing trend as a result of a component of mare basalt or mare glass, not as a result of less anorthosite; section 5.1.4.) Third, Th is strongly correlated with Sm in Apollo 16 soils (Fig. 7). Soil samples plotting at the high-Sc and high-Sm end of the mixing trend contain about 2.5 μg/g Th, which is the average Th concentration of the Cayley Plains immediately west of the landing site as determined from orbit (*Metzger et al.,* 1981). Because of the strong correlations between pairs of ITEs and between incompatible and compatible lithophile elements in Apollo 16 soils (Figs. 4 and 7; *Korotev,* 1981), knowledge of the Th concentration of the Cayley Plains effectively fixes the average concentration of other lithophile elements. The only evidence

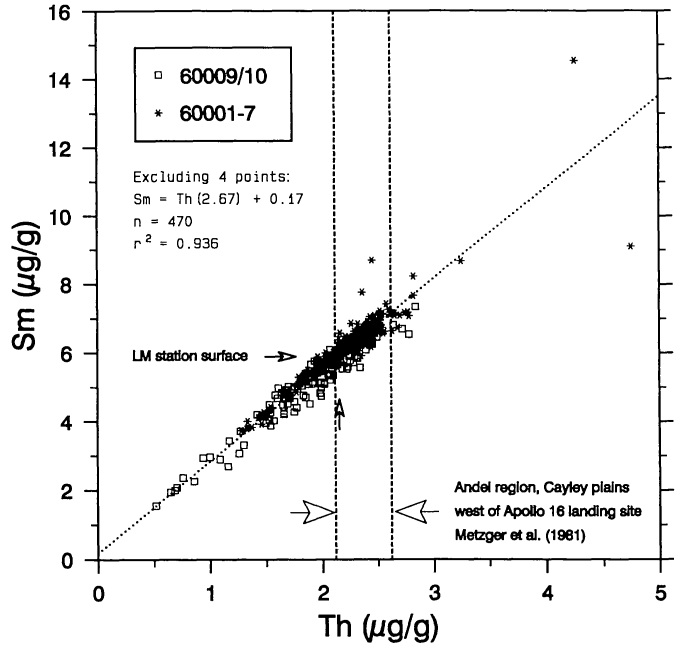

Fig. 7. Variation of Sm with Th in samples from the two cores. The vertical lines represent the range in Th concentration obtained from the Apollos 15 and 16 orbiting gamma-ray experiments for the Andel region, which consists mostly of the Cayley Plains immediately west of the landing site (*Metzger et al.,* 1981). The small arrows locate the concentrations at the surface of the LM Station based on the top 10 cm of soil from the two cores and 60601 (Fig. 1). The data show that the most Th- and Sm-rich soils in the cores (excluding a few anomalous samples) are typical of the surface of the local Cayley Plains. Soil as poor in Th as the most Th-poor soils in 60009/10 is found at the surface immediately east of the Apollo 16 landing site [Descartes and Kant regions; *Metzger et al.* (1981)]. The regression line [method of *York* (1969); see section A2] excludes the four data points that are most deviant.

TABLE 2. Petrographic data for three depth intervals in 60009/10 from *McKay et al.* (1976, 1977); values in modal (volume) percent*.

Sample Number:	60009,457		60010,3107	60009,458
Nominal Depth (cm):	54		20	58
Scandium Concentration:	low		high	high
	raw	minus plag.	raw	raw
(1) Metamorphosed Breccia	4.7	*16.*	11.0	11.7
(2) Poikilitic Rocks	3.0	*10.*	28.1	12.5
(3) Plagioclase Single Crystals	73.8	*11.3*	11.5	11.1
SUM (1-3)	81.5	*37.5*	50.6	35.3
(4) Brown Matrix Breccia	2.4	*8.2*	8.1	13.8
(5) Agglutinates	5.0	*16.9*	10.9	26.1
SUM (1-5)	88.9	*62.6*	69.5	75.2

*Mass weighted mean of three size fractions (90-500 μm). The column labeled "minus plag." results from mathematically removing "plagioclase single crystals" until the normalized percentage is 11.3, the mean value of the other two depth intervals.

suggesting that the Cayley soil component may be slightly more mafic than the most Sc-rich soils in 60009/10 is that the three >1-mm particles from 60009/10 identified as regolith breccias plot on the mixing trend at slightly higher concentrations of Sc and Sm (Fig. 5a; section 3.2). However, most Apollo 16 regolith breccias are less mafic than the three particles from 60009/10 (section 6.2).

4.2.2. But not perfectly well mixed. In their study of the core, *McKay et al.* (1977) concluded that modal petrographic variations among soils from different depths involved mainly three components. In this section I show that some of the scatter about the binary mixing line of Fig. 4 is caused by variation in the proportions of the components identified by *McKay et al.* (1977) and that the Cayley soil component does not have a unique chemical and mineralogical composition, but is variable within limits.

The modal petrography of *McKay et al.* (1977) is summarized in Table 2. The table lists percentages of five components that account for 70-90% of the volume of the core samples. *McKay et al.* (1977) argue that most of the petrographic variation involves three lithologies, "plagioclase single crystals," "poikilitic rocks" (*Simonds et al.,* 1973), and "metamorphosed breccia." At one extreme is the soil from 54 cm depth in 60009, which contains >70% plagioclase single crystals. Within the 60009 section, the other extreme is at 58 cm depth, which contains the lowest fraction of plagioclase single crystals, 11%, and the highest fractions of poikilitic rocks and metamorphosed breccia. The two latter components are approximately equally abundant. Other soils in 60009 (not listed in Table 2) appear to be mixtures of these two extreme soils in that the ratio of poikilitic rocks to metamorphosed breccias remains fairly constant at 1 to 1 and only the ratios of plagioclase single crystals to the sums of the other two components change. This variation defines one mixing trend. Another petrographic mixing trend occurs in the 60010 section of the core. The most extreme soil in 60010 is that at 20 cm depth, which contains the lowest fraction of plagioclase single crystals, 11.5%, which is nearly identical to that of the soil at 58 cm depth in 60009. However, the ratio of poikilitic rocks to metamorphosed breccia is 2.4 to 1 and other soils in 60010 maintain this ratio. On triangular plots on which these three components are normalized to 100%, two distinct mixing trends occur, one for 60009 and the other for 60010 (Figs. 8 and 9 of *McKay et al.,* 1977).

Why are the two mixing trends, which are strikingly obvious on the plots of *McKay et al.* (1977), not apparent in the compositional data? The principal criterion distinguishing the two trends on the plots of *McKay et al.* (1977) is the ratio of poikilitic rocks to metamorphosed breccias. In order for the petrographic mixing trends to be apparent on compositional plots, these two components must be (1) volumetrically significant constituents of the soil and (2) compositionally distinct. The triangular (normalized) plots of *McKay et al.* (1977) obscure the fact that the only significant difference between the soils at 20 cm and 58 cm depth is that the soil at 20 cm depth contains a higher concentration of "poikilitic rocks"; concentrations of the other two components are nearly the same in the two mafic soils. The difference of 15.6% in the concentration of poikilitic rocks between the two mafic soils is small compared with the range of 11% to 74% in the concentration of "plagioclase single crystals" between the mafic soils (Sc-rich) and the feldspathic (Sc-poor) soils. Thus, the volumetric importance of the petrographic difference between the 20-cm soil and the 58-cm soil is not as great as the volumetric importance of the difference in plagioclase concentration of these two soils and the 54-cm soils. Only if the "metamorphosed breccia" and the "poikilitic rocks" components were significantly different in composition would we expect to see a compositional difference.

The >1-mm particles were studied in large part to associate chemical compositions with the poikilitic rocks and metamorphosed breccia components of *McKay et al.* (1976, 1977). All the particles with poikilitic textures are impact-melt breccias with relatively high Sc concentrations and Sm concentrations exceeding 10 μg/g (Fig. 5). Rocks such as this are common at Apollo 16 (*Vaniman and Papike,* 1980) and are a major carrier of Sc and the principal carrier of ITEs such as Sm in the soil; no other common Apollo 16 lithologies are richer in Sc or ITEs or have a higher Sm/Sc ratio. Thus, the compositional fingerprint of the relative enrichment of the soil

at 20 cm depth in "poikilitic rocks" is that the seven samples from this zone tend to plot on the high-Sm side of the mixing line (Fig. 4), but only slightly.

The three samples of <1-mm fines from 58 cm depth plot on the low-Sm side of the mixing line at a relatively high Sc concentration in Fig. 4. This suggests that the "metamorphosed breccia" component is a relatively mafic (e.g., noritic anorthosite) but Sm-poor lithology. Two of the >1-mm particles from 58 cm depth (58-D and 58-G, Table A2) are granulitic (granoblastic) breccias that would probably fall in the "metamorphosed breccia" category of *McKay et al.* (1976). Both are poor in Sm (<1 μg/g) but have moderate Sc concentrations (6-7 μg/g). (These are the two squares in the "FrBx & GrBx" field of Fig. 5.) Thus, I suspect that many of the "metamorphosed breccia" fragments reported by *McKay et al.* (1976, 1977) are Sm-poor lithologies. However, among the >1-mm particles studied here are a few Sm-rich particles that are impact-melt breccias with recrystallized textures that may also have been classified as "metamorphosed breccias" in the scheme of *McKay et al.* (1976, 1977; also *Vaniman et al.,* 1978). Thus, a unique composition for the "metamorphosed breccia" component of *McKay et al.* (1977) cannot be unambiguously assigned.

In summary, most of the compositional variations in the 60009/10 soils result from varying proportions of an anorthosite containing a very high percentage of plagioclase feldspar (~99%) and more mafic soil, the Cayley soil component. The mafic subcomponents of the Cayley soil component are generally fine grained and reasonably well mixed, but vary slightly in proportion with depth in the core. This variation is small compared with the large variation in the fraction of modal plagioclase among the samples, but it causes most of the scatter about the mixing line in Fig. 4. Variation in average plagioclase composition also causes some of the scatter for "plagiophile" elements in plots such as those in Fig. 6. Considering the wide variation in the composition of the constituent particles of the soils (Fig. 5), the trends of Figs. 4 and 6 are strong evidence that the more mafic components of the soil were well mixed prior to admixture of the anorthosite component.

4.3. Magnetic Fractions and "Ancient" Fe-Ni Metal

I diverge here to discuss a once-popular topic that a review of early literature on 60009/10 reveals was abandoned, but never completely resolved—that of magnetic fractions of lunar soils. Magnetic separates are typically enriched in Fe (expected) as well as Sc, Cr, and ITEs (not necessarily expected) compared with nonmagnetic fractions (*Rhodes et al.,* 1975; *Blanchard et al.,* 1976). *Rhodes et al.* (1975) argued that magnetic separates are enriched in agglutinates (below) and that the compositional differences between magnetic and nonmagnetic fractions resulted from some chemical fractionation process that occurred during the formation of agglutinates. This idea fell from favor when electron microprobe studies showed little difference in composition between the glassy matrix of agglutinates and the soils in which the agglutinates occurred (*Gibbons et al.,* 1976; *Hu and Taylor,* 1977). However, the observation that magnetic fractions contained higher concentrations of nonferromagnetic elements was never satisfactorily explained, although *Via and Taylor* (1976) noted that magnetic fractions contained "magnetic nonagglutinates consisting of glass-free microbreccias with 30-60 μm native FeNi grains." As magnetic separation techniques may be used in the future to separate metal from lunar soils at a lunar base, I reexamine this issue in this section. The discussion also introduces the subject of "ancient" Fe-Ni metal, which is important in a subsequent discussion.

4.3.1. Agglutinates and single-domain iron. Agglutinates are small glassy-matrix particles containing mineral and lithic clasts and are believed to be produced at the surface of the regolith by melting of fines during micrometeorite impact (*McKay et al.,* 1974; *Papike et al.,* 1981; *McKay and Wentworth,* 1990). The fraction of agglutinates (Table 2) is a measure of the maturity (duration and extent of surface exposure) of a soil (*McKay et al.,* 1974). Agglutinates contain fine-grained (<30 nm) particles of nearly pure, single-domain Fe metal that is produced by exposure-related reduction (micrometeorite impact or solar-wind protons) of Fe(II) in iron silicates (*Housley et al.,* 1974; *Morris,* 1976, 1980). The parameter I_s/FeO, which is a measure of the amount of single-domain iron normalized to total iron concentration (*Morris,* 1976), increases with surface exposure. *Rhodes et al.* (1975) used magnetic separation to obtain "agglutinate fractions" of several lunar soils. These "agglutinate fractions" were, more precisely, magnetic fractions containing agglutinate particles.

Blanchard et al. (1976) analyzed both "magnetic fractions" and "nonmagnetic fractions" in their study of 60009. They never explicitly declared their purpose in studying the fractions, but in their modeling they implied a relationship between the proportion of "magnetic fraction" and soil maturity. The magnetic fractions were considerably enriched in Ni and Co compared with the nonmagnetic fractions, as they were in the study of *Rhodes et al.* (1975). If the metal in magnetic fractions is derived only from the reduction of Fe silicates, an enrichment of Ni and Co would be unexpected because the metal produced in this manner is nearly pure Fe (*Morris et al.,* 1975). However, as shown below, much of the metal in the magnetic separates is Fe-Ni metal of meteoritic derivation.

4.3.2. "Ancient" Fe-Ni metal. Iron-nickel metal alloys are a common component of Apollo 16 soils. This metal is generally believed to be of meteoritic origin, although most of it is considerably different in composition from metal in ordinary chondrites. A common composition, particularly at Apollo 16, is metal containing ~6% Ni (H, L, and LL chondrites: 8-30%) with a Ni/Co ratio 15.5 ± 3 (most chondrites: 21 ± 2) and a Au/Ir ratio as high as 1.0 (chondrites: ~0.3) (*Korotev,* 1987b; *Anders et al.,* 1973; *Wlotzka et al.,* 1973; *Goldstein and Axon,* 1973). Metal of identical composition is prevalent (up to 1-2%) in mafic impact-melt breccias from Apollo 16 (*Korotev,* 1987b,c, 1990a). These breccias were formed 3.8-3.9 Ga ago during formation of the major lunar basins. Much of the Fe-Ni metal in the soil is contained in fragments of these ancient melt breccias. For example, the Sm-rich (>10 μg/g), impact-melt breccias among the >1-mm particles (Fig. 5a) have a high average Ni concentration, 710 μg/g (Table A2), which corresponds to about 1% Fe-Ni

metal (*Korotev,* 1987c). However, some Fe-Ni metal in the soil is also found as free grains (e.g., section 3.1.5) that were either formed directly as molten droplets at the time of the ancient impacts (*Goldstein et al.,* 1975) or released from the breccias by subsequent impacts.

The soils also contain a meteoritic component from more recent crater-forming impacts (*Anders et al.,* 1973), some of which may also be Fe-Ni metal. For example, there are many samples of glass "impact-melt splashes" from Apollo 16 that are believed to have formed during the South Ray Crater impact (Fig. 1), about 2 Ma ago (*Morris et al.,* 1986). The Au/Ir ratios of these glasses are chondritic (*Ganapathy et al.,* 1974) and the Ni/Fe^0 ratio in many of these samples is ~0.4, consistent with an LL chondrite (*Morris et al.,* 1986,) but inconsistent with Fe-Ni metal found in the melt breccias ($Ni/Fe^0 = 0.06$).

To distinguish it from metal that may derive from more recent crater-forming impacts, I will refer to Fe-Ni metal such as that found in ancient melt rocks as the "ancient" Fe-Ni metal component. I use the term "ancient" because this metal has been a component of the regolith longer than metal from meteorites causing local craters. Also, it is the carrier of the siderophile-element signatures of those "ancient meteorite groups" of *Hertogen et al.* (1977) that are characteristic of Apollo 16 (*Korotev,* 1987b,c).

4.3.3. Correlation of nonferromagnetic elements with ancient Fe-Ni metal. Nickel and Co concentrations indicate that a large portion of the metal in the magnetic separates of *Blanchard et al.* (1976) is ancient Fe-Ni metal. For the 90-150-μm grain-size fractions, the ratio of the difference between the Ni concentrations in the magnetic and nonmagnetic fractions to the corresponding difference for Co averages 15.1 for the five samples analyzed. Thus, the "excess" Ni and Co in the magnetic fractions compared with the nonmagnetic fractions is consistent with ancient Fe-Ni metal, but not with metal from ordinary chondrites. As expected, the magnetic fractions also have higher concentrations of Fe than the nonmagnetic fractions (total Fe reported as FeO). If the excess Ni in the magnetic fractions is carried by Fe-Ni metal containing 6% Ni, then on the average about half the excess Fe in the 90-150-μm grain-size fractions results from Fe-Ni metal and the other half from exposure-related reduction of Fe^{2+}. For the <20-μm grain-size fractions, the magnetic fractions are also enriched in Fe, Ni, and Co, but the Ni/Co ratio of the excess averages 18.5, more nearly the chondritic ratio. The <20-μm fractions probably contain both ancient Fe-Ni metal (Ni/Co = 15.5) and a chondritic meteorite component (Ni/Co = 21). *Blanchard et al.* (1976) acknowledge that the Ni/Co ratios of the <20-μm material were more nearly "meteoritic," but mention only that the 90-150-μm fraction requires a different kind of Ni-rich material (i.e., lower Ni/Co, as in ancient Fe-Ni metal).

Thus, magnetic separates of Apollo 16 soil preferentially contain metal-bearing fragments of mafic, ITE-rich, impact-melt breccias as well as free Fe-Ni metal. This is the reason magnetic separates of Apollo 16 soils are enriched in ITEs and elements associated with ferromagnesian minerals at the expense of elements associated with plagioclase in the data of *Rhodes et al.* (1975) and *Blanchard et al.* (1976). The physical association of Fe-Ni metal with the most mafic and ITE-rich components of the soil leads to correlations among siderophile elements, ITEs, and elements associated with mafic mineral phases (*Korotev,* 1990a). Correlations such as these would not be expected to result from igneous differentiation processes.

The effect of meteoritic material on the siderophile elements can be seen in Fig. 8. Four components are represented in the plots: (1) ferroan anorthosite with effectively zero concentrations of all four elements, (2) mafic silicates that contain appreciable concentrations of Co as well as Fe and Sc, but little Ni, (3) ancient Fe-Ni-Co metal, and (4) chondrites. Soil samples with greater than ~30 μg/g Co (Fig. 8a) are usually submature to mature. They contain a large proportion of Cayley soil component and thus derive a high proportion of their mafic silicates from ancient melt breccias of which they are in part composed. They also contain both a chondritic component from accumulation of micrometeorite material and debris from occasional impacts of larger ordinary chondrites (e.g., South Ray Crater; section 4.3.2), and an ancient Fe-Ni metal component from the melt breccias (*Korotev,* 1987b). Addition of ferroan anorthosite, such as for the anorthositic soils from 60009, simply dilutes the concentrations of all four elements in Fig. 8. Thus, although four components are represented in the plots, linear trends occur because both the Ni-rich components are associated with the Cayley soil component and not with the anorthosite component.

As a result of large metal grains that occur infrequently, samples with anomalously high concentrations of Ni and Co deviate from the main cluster of points along a trajectory more consistent with an Fe-Ni metal component than a chondritic component (Fig. 8a). These same samples are enriched in Fe to such an extent that a significant fraction of the total Fe in the sample is of meteoritic origin (Fig. 8b). On the Fe-Sc plot, the main trend of the data is simply the anorthosite mixing trend discussed above; the deviations from this trend in the high-Fe direction result from grains of Fe-Ni metal or other meteoritic material (*Haskin et al.,* 1973). The unreliability of the total Fe concentration as an indicator of the mafic silicate concentration is why I choose to plot the trace element Sc instead of the major element Fe on plots such as Figs. 4 and 6.

4.4. Mixing Model

To demonstrate the mixing concepts discussed above, I have modeled the <1-mm fines from 60009/10 as mixtures of two primary components, an anorthosite component and the "Cayley soil component." I have also included three minor components to account for siderophile elements and deviations from the mixing line. The compositions of the components are listed in Table 3. Below, I describe how those compositions were obtained and discuss the model results.

4.4.1. Model components. Because the anorthosite component of the 60009/10 soils is ~99% plagioclase and indistinguishable in composition from the plagioclase particles separated from the >1-mm grain-size fraction (section 4), I use the mean composition of seven plagioclase particles for the anorthosite component of the model. These include the six plagioclase particles discussed above (sections 3.2 and 4.1.1) and particle 2.25 from 60002 (section 5.2.4). For elements with concentrations below detection limits (e.g., Au), concentration values were assumed.

A composition to represent the Cayley soil component is not so directly obtained because none of the analyzed >1-mm particles represents the Cayley soil component. One of the <1-mm fines samples from 18-21 cm depth that plots at the extreme end of the mixing line could be used to represent this component. However, these samples were each radioassayed only once (section 2.2), and for a mixing model component, a more precisely known composition is preferable. Thus, the mean composition of the six replicate samples of 60601 (Table A6; each was radioassayed several times) serves as a starting point for establishing a composition for the Cayley soil component. Soil 60601 plots very near the mixing lines of Figs. 4 and 6 (not shown), but it does not plot at the extreme high-Sc end, i.e., it contains a small component of anorthosite. Thus, for the purpose of the model, I define the Cayley soil component as that composition that, when mixed in seven parts with one part of the anorthosite component, yields the mean composition of 60601. The choice of these proportions was somewhat arbitrary, but they were selected such that the Sc concentration of the Cayley soil component ("+" on Fig. 4) is just slightly greater than the most Sc-rich soil sample; there is no particular necessity that the proportions be integer values.

Variation in the ratio of the anorthosite component to the Cayley soil component accounts for most of the variation in lithophile-element concentrations in the soils, but does not account for the siderophile-element variations. Most mixing models for lunar soils contain a component of carbonaceous chondrite to account for "extralunar" siderophile elements derived from the continuous flux of micrometeorites striking the surface (e.g., *Boynton et al.,* 1975, 1976; *Morris et al.,* 1989), and this is usually adequate for soils from mare sites. However, as discussed in section 4.3, a significant fraction of the siderophile elements in Apollo 16 soils is not derived from micrometeorites, but is carried by ancient Fe-Ni metal associated with the mafic impact-melt breccias formed 3.9 Ga ago. For example, in a typical submature to mature (Cayley) soil from Apollo 16, 50% of the Ni is carried by the carbonaceous chondrite component and 50% by the ancient Fe-Ni metal component (*Korotev,* 1987b). Thus, I include two meteorite components in the model. One, designated the CI component, represents both carbonaceous chondrites (primarily micrometeorites) as well as debris from larger, ordinary chondrites (*Anders et al.,* 1973; *Morris et al.,* 1986). The other, the ancient Fe-Ni metal component, represents the metal associated with mafic impact-melt breccias. For the CI component, the composition used is the "mean C1 chondrite" composition of *Anders and Grevesse* (1989), but with all concentration values multiplied by 1.36 to convert to a volatile-free basis. For the Fe-Ni component, I use the average composition of metal separates from three Apollo 16 impact-melt breccias (*Korotev,* 1990a).

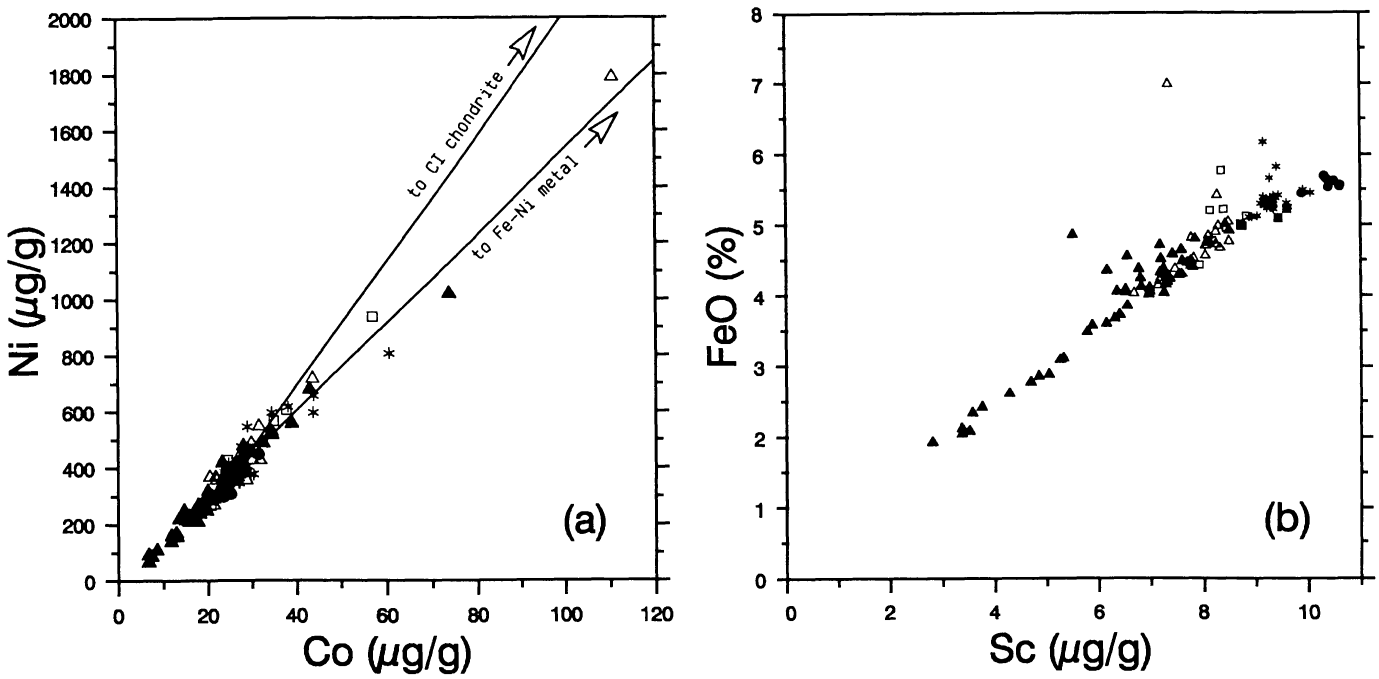

Fig. 8. Variation in Ni and Co concentrations and FeO and Sc concentrations in <1-mm fines from 60009/10; the symbol key is the same as in Figs. 3-6. **(a)** The lines indicate the effect of adding carbonaceous (CI) chondrites (Ni/Co = 21; the Ni/Co ratio of ordinary chondrites is essentially the same) or "ancient" Fe-Ni metal such as found in Apollo 16 mafic impact-melt breccias (Ni/Co = 16) to the average composition of the 60009/10 soils. Typical submature to mature Apollo 16 soil (32 μg/g Co, 460 μg/g Ni) receives about half its Ni from each of these two sources (*Korotev,* 1987b). For the <1-mm fines, the low-Ni part of the linear trend is caused mainly by the dilution effect of plagioclase in these plagioclase-rich soils (36-57 cm depth; Fig. 4); the high-Ni part of the trend is caused primarily by the variation in the amount of Fe-Ni metal. **(b)** FeO should correlate well with Sc if iron were carried only by mafic silicates, but Ni-rich samples contain excess Fe (total Fe as FeO). For these samples, a large fraction of the total iron is carried by Fe-Ni metal.

TABLE 3. Compositions of mixing model components.

	Unit	Weight Factor	Cayley Soil	Anor-thosite	CI	Ancient Fe-Ni	Mare Basalt	Sodic Plag.	Impact Melt
Na_2O	%	2	0.468	0.368	0.917		0.500	1.05	0.522
CaO	%	3	15.3	18.9	1.77		10.5	17.7	13.9
Sc	μg/g	2	10.79	0.34	7.92		82.9	0.78	10.8
Cr	μg/g	2	856.	10.	3618.		2184.	21.	970.
FeO	%	2	5.30	0.23	33.31	120.7	20.2	0.87	6.42
Co	μg/g	2	9.3	0.4	683.	3600.	27.3	0.9	29.1
Ni	μg/g	5	48.	1.	14960.	57800.	2.0	1.	412.
Sr	μg/g	5	181.	170.	10.6		170.	342.	160.
Zr	μg/g	10	218.	0.3	5.4		435.	5.	380.
Ba	μg/g	4	167.	7.0	3.2		310.	52.	262.
La	μg/g	2	14.86	0.15	0.319		26.9	2.05	27.4
Sm	μg/g	2	6.90	0.058	0.200		20.9	0.547	12.3
Eu	μg/g	2	1.273	0.810	0.076		2.29	2.225	1.43
Tb	μg/g	4	1.36	0.01	0.049		4.6	0.08	2.46
Yb	μg/g	2	4.88	0.02	0.221		16.9	0.22	8.46
Lu	μg/g	2	0.677	0.003	0.033		2.46	0.026	1.17
Hf	μg/g	2	5.23	0.04	0.141		15.6	0.14	9.18
Ta	μg/g	5	0.62	0.006	0.019		2.5	0.02	1.09
Ir	ng/g	5	0.	0.	654.	1380.	0.	0.001	9.
Au	ng/g	5	0.	0.	190.	1315.	0.	0.001	8.
Th	μg/g	3	2.53	0.01	0.040		2.6	0.05	4.52
U	μg/g	5	0.66	0.003	0.011		0.50	0.01	1.22

Weight factor: Approximate analytical uncertainty of soil concentrations in percent (*Boynton et al.,* 1975).
Cayley soil: Based on 60601 (Table A6), see text.
Anorthosite: Ferroan anorthosite containing ~99% plagioclase: mean of particles 20-L, 20-M, 54-G, 54-H, 54-I, and 58-I from 60009/10 (Table A2) and 2.25 from 60002 (Table A5).
CI: Volatile-free CI chondrite: values of *Anders and Grevesse* (1989) times 1.36.
Ancient Fe-Ni: Fe-Ni metal from ancient impact melt breccias: mean of three from *Korotev* (1990a).
Mare basalt: Apollo 11 high-K basalt: mean from *Beatty et al.* (1979).
Sodic plag.: An_{90-91} plagioclase from 60002: mean of particles 2.13 and 2.31 (Table A5); used to model MPU-A soils only.
Impact melt: ITE-rich mafic impact melt breccias: mean of particles 1.05, 1.06, 2.24, and 2.32 from 60001 and 60002 (Tables A4 and A5); used to model MPU-A soils only.

The need for two meteoritic components can be seen in the Au/Ir ratio profile of Fig. 2. The Au/Ir ratio of carbonaceous and most ordinary chondrites is 0.3, whereas the Au/Ir ratio of Fe-Ni metal in the ancient impact-melt breccias from Apollo 16 is usually greater, with values of about 1.0 being common ("ancient meteorite groups" 1H and 1L of *Hertogen et al.,* 1977; *Korotev,* 1990a). Ratios for the soils are intermediate; thus, the model's selectivity for the two meteorite components results mainly from accounting for the Au/Ir ratio of the soil (and, to a lesser extent, the Ni/Co ratio). Because soil sample 60601 contains both meteorite components, the composition of the Cayley soil component was further modified by algebraically removing 1.08% CI component and 0.42% Fe-Ni metal component; these are the unique proportions that result in concentrations of zero for Au and Ir. Thus, the Cayley soil component, as used in the mixing model, is free of extralunar siderophile elements.

I have also included a mare basalt component in the model for the 60009/10 soils mainly for consistency with the modeling of the 60001-7 soils, which, as shown below, require a mare basalt component. The composition used is the mean composition of several fragments of Apollo 11 high-K basalt reported by *Beatty et al.* (1979). (Because the proportion of mare basalt is so low, the model is insensitive to exactly which type of mare basalt is used.) Like the anorthosite component and the two meteoritic components, soil 60601 probably contains a small fraction of mare-derived material and, for consistency, it would be appropriate also to remove this component from the composition of the Cayley soil component. However, unlike the other three components, there is no objective way to know how much mare basalt to remove. Thus, the model results for the mare basalt component represent mare basalt in *excess* of any that may be present in the Cayley soil component.

4.4.2. Model calculations and results. I have modeled the concentrations of all 20 elements in each of the 121 samples of <1-mm fines from 60009/10 with a multielement, weighted, least-squares mass-balance model such as that described by *Boynton et al.* (1975). Table 4 summarizes the results for the mean composition of the 121 samples. The best fit composition ("calc.") agrees very well with the observed mean composition ("obs."). (The agreement for individual samples is not always this good, however.) The percentages of the five model components that best fit the mean core

TABLE 4. Mixing model results for average core soils.

		60009/10		60001-7			
		All		MPU-(B,C,D)		MPU-A	
		Obs.	Calc.	Obs.	Calc.	Obs.	Calc.
Na_2O	%	0.448	0.444	0.456	0.458	*0.506*	*0.485*
CaO	%	16.1	16.1	15.4	15.4	15.2	15.2
Sc	μg/g	7.82	7.80	9.69	9.69	9.80	9.76
Cr	μg/g	639.	654.	786.	792.	812.	801.
FeO	%	4.61	4.63	5.51	5.56	5.43	5.47
Co	μg/g	26.5	26.9	31.2	31.4	25.9	26.0
Ni	μg/g	394.	399.	457.	470.	343.	368.
Sr	μg/g	n.a.	n.a.	177.	176.	179.	181.
Zr	μg/g	n.a.	n.a.	196.	188.	247.	208.
Ba	μg/g	119.	122.	141.	145.	157.	158.
La	μg/g	10.80	10.73	12.90	12.85	14.25	14.35
Sm	μg/g	5.01	4.96	6.05	6.00	6.58	6.69
Eu	μg/g	1.12	1.13	1.20	1.20	*1.22*	*1.27*
Tb	μg/g	0.96	0.98	1.19	1.18	1.33	1.32
Yb	μg/g	3.54	3.50	4.25	4.25	4.68	4.67
Lu	μg/g	0.485	0.485	0.589	0.590	0.639	0.648
Hf	μg/g	3.82	3.76	4.60	4.54	5.18	5.02
Ta	μg/g	0.43	0.44	0.53	0.54	0.602	0.594
Ir	ng/g	12.3	11.7	14.8*	14.3	11.0	10.8
Au	ng/g	7.2	6.8	8.0*	7.7	6.6	6.2
Th	μg/g	1.86	1.83	2.18	2.18	2.40	2.41
U	μg/g	0.46	0.48	0.56	0.57	0.62	0.63
Components (%)							
Cayley soil		72.3 ± 0.8		85.7 ± 0.6		76.8 ± 6.0	
Anorthosite		26.5 ± 1.3		11.7 ± 0.8		7.0 ± 4.9	
CI		1.03 ± 0.10		1.37 ± 0.07		0.95 ± 0.15	
Ancient Fe-Ni		0.36 ± 0.02		0.39 ± 0.02		0.26 ± 0.04	
Mare basalt		-0.2 ± 0.2		0.36 ± 0.16		3.2 ± 5.5	
Sodic plag.		n.u.	n.u.	n.u.	n.u.	3.6 ± 2.0	
Impact melt		n.u.	n.u.	n.u.	n.u.	9.5 ± 1.5	

*Excludes all samples with >20 ng/g Au.

n.a. = not analyzed.
n.u. = not used in model.

composition are also listed in Table 4. Note that the concentrations of the two meteorite components, 1.03% CI and 0.36% Fe-Ni, are nearly the same as the concentrations removed from the Cayley soil component (above); this is a necessary consequence of the fact that the mean siderophile-element concentrations in 60601 (Table A6) are similar to those of the average 60009/10 soil. Note also that the concentration of the mare basalt component is zero, within model uncertainty, for the average soil (-0.2 ± 0.2%). The proportion of mare basalt component predicted by the model depends primarily on the concentration ratio of other elements to Sc (e.g., Sm/Sc, Fe/Sc). Because the mixing line of Fig. 4 passes just slightly to the low-Sc side of the point for the Cayley soil component, the average soil (which, of course, plots on the mixing line) is modeled as having a very slightly negative component of mare basalt (-0.2%).

Depth profiles for the proportions of the five components as predicted by the model are plotted in Fig. 9. As expected, the shape of the Cayley soil profile is the same as that of the Sc and Sm profiles of Fig. 2. The model predicts about 73% anorthosite component for the most anorthositic soils, those at 54 cm depth. This is almost exactly the fraction of plagioclase single crystals observed petrographically in this soil (73.8%, Table 2). The CI chondrite component varies between about 0% and 2% with a peak at about 13-15 cm depth and a minimum in the vicinity of the anorthosite maximum. The concentration of Fe-Ni metal component is highly variable from sample to sample and shows no systematic variation with depth.

The concentration of mare basalt component fluctuates unsystematically about zero. It is important to note that mare basalt is the only component included in the model that can account for deviations from the binary mixing lines of Figs. 4 and 6. The most compositionally distinct aspect of the mare basalt component is its very high concentration of Sc (and, to a lesser extent, Fe and Cr). Thus, any sample plotting on the high-Sc side of the mixing line of Fig. 4 is interpreted by the model as having a positive component of mare basalt. For example, the model predicts about 1% mare basalt component for samples at 58 cm depth. A component of mare basalt usually lowers the La/Sm ratio as well as the Sm/Sc ratio, and the La/Sm ratio is remarkably constant among the 60009/10 soils, including those from 58 cm depth (Fig. 2). Although the 58-cm samples may actually contain a small component of

mare basalt, the actual cause of the low Sm/Sc ratio is more probably a component of "metamorphosed breccia" with a very low Sm/Sc ratio, not mare basalt (section 4.2.2). Thus, it is likely that the range of variation in the true concentration of mare basalt in the 60009/10 samples is less than that implied by Fig. 9.

5. 60001-7 RESULTS

5.1. <1-mm Fines

The deep drill core consisted of seven sections numbered consecutively from the bit (60001) to the topmost section (60007). A schematic cross section of the core indicating section numbers, penetration depths, and recovery information is given in Fig. 10. Unlike that for 60009/10, there is considerable uncertainty in the depth scale for 60001-7 (Fig. 11). For purposes of discussion of specific samples and for plotting data in the figures, I use the depth scale of *Allton et al.* (1981) and *Allton and Waltz* (1980), which assumes that the top of the lower half of the core (top of 60004) represents 102 cm depth and that the 60006/7 soils represent a continuous plug with the top of 60007 representing the lunar surface. I plot the 60005 samples at the depth at which they were recovered in the core tube, but recognize that this soil is greatly disturbed and assume that no stratigraphic information is preserved. In addition, I show below that the 60006 soils are also greatly disturbed and are discontinuous with the 60007 soils.

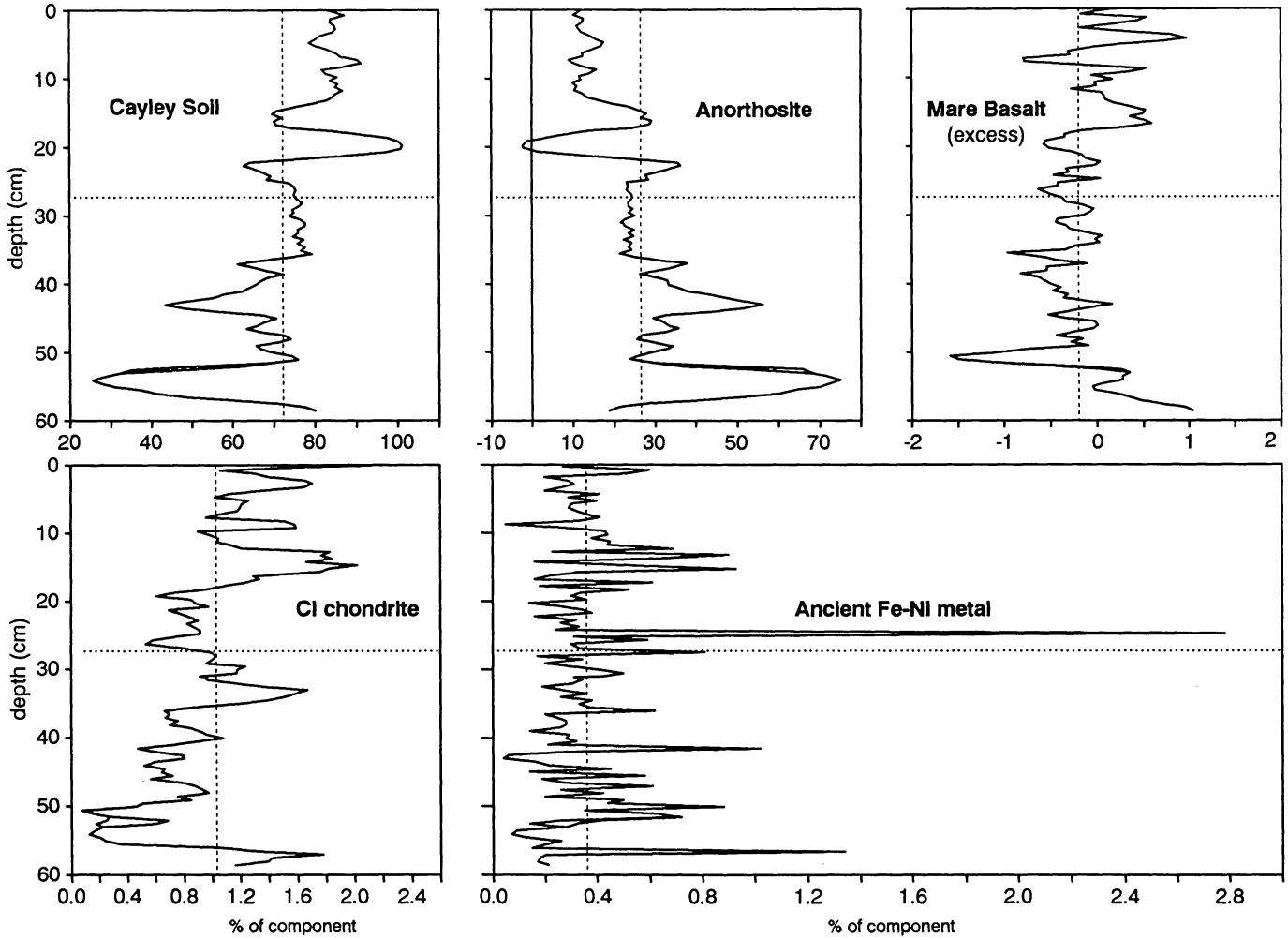

Fig. 9. Mixing-model results for <1-mm fines from 60009/10. The five components are those of Table 3. The horizontal line represents the results for the mean core composition. For clarity, the results for each component except the ancient Fe-Ni metal component have been subjected to a simple three-point smooth [(1+1+1)/3]. The mare basalt component represents any mare material in excess of that carried by the Cayley soil component (see text).

Analytical results for the <1-mm fines samples from the 60001-7 core are listed in Table A3. Depth profiles for several elements and element ratios are plotted in Fig. 12. Most of the 60001-7 soils plot along the Sc-Sm mixing line (and within the scatter about that line) defined by the 60009/10 soils

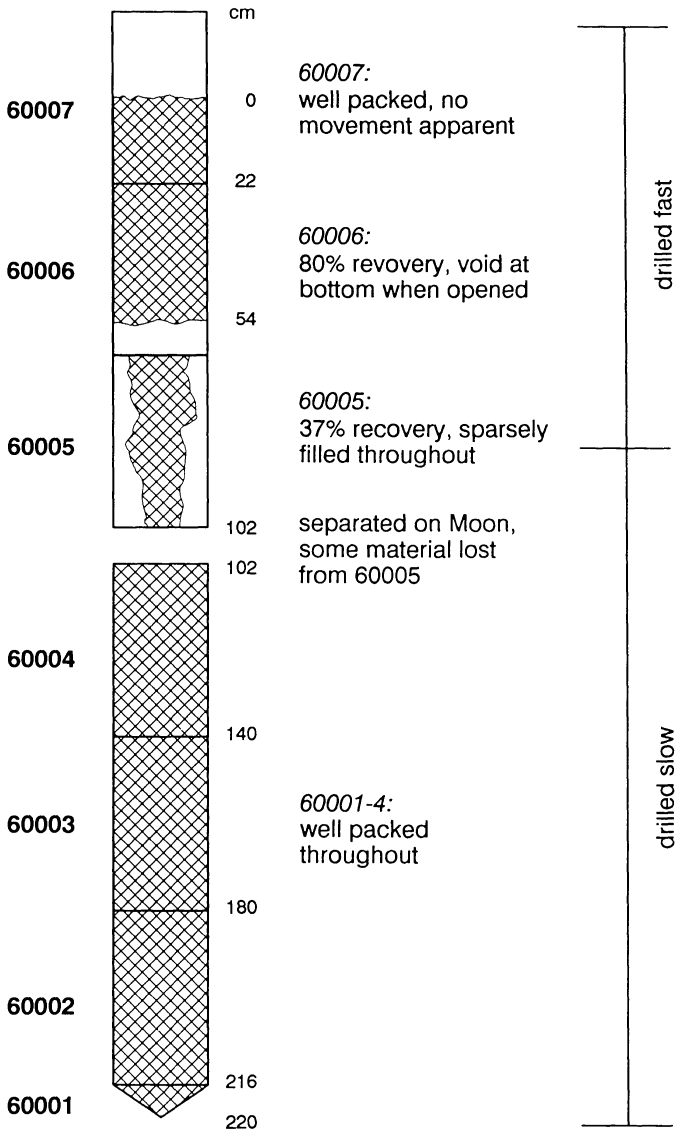

Fig. 10. Schematic cross section of deep drill core 60001-7 (based on *Allton and Waltz,* 1980). Because the entire 60001-7 drill string was 2.4 m long, it was separated into two halves for return to Earth. When the core was opened in Houston, the lower half (sections 60001-4) was completely filled with soil but the upper half (sections 60005-7) contained voids; the 60005 section contained only 37% of its capacity and the 60006 section was only 80% full. Discussions of the taking of the core and various scenarios for why the upper half is incompletely filled are provided by *Carrier* (1974), *Nagle et al.* (1975), *Duke and Nagle* (1976), and *Allton and Waltz* (1980). The favored scenario is that the lower half (60001-4) is not seriously disturbed and the upper half is incompletely filled as a result of (1) a very fast drill rate (2.5 cm/sec) for the first 80 cm and (2) spillage from the bottom of 60005 on the lunar surface after the halves were separated (*Allton and Waltz,* 1980).

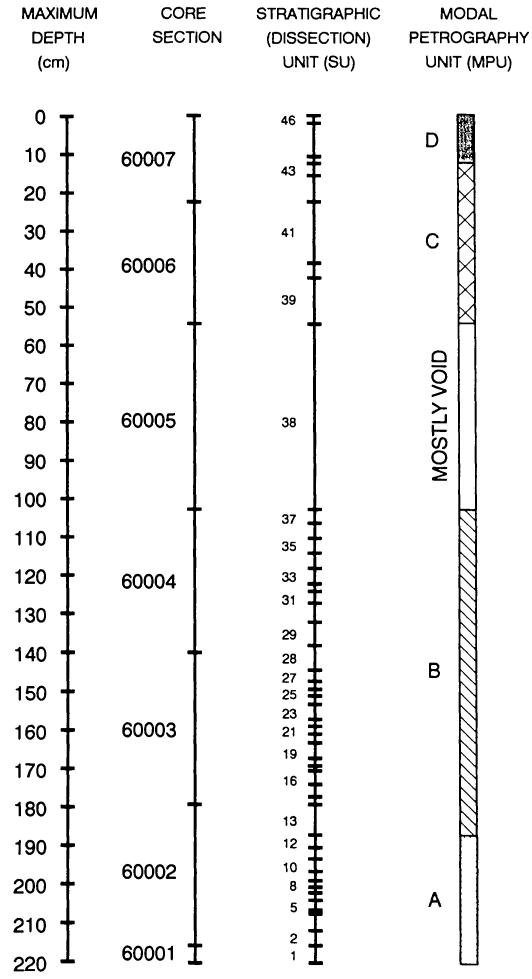

Fig. 11. Correlations of the maximum depth scale (*Allton et al.,* 1981), core tube numbers (6000X), stratigraphic units (SU) of *Duke and Nagle* (1976), and modal petrography units (MPU) of *Vaniman et al.* (1976) in 60001-7. The maximum depth scale of *Allton et al.* (1981) differs slightly from the preliminary maximum depth scale of *Duke and Nagle* (1976) that was used by most previous workers. Thus, statements in the text such as "... samples between 177 cm and 187 cm in depth ..." may not refer exactly to the same samples plotted within this depth interval in other work (e.g., *Gose and Morris,* 1977). However, Table A2 lists parent split numbers as well as the stratigraphic units (SU) of Duke and Nagle, which allow cross reference of data from this work with the work of others. The most important discrepancy of this type involves the location of the boundary between MPU-A and MPU-B. This boundary occurs between SU12 and SU13, which is at 189.7 cm maximum depth on the scale of Duke and Nagle but 186.8 cm depth on the scale of *Allton et al.* (1981). In their study of modal petrography based on the continuous thin sections, *Vaniman et al.* (1976) put the boundary between their MPU-D and MPU-C at about 9 cm; they do not give an exact value for the boundary because of gaps in the thin sections. *Gose and Morris* (1977) put the boundary between MPU-C and MPU-D boundary at 13 cm because they observed a discontinuity in their Fe concentration profile at this depth (see also *Heymann et al.,* 1978). In the high-resolution concentration profiles of Fig. 12, no sharp break occurs within 60007 for any element, only a gradual change with depth, thus there is no distinct compositional boundary between these units. For consistency with *Gose and Morris* (1977), the boundary between MPU-C and MPU-D is plotted at 13 cm depth in all figures.

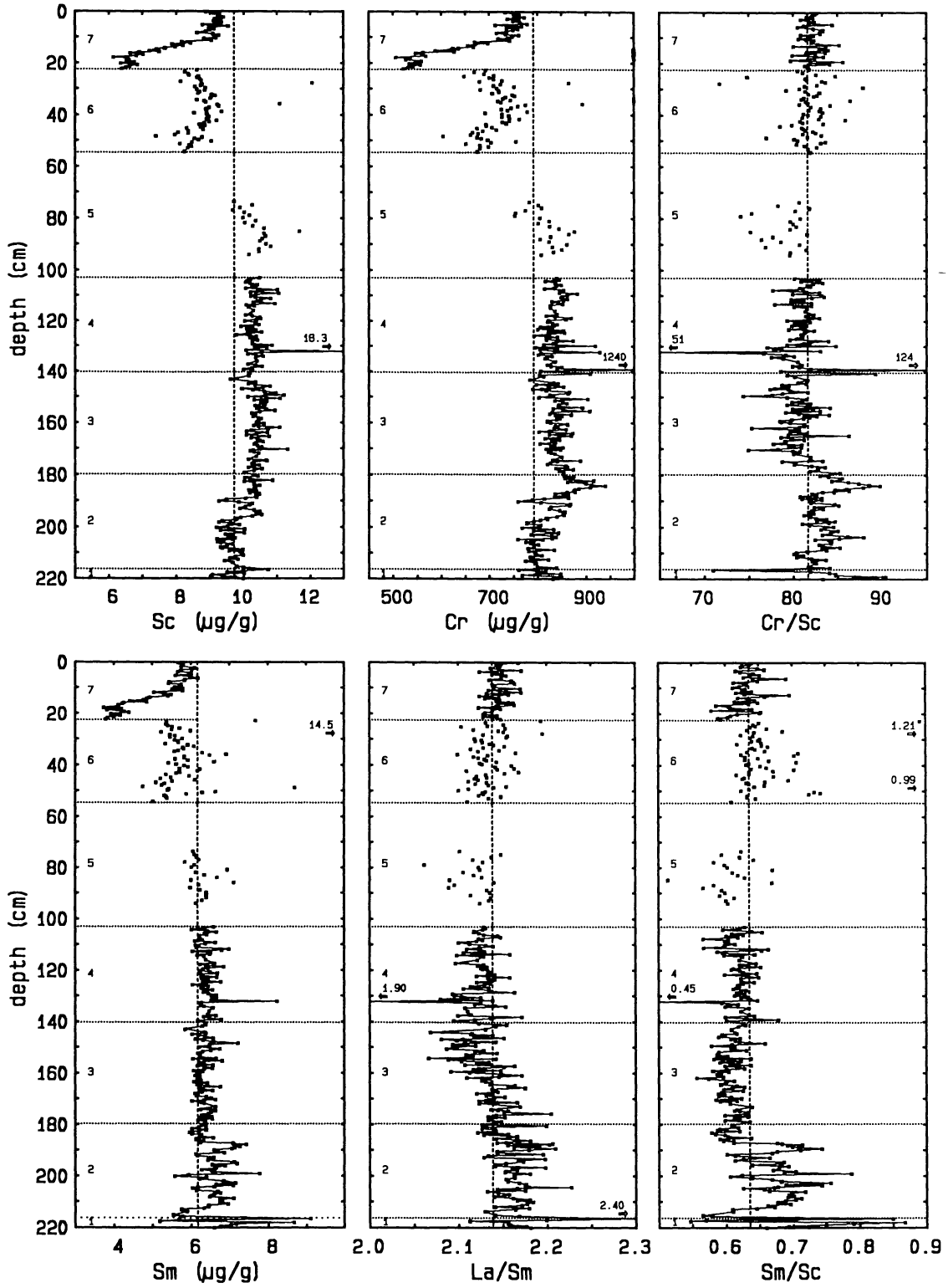

Fig. 12. Depth profiles of element concentrations and concentration ratios for <1-mm fines from 60001-7 [depth scale of *Allton et al.* (1981); data from Table A3]. Data for samples from 60005 and 60006 are plotted at the position at which they were found in the core tubes. These soils have been disturbed and mixed; the original stratigraphic positions are not known (Fig. 10). The horizontal dotted lines indicate the boundaries between core sections; the vertical dashed lines indicate the mean concentration or ratio of all 353 samples. Au, Ir, and Au/Ir data are plotted on a logarithmic scale.

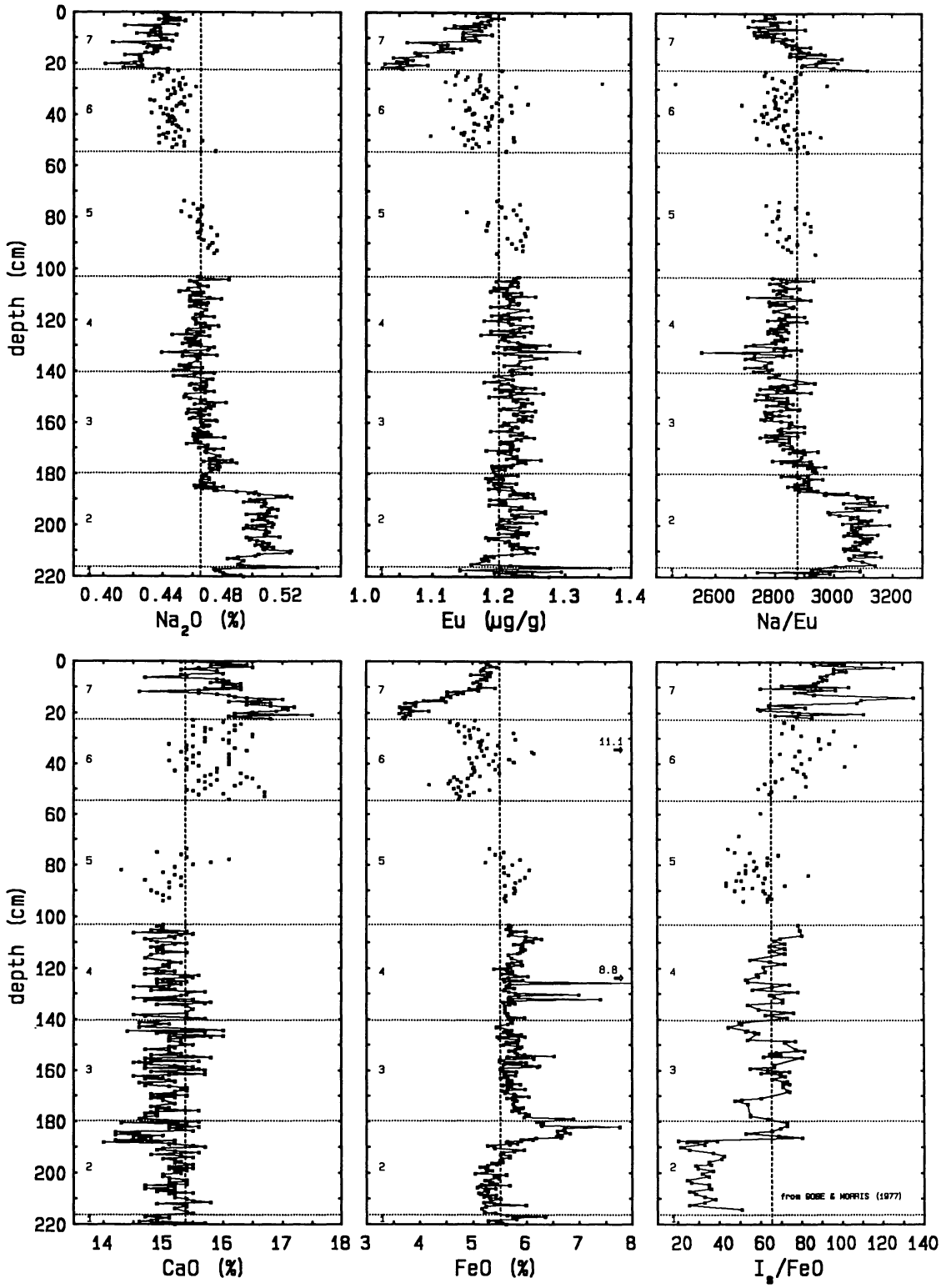

Fig. 12. (continued).

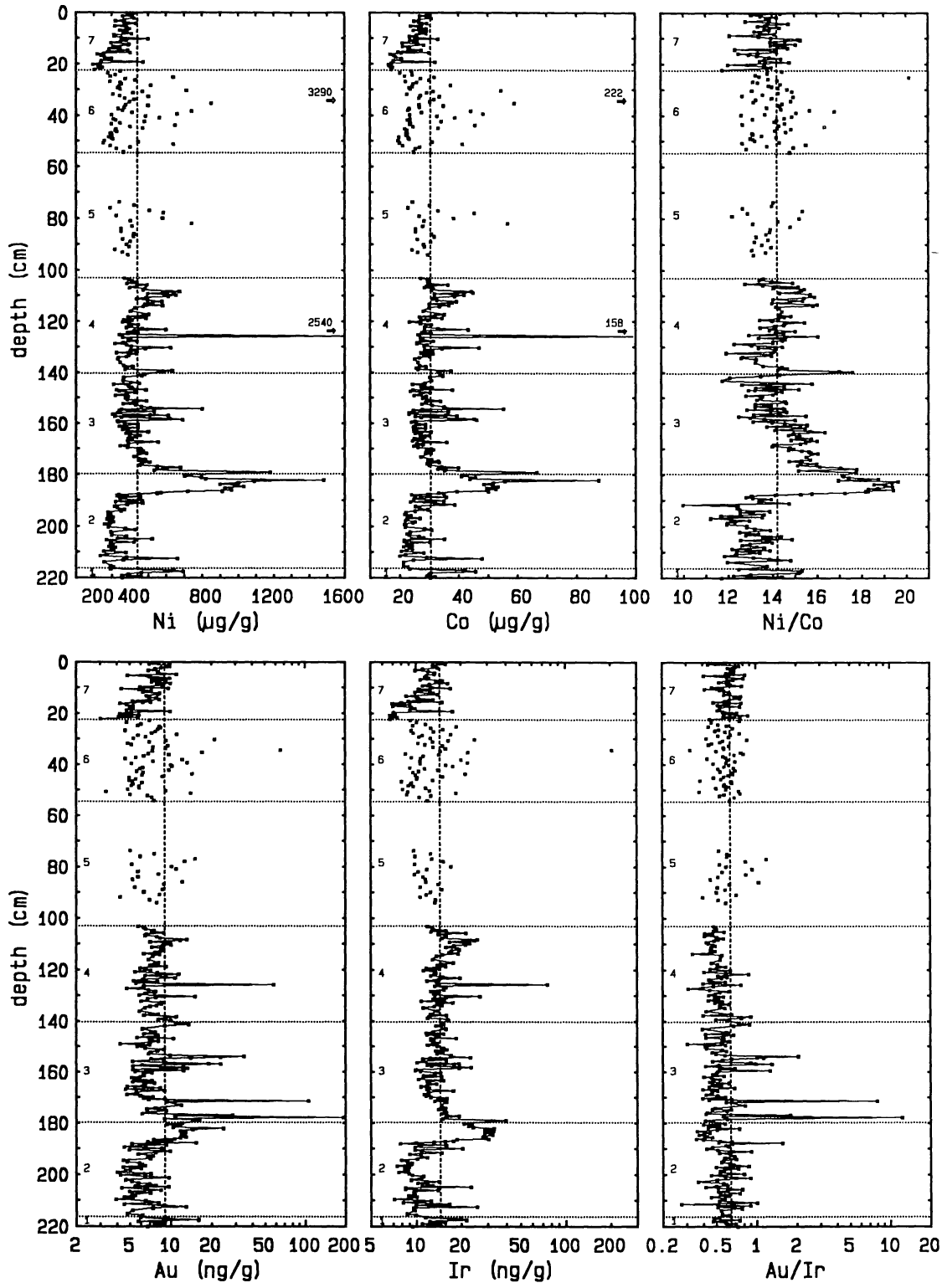

Fig. 12. (continued).

(Figs. 13 and 14), indicating that mixing between anorthosite containing about 99% plagioclase and the Cayley soil component dominates the compositional variation in lithophile elements in this core as well. However, some of the 60001-7 samples show deviations from the 60009/10 trend. Below, I discuss features of the profiles and deviations from the mixing trend, starting from the top and proceeding downward.

5.1.1. 60007 (MPU-C and MPU-D). Like the 60009/10 core, there is little variation in composition with depth for the first 10 cm. In this zone Sc and Sm concentrations average about 2% lower than for soils from the top of 60009/10. Most soils from the surface of Stations LM, 1, and 2 (Fig. 1) are indistinguishable from each other in composition (*Korotev,* 1981).

The largest compositional changes in the core occur just below the surface layer, in the 60007 section. Between about 10 cm and 17 cm depth the concentrations of all elements except Ca decrease systematically with depth while Ca concentrations increase. Between 17 cm depth and the bottom of the 60007 section at 22 cm depth, soil compositions remain relatively constant. The zone of greatest change in composition with depth (10-17 cm) corresponds to one of the two major stratigraphic boundaries recognized in previous studies of the core, that between MPU-D and MPU-C (MPU = modal petrography unit, Fig. 11).

The soils at the bottom of the 60007 section (MPU-C) are compositionally the most anorthositic soils in the core. By analogy with 60009/10 we would expect these soils to contain

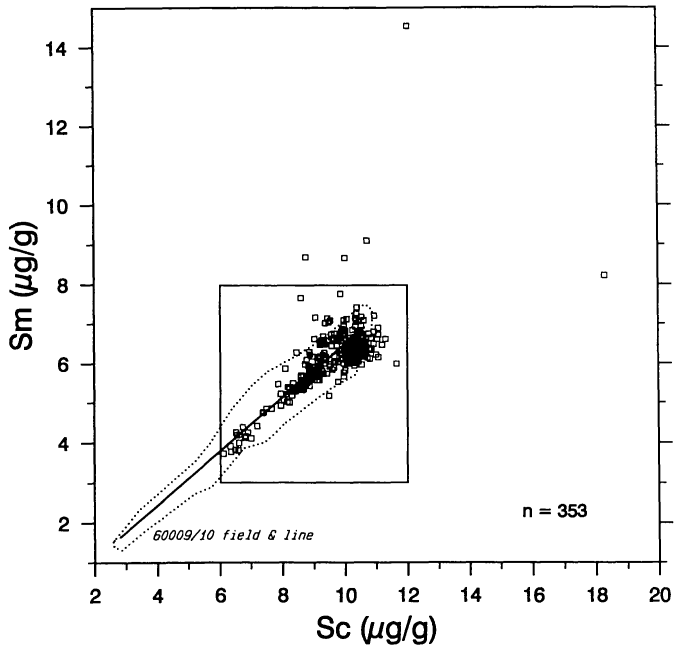

Fig. 13. Variation of Sm and Sc concentrations in <1-mm fines from 60001-7 (data from Table A3). The dotted field indicates the range of the 60009/10 data and solid line is the best fit to the 60009/10 data (from Fig. 4). The interior box indicates the area of Fig. 14.

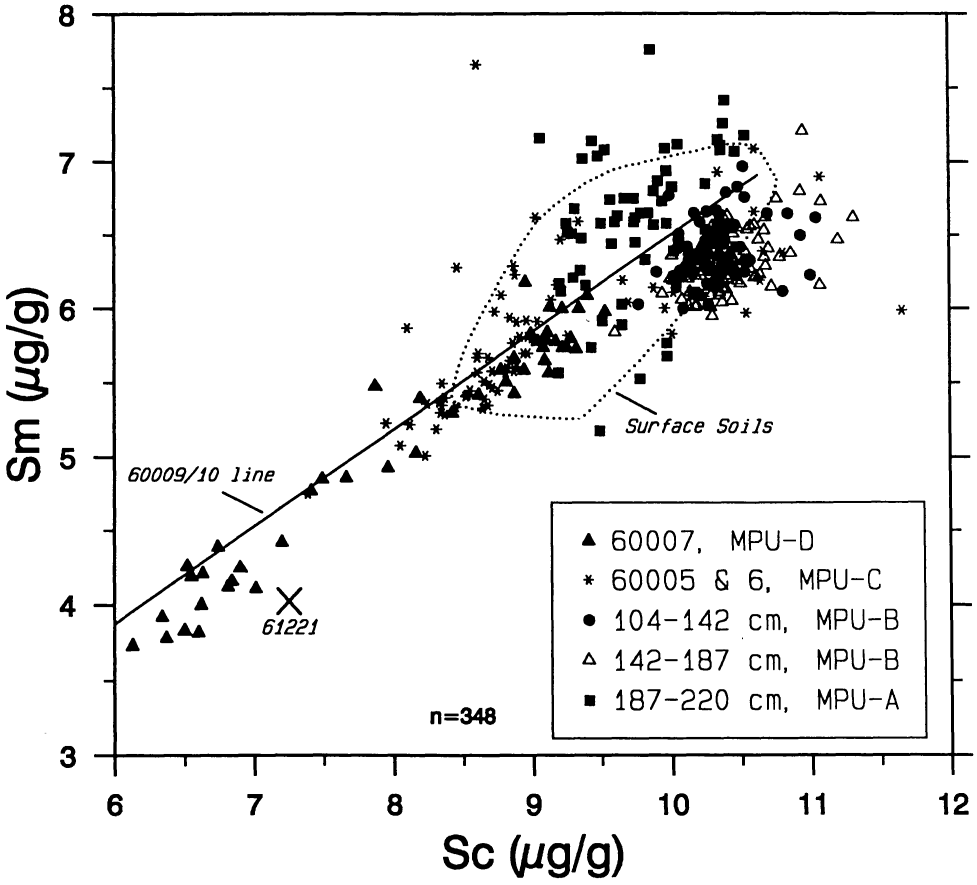

Fig. 14. Detail from Fig. 13, with samples keyed according to depth. Trench soil 61221 is the most anorthositic of Apollo 16 surface and trench soils (some soils from North Ray Crater are equivalently anorthositic; Table A7). The dotted field labeled "Surface Soils" encloses the range of Apollo 16 surface soil samples (6XXX1, n = 23) from all stations except those contaminated with ejecta from North Ray Crater (i.e., Stations 7 and 13). Also excluded are all trench soils (61221, 61241, and 64421) and some surface soils believed to have a component of subsurface ejecta from local craters (60051, 64501); some of these plot in the gap between the surface soils and 61221.

the greatest proportion of anorthosite, and that is indeed the case. Petrographically, MPU-C is distinguished by large, single plagioclase grains that are absent in MPU-D above it (*Nagle et al.,* 1975; *Vaniman et al.,* 1976).

5.1.2. 60006 disturbance. A sharp discontinuity occurs in most element profiles at the break between the 60007 section and the 60006 section of the core (Fig. 12). Within the 60006 section, ITEs and elements associated with mafic mineral phases (Sm and Sc) show a bow-shaped profile, increasing toward the middle of the section and then decreasing toward the bottom. Soil from the bottom of the 60006 core section is distinctly different from the average material in the 60005 section (Fig. 15), which was mostly void when opened and known to be highly disturbed (Fig. 10). The 60006 section was 20% void (Fig. 10). These data strongly suggest that as a result of the void space, routine handling of the 60006 section at JSC caused the contents to be partially mixed after it was separated from the 60007 and 60005 sections. *Duke and Nagle* (1976) and *Allton and Waltz* (1981) indicate that the void space in 60006 was at the bottom when processed, but sketches of the X-radiograph taken before the sections were disassembled clearly show voids at both the top and bottom (*Duke and Nagle,* 1976, Fig. 16-11). Thus, I am forced to conclude that most of the stratigraphic information in 60006 has been erased, but infer that the anorthosite-rich layer in 60007 continued into the region of the core sampled by the 60006 section and that contact between the bottom of the anorthositic layer and more mafic underlying soil (60004) has not been retained (Fig. 15).

Because of the disturbance in 60005 and 60006 and the rapid drilling rate during the first 80 cm (Fig. 11), it cannot be assumed that the stratigraphy of 60007 has been accurately preserved. In particular, what may be a sharp contact on the lunar surface may have been degraded into the gradual contact between MPU-C and MPU-D that appears in Figs. 12 and 15. If such degradation has occurred, it would affect some interpretations, such as those of *Gose and Morris* (1977).

5.1.3. 60004–60003 (MPU-B). There is no indication of disturbance in the lower half of the drill core. As others have noted, the compositions of samples from 60003 and 60004 (102-140 cm depth) are remarkably constant (*Gose and Morris,* 1977; *Ehmann et al.,* 1977). For most elements, the variation in the topmost 21 samples of 60004 is less than that in all 21 samples of 60005 (Table A6), which were presumably mixed and partially homogenized. This constancy, particularly when compared with large variations seen in 60009/10, might be cause to question (as did *Heymann et al.,* 1978) whether the rotary-percussion drill used to take 60001-7 was less effective at preserving stratigraphy than the drive tubes like 60009/10. However, lower in the core are some distinct compositional variations in profiles of several elements that do not appear to have been "smeared" (Fig. 12).

Before discussing these features, I discuss some minor features. There is a hint of a compositional discontinuity at about 145 cm depth, particularly in the profiles of Sc and the Na/Eu ratio (Fig. 12), just below the break between the 60004 and 60003 core sections. This occurs approximately at the break between SU28 and SU27 of *Duke and Nagle* (1976) (SU = stratigraphic unit; Fig. 11). *Heymann et al.* (1978) review a variety of data and conclude that a stratigraphic break probably occurs at the SU27/SU28 boundary. They note that this boundary was "visually . . . quite striking"; SU28 is uniform and massive whereas SU27 is marbled and laminated (*Duke and Nagle,* 1976). *Heymann et al.* (1978) also argue, on the basis of the petrographic data of *Vaniman et al.* (1976), that a discontinuity occurs somewhere near the 60003/4 boundary, but they could not locate the exact position because of gaps in the thin sections.

5.1.4. Mare basalt in 60003 and 60004 (MPU-B). At 132 cm depth, the subsample of 60004,214 analyzed here is anomalously enriched in Sc and Sm, but has low La/Sm and Sm/Sc ratios. This is almost certainly the result of a fragment of mare basalt with relatively high ITE concentrations. The composition of this sample can be duplicated by mixing 10% Apollo 11 high-K basalt (Table 3), for example, and 90% soil from adjacent depth intervals. The geochemical signature of mare basalt is high Sc and Cr concentrations and a low La/Sm ratio. Scandium and Cr concentrations reach their maximum in the 60003-5 core sections because (1) these soils contain less anorthosite than soils higher in the core and (2) they contain a small component of mare material. The La/Sm ratio reaches a minimum in this unit (Fig. 12) and is lower than that of any samples from the 60009/10 core (Fig. 2). Also, the MPU-B soils plot distinctly to the high-Sc side of the mixing line defined by the 60009/10 soils in Fig. 14. The enrichment in mare material is slightly greater below the SU27/SU28 discontinuity (145-187 cm) than above it (104-145 cm).

5.1.5. Lithophile element anomalies. In addition to the sample containing an anomalously large amount of mare material, some samples contain an excess of Sm with respect to the amount of Sc (Figs. 12 and 13). These almost certainly result from large particles of ITE-rich impact-melt breccias in the analyzed subsamples because such rocks are the only components of the Apollo 16 regolith having high Sm concentrations as well as high Sm/Sc ratios (e.g., Fig. 5). Curiously, of the five fines samples with Sm/Sc exceeding 0.8, three occur in the disturbed 60006 section of the core. The two others are from the bit (60001), which consisted only of coarse-grained material (section 2.1.2). A sample of 60003 (139 cm depth) has an anomalously high Cr concentration (as does a sample of 60009 at 33 cm depth; Fig. 2). This may result from a single grain of chromite or from contamination from the drilling or processing hardware (a Cr anomaly was also reported from a sample at 147 cm depth in 60003 by *Korotev,* 1982). Several samples contain concentrations of Zr and Hf that are anomalously high compared with trivalent ITEs like the REE (Table A3). These probably result from small zircons (*Morris et al.,* 1989).

5.1.6. Siderophile-element anomalies. Throughout the core there are samples with anomalously high concentrations of siderophile elements compared with adjacent samples. Nickel concentrations exceed 0.25% for the analyzed subsamples of 60006,89 (plotted at 34 cm depth; Fig. 12) and 60004,244 (126 cm). As Ni/Co ratios for both samples are subchondritic at 15-16, these anomalies are probably caused by large grains (2-3 mg) of Fe-Ni metal (section 4). The sample at 34 cm depth has a chondritic Au/Ir ratio of 0.32, but the ratio for the sample at 126 cm depth (Au/Ir = 0.76)

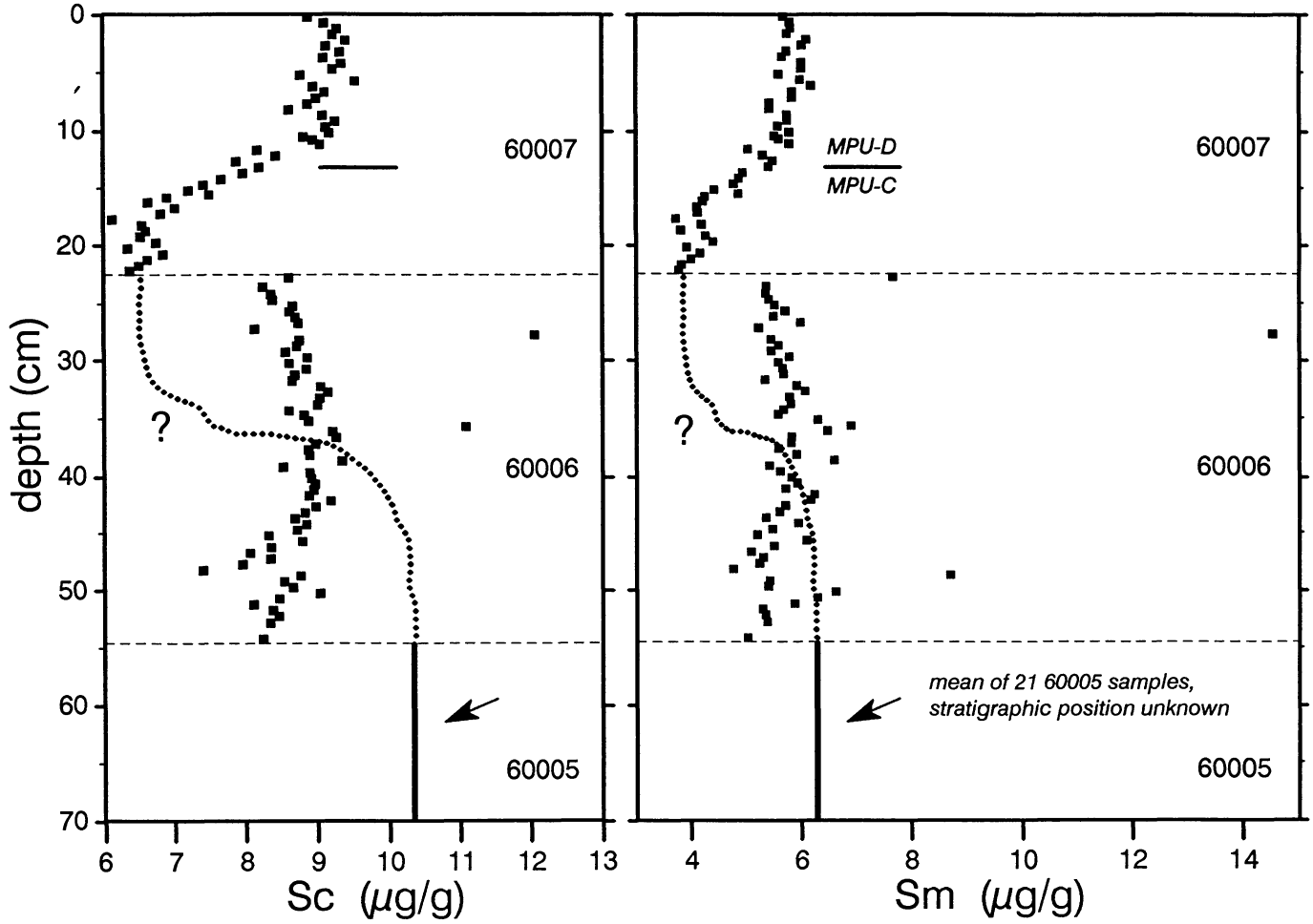

Fig. 15. Profiles for Sc and Sm at the top of the deep-drill core. The profile for the 60006 samples is discontinuous with that for the overlying 60007 samples as well as with that of the mean of the underlying 60005 samples, which are known to be disturbed. This suggests that the contents of the partially full 60006 core tube were mixed *after* it was disconnected from the other two sections. The actual profiles through this core section probably resemble those suggested by the dotted lines. The boundary between MPU-C and MPU-D is indicated at 13 cm depth, as advocated by *Gose and Morris* (1977).

is more similar to metal from ancient impact-melt breccias (typically about unity; Table 3). Several samples, most notably two from 60003 at 171 and 178 cm depth, have very high concentrations of Au compared with other siderophile elements.

5.1.7. Siderophile-element enrichment at the bottom of MPU-B. All samples between about 177 and 187 cm depth (i.e., those from SU13 at the top of 60002 and SU14 at the bottom of 60003) are strongly enriched in Ni, Co, Ir, and Au and slightly enriched in Cr (Fig. 12). High concentrations of siderophile elements occurring over several stratigraphically consecutive samples have not been observed in previous high-resolution studies (*Korotev et al.,* 1984; *Morris et al.,* 1989), although there is a hint of such an enrichment in 60010 (section 3.1.5). *Ehmann et al.* (1977) also report Ni and Co enrichment in two samples from the bottom of 60003, but because of the wider spacing of the samples they analyzed, it is not evident that a zone of enrichment occurs.

The enrichment in siderophile elements in SU13 and SU14 is accompanied by an enrichment in metallic iron (*Gose and Morris,* 1977), suggesting that the siderophile elements are carried by Fe-Ni metal of meteoritic origin. However, the enrichments are not the result of a concentration of ancient Fe-Ni metal (section 4.3), but of a component of ordinary chondrite. This is demonstrated by the data in Table 5 where mean siderophile-element concentrations and ratios in soils from SU13 and SU14 are compared with those from SU18 and SU19, which are about 16 cm higher in the core and have more nearly "normal" concentrations of siderophile elements. The differences in concentrations between these two levels are the "excess" attributed to the meteoritic component causing the anomalies.

The enrichment in Cr as well as siderophile elements argues that the anomaly is not simply the result of a concentration of Fe-Ni metal. The Cr/Fe_{total} ratio of the component causing the enrichments is 0.0063 ± 0.0016. Although this is only about half the chondritic ratio (Table 5), the data are still

TABLE 5. Siderophile-element ratios for meteoritic component in region of high siderophile-element concentration (SU13 and SU14) estimated by comparison with nearby region with "normal" concentrations (SU18 and SU19).

		Normal	Enriched	Difference	Meteorite	
SU:		18 & 19	13 & 14	(excess)		
Depth (cm):		164-169	177-187		CI	H
Fe^0	mg/g	6.1	12.2	6.1		
	±	0.7	1.0	1.1		
Fe_{total}	mg/g	44.2	50.7	6.5		
	±	0.3	0.7	0.8		
Ni	mg/g	0.41	0.89	0.48		
	±	0.02	0.05	0.05		
Co	μg/g	27.4	49.2	22.		
	±	1.0	2.8	3.		
Ir	ng/g	12.5	26.5*	14.1		
	±	0.6	1.5	1.6		
Au	ng/g	6.2	11.6*	5.4		
	±	0.5	1.0	0.7		
Cr	mg/g	0.836	0.877	0.041		
	±	0.006	0.006	0.009		
Fe^0/Fe_{total}	g/g			0.93	~0	0.6
	±			0.21		
$Ni/(Ni+Fe^0)$	g/g			0.073	~0	0.092
	±			0.016		
Ni/Co	g/g			22.	21.1	19.7
	±			4.		
Au/Ir	g/g			0.39	0.31	0.28
	±			0.06		
Cr/Fe_{total}	mg/g			6.3	14.6	13.3
	±			1.6		

*Data from 2 of 17 samples are excluded for Ir and Au because of anomalously high Au concentrations (Fig. 16).

Fe^0 (metal) data from *Gose and Morris* (1977); meteorite data from *Wasson* (1985), *Wasson and Kallemeyn* (1988), and *Rambaldi* (1977).

consistent with a component of ordinary chondrite if there has been some separation of metal and silicate, namely, relative loss of silicate material.

The Ni/Co ratio of 22 ± 4 is consistent with a chondritic component, but inconsistent with ancient Fe-Ni metal (Table 3). A representative Au/Ir ratio for the meteoritic component is more difficult to determine because the ratios are highly variable among the individual samples. Most of the samples between 177 and 187 cm depth deviate from "normal" samples (164-169 cm) along a trend more consistent with a chondritic component than with ancient Fe-Ni metal, but two samples with anomalously high Au concentrations (>20 ng/g) clearly do not follow this trend (Fig. 16). For the purpose of Table 5 these two samples were excluded from the mean.

The Ni concentration of the metal phase (assuming that the Ni excess is contained entirely in the metal phase) is calculated by dividing the excess Ni by the sum of excess Ni and Fe^0. This leads to 7.3 ± 1.6% Ni in the metal (Table 5). For low concentrations of Ni such as this, the concentration of Fe^0 reported by *Gose and Morris* (1977) is actually the total concentration of alloyed metal (*Pearce et al.*, 1973; *Morris*, 1976); thus, the Ni concentration of the metal may actually be as high as 0.48/6.1 = 7.9%. Among ordinary chondrites this value is consistent only with the H group. The Fe^0 concentrations reported by *Gose and Morris* (1977) were determined on fewer samples and samples that were distributed differently throughout SU13 and SU14 than those analyzed here, but if the data are taken at face value, then nearly all the meteorite-derived Fe is in the metal phase, i.e., Fe^0/Fe_{total} is 90 ± 20% (Table 5). This is a large value for ordinary chondrites, even H chondrites (typically 60%). As with the Cr/Fe_{total} ratio, however, the data are consistent with an H-chondrite source if the metal/silicate ratio of the meteoritic debris is higher than average, perhaps as a result of selective loss of silicate material. The constraints posed by the Cr/Fe_{total} and the Fe^0/Fe_{total} ratios can both be achieved with a component of H chondrite that contains ~40% metal instead of the usual 15-20%.

Other data confirm that the zone of siderophile-element enrichment is enriched in meteoritic lithophile elements as well as siderophile elements. The only three samples from the deep drill core studied by *Boynton et al.* (1976) are, coincidentally, from the top of 60002, right in the peak of the zone of siderophile-element enrichment (parent splits 23, 25, and 27 at about 181-182 cm depth). In addition to being enriched in Fe, Cr, and siderophile elements, the 60002 soils of *Boynton et al.* (1976) also have high Mg concentrations for Apollo 16 soils (mean: 7.4% as MgO). Similarly, the single sample from this zone in the data of *Nava et al.* (1976) (60002,206, parent split 31 at ~183 cm depth) contains 7.04% MgO, compared with a mean concentration of 6.29% for 11

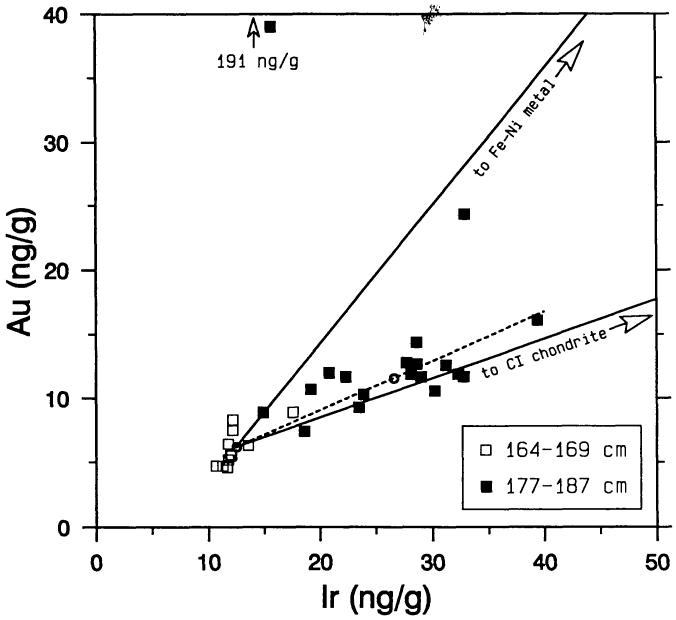

Fig. 16. Variation of concentrations of the siderophile elements (SE) Au and Ir in <1-mm fines from the SE-rich region of 60002 and 60003 (177-187 cm depth, SU13 and SU14) compared with a nearby region of "normal" SE abundances (164-169 cm depth, SU18 and SU19). The open circles represent the mean concentrations of soils in each region, except that the two high-Au samples (Au > 20 ng/g) were excluded from the SE-rich mean. The dashed line is defined by the two means (open circles). As in Fig. 8, the solid lines indicate the effect of adding Fe-Ni metal such as found in mafic impact-melt breccias from Apollo 16 (Au/Ir = 1) or CI chondrites (Au/Ir = 0.3) to the mean composition of the "normal" soils. The plot shows that the zone of SE enrichment is more consistent with a chondritic component than with Fe-Ni metal.

samples of 60002 below 187 cm depth. I avoid applying any arguments such as used for Table 5 to these data to further constrain the nature of the meteoritic component for two reasons. In the data of *Boynton et al.* (1976) no "normal" core soils were studied with which to compare the results, and there are indications of some systematic differences between their data and those obtained here. Chromium and Fe concentrations (INAA) are 12-13% higher than those obtained here for samples from the same parent splits and were obtained on different subsplits than were the siderophile-element abundances (RNAA). Magnesium concentrations (not determined well by INAA) are high compared with the values of *Nava et al.* (1976) (well determined by atomic absorption spectrophotometry). Systematically high values for Fe and Mg are the probable cause of the high mixing-model sums (103-108%) obtained by *Boynton et al.* (1976) for these three soils.

The phase carrying the siderophile elements in SU13 and SU14 has not been positively identified, although there is some evidence that it is a form of vesicular, glassy breccia. Samples from SU10 and SU15 were studied petrographically, but none from SU13, the zone of greatest siderophile-element enrichment (*Meyer and Tsai,* 1975; *Meyer and McCallister,* 1976). There are no striking petrographic anomalies for this zone in the data of *Vaniman et al.* (1976) based on the set of continuous thin sections of the core (primarily, sections 389, 390, and 391 of 60002). The description made during core processing of SU13 indicates that it is "finer [grained] than the rest of the core" and that "frothy to vesicular spattered glassy agglutinates are especially abundant in this sub-unit" (*Duke and Nagle,* 1976). Although agglutinates are thought to be the product of micrometeorite impact, agglutinate particles are not necessarily enriched in siderophile elements. For example, agglutinate particles from Apollo 17 and Luna 24 have Ni concentrations similar to typical <1-mm fines (*Blanchard et al.,* 1975; *Korotev,* 1989). The single agglutinate particle studied from 60009 (particle 58-F, section 3.2) and one of the two studied from 60002 (particle 2.02, section 5.2.3) have lower Ni concentrations (250 and 295 μg/g; Tables A2 and A5) than the average core soil (394 and 439 μg/g; Tables A1 and A3). However, the other agglutinate particle identified among the >1-mm particles from 60002, particle 2.16, is highly enriched in siderophile elements (1550 μg/g Ni). Similarly, regolith breccia 63507 is unusual among Apollo 16 regolith breccias in containing both a high proportion of agglutinates as well as high concentrations of siderophile elements (*McKay et al.,* 1986). In fact, concentrations of all lithophile and siderophile elements in both particle 2.16 and regolith breccia 63507 are quite similar to those in the 60002 soils with the highest concentrations of siderophile elements, and both have chondritic Au/Ir ratios. Although not conclusive, these observations suggest that the siderophile-element enrichment between 177 and 187 cm depth results from an agglutinate-like component (see also section A1.3).

5.1.8. Boundary between MPU-B and MPU-A. The zone of siderophile-element enrichment is gradually terminated at the top, but abruptly terminated at the bottom exactly at the boundary between SU12 and SU13 at 187 cm depth (Fig. 17). The boundary between these two stratigraphic units is the second of the two major stratigraphic boundaries recognized in the core in previous studies, that between MPU-A and MPU-B (Fig. 11). Below 187 cm depth distinct changes occur in modal petrography (*Vaniman et al.,* 1976), I_s/FeO (Fig. 12), and $^{40}Ar/^{36}Ar$ ratios (*Heymann et al.,* 1978). The data obtained here show that these changes are also accompanied by distinct compositional changes. In addition to the abrupt decrease in siderophile-element concentrations, discontinuities occur in the concentrations of some lithophile elements across the boundary. A compositional discontinuity was not discerned in previous studies because of vagaries in spacing and allocation of samples and the limited number of samples and elements determined (*Nava et al.,* 1976; *Gose and Morris,* 1977). [Based on one sample from above the boundary compared with several below, *Heymann et al.* (1978) suspected that differences in Fe and Mg concentrations in the data of *Nava et al.* (1976) represented a concentration change associated with the boundary.]

5.1.9. Sodium enrichment in MPU-A. For all elements determined here except Na, the soils from MPU-A have concentrations generally typical of Cayley soils. Below 187 cm

depth, concentrations of ITEs become more variable from sample to sample. This is probably a grain-size effect resulting from the greater proportion of coarse-grained fragments in this unit (*Nagle et al.,* 1975). On the average, however, the MPU-A soils plot at the high-Sc end of the Sc-Sm mixing line defined by the 60009/10 soils and slightly to the high-Sm side of that line (Fig. 14). Thus, the MPU-A soils probably do *not* contain the component of mare basalt that occurs in MPU-B soils. Because the MPU-A soils have slightly lower Sc concentrations (also Fe and Cr) and slightly higher ITE concentrations (Sm) than the MPU-B soils, there is a distinct discontinuity in the profile of the Sm/Sc ratio at the boundary at 187 cm (Fig. 12).

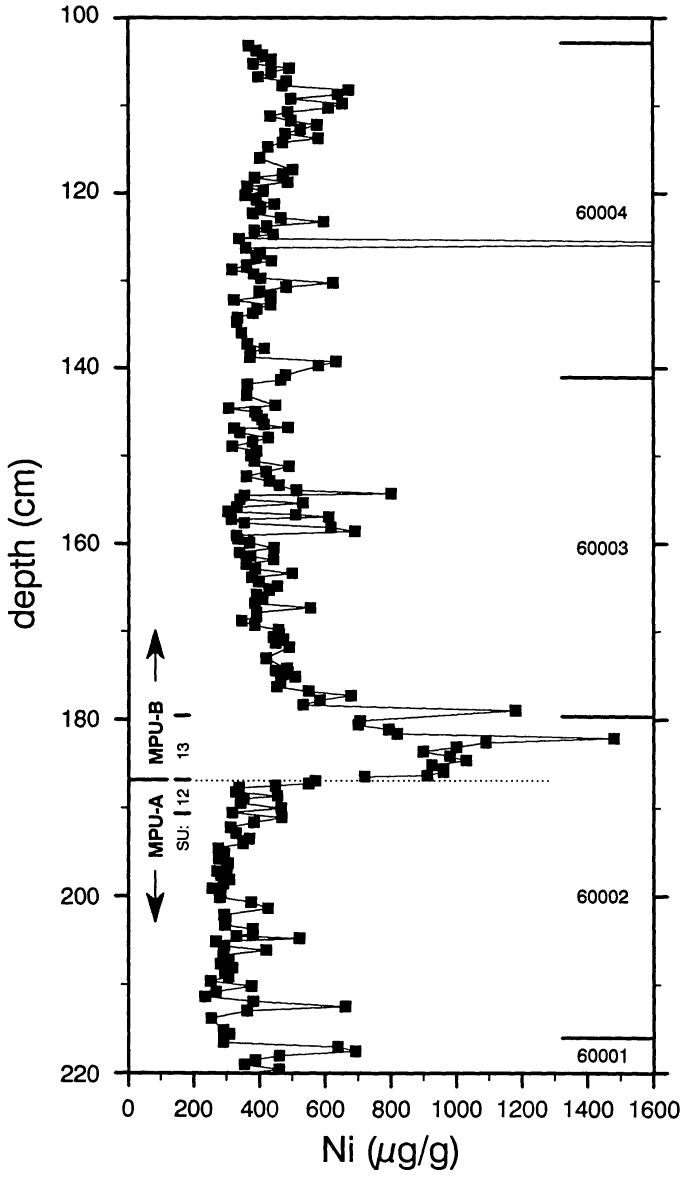

Fig. 17. Depth profile for Ni in the lower half of 60001-7 (detail from Fig. 12).

The most striking compositional change, however, is that MPU-A soils are richer in Na than soils above this depth (Fig. 12); the average MPU-A soil is enriched in Na by a factor of 1.08 compared with the average of all samples above MPU-A. Such a change requires only a small increase in the average albite concentration of the plagioclase (e.g., from $Ab_{5.1}$ to $Ab_{5.7}$). Curiously, there is no change in the Eu concentration, which usually increases with increasing Na_2O concentration in plagioclase (Fig. 6). To help assess the cause of the Na enrichment, I studied a number of >1-mm particles from MPU-A in 60002.

5.2. 60002 and Other Particles

Like the particles from 60009/10, the particles studied from 60001-7 (mostly from 60002) encompass a wide variety of compositions and lithologies. Although most of the particles are not directly relevant to the question of why the <1-mm fines from MPU-A are compositionally distinct, some of them relate to other issues discussed here, so I briefly discuss the particles below.

5.2.1. Subsamples of particles 2.19 and 2.34. Two of the 60002 particles were too large to analyze conveniently as single particles, so they were subdivided into several smaller subsamples (section 2.1.2). Under the binocular microscope particle 2.34 was identified as a breccia with a very dark, fine-grained matrix containing a portion of a large, lighter-colored clast that appeared glassy and heterogeneous. The four subsamples of particle 2.34 differ greatly from each other in composition (Fig. 18). Samarium correlates well with Sc, suggesting binary mixing. This is substantiated by the sample descriptions. The subsample with the lowest concentrations of Sc and Sm (2.34B) is nearly pure dark matrix; the subsample with the highest Sc and Sm concentrations (2.34C) contains the largest amount of the glassy clast. The other two subsamples are intermediate. Thus, the glassy clast must carry an ITE-rich component.

The large particle designated 2.19 was a breccia with a fine-grained, light gray matrix and veins of lighter material. Upon being broken into smaller pieces for analysis, the particle tended to fracture along the veins. The eight subsamples of particle 2.19 are similar to each other in composition, but systematic differences occur (Fig. 18). The Sm concentrations are low, similar to those from ferroan anorthosites, but the Sc concentration are much greater (Fig. 5b). Scandium and Sm concentrations are correlated, again suggesting that the correlation results from varying proportions of two components in the different subsamples (matrix and vein material?).

The mass-weighted mean concentrations for particles 2.19 and 2.34 are listed in Table A5 and single points corresponding to these values are plotted in subsequent figures.

5.2.2. Unusual particles. The particle with the greatest concentrations of Sc and Sm (particle 4.03, Fig. 19) is a poikilitic impact-melt breccia from 60004. This particle is one that I removed from the <1-mm fines because it was large (section 2.1.2); smaller particles similar to this that were *not* removed are the likely cause of some of the positive anomalies in ITEs, like Sm, in Figs. 12 and 13. Although not examined petrographically, particles 1.05, 1.06, 2.24, and 2.32 (Fig. 19)

are probably also mafic impact-melt breccias because they are compositionally similar to melt breccias from 60009/10 and large samples of melt breccias from Apollo 16 (*Vaniman and Papike,* 1980).

Particle 2.15 is a single crystal of olivine, which accounts for the high Co concentration (59 μg/g). The low Na_2O, CaO, and Eu concentrations (0.02%, 0.3%, and 0.033 μg/g) are expected for a particle containing no plagioclase. Particle 2.29, which has the highest Sc concentration of the particles studied, is a medium-grained anorthositic gabbro.

The spherical particles, which are presumably impact melts shaped during free fall, show a wide range in compositions. For spheres 2.35 and 3.02, the low concentrations of Sc, Cr, and Fe and relative concentrations of REE suggest that they have only a small mafic component and probably derive from plagioclase-rich rocks. Sphere 2.20 is a nearly colorless glass containing many vesicles and is similar to the MPU-A soil in composition, except that it is not enriched in Na. Sphere 2.01 has no Eu anomaly and is relatively enriched in heavy REE compared to the typical soil. Sphere 2.36 has an unusually high Co/Ni ratio and its Hf concentration is high compared with other ITEs. Because the compositions of many of these spheres are unusual and are not those of average materials, they are probably not portions of large melt volumes; they are more likely to be small melts derived from special targets.

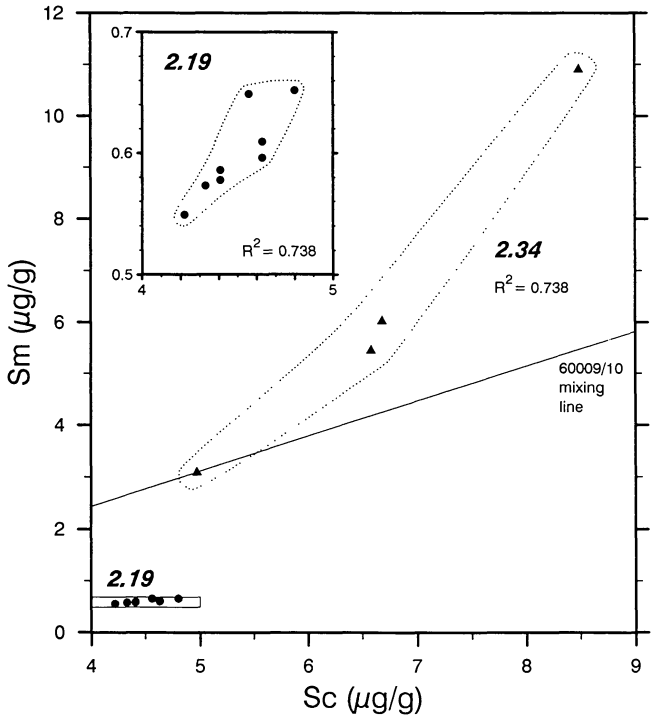

Fig. 18. Variation of Sm and Sc concentrations in subsamples of two large particles from 60002 (sections 2.1.2 and 5.2.1). A simple linear regression of Sm against Sc for the subsamples of particle 2.19 (expanded scale in the upper left corner) yields a line that crosses the Sc axis at 0.9 μg/g Sc.

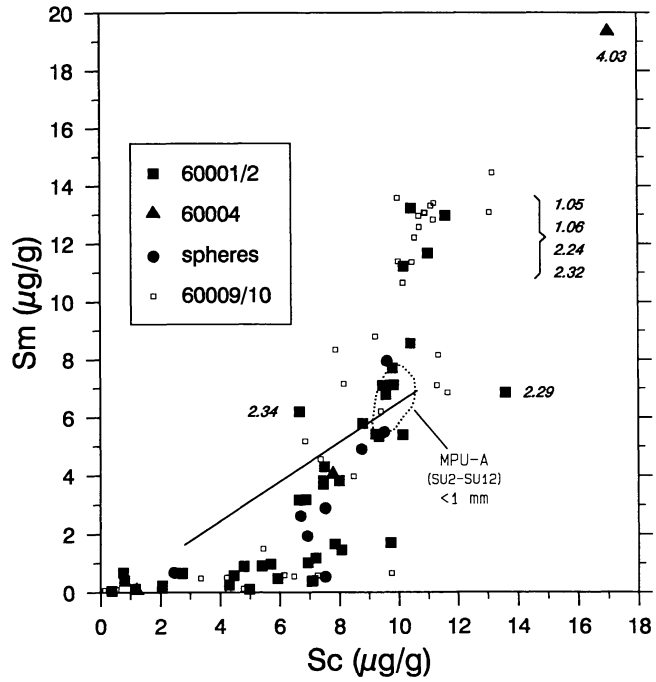

Fig. 19. Variation of Sm and Sc concentrations in >1-mm particles and spheres from 60001-7 (section 2.1.2; data from Tables A4 and A5). Data for >1-mm particles from 60009/10 (Fig. 5) are shown for comparison. The solid line is the mixing line for <1-mm fines from 60009/10 (Fig. 4). Labels such as "4.03" are particle numbers for samples discussed in the text (section 5.2). The dotted field shows the range of <1-mm fines samples from SU2 through SU12 in 60002 (i.e., the Na-rich samples from MPU-A). Thin sections were made of eight of the 60001/2 particles plotting in or near this field; four or five are regolith breccias.

5.2.3. Regolith breccias and agglutinates. Compared with 60009/10, a larger fraction of the >1 mm-particles from 60001 and 60002 are similar in composition to the corresponding <1-mm fines (Figs. 18 and 20). Study of thin sections of the eight particles that are the most soil-like in composition show them to be petrographically diverse. Two appear to be impact-melt breccias; one is crystalline (particle 2.27) and the other is glassy and clast-laden (particle 2.06). Both of these have low Ni concentrations (~70 μg/g). The remaining six are either regolith breccias (particles 1.04, 2.07, 2.28, and 2.33) or agglutinates (particles 2.02 and 2.16). The agglutinates have lower Na_2O concentrations (mean: 0.48%) than the regolith breccias (mean: 0.54%); the two regolith breccias with the greatest Na_2O concentrations (particles 2.07 and 2.33) each contain medium-sized clasts (up to 0.4 mm) of shocked anorthosite.

5.2.4. "Sodic plagioclase." Most of the particles from 60002 have Na_2O abundances similar to those of particles from other regions of the core and to the particles from 60009/10 (Fig. 21). However, two of them, particles 2.13 and 2.31 from about 204 cm and 194 m depth, have anomalously high

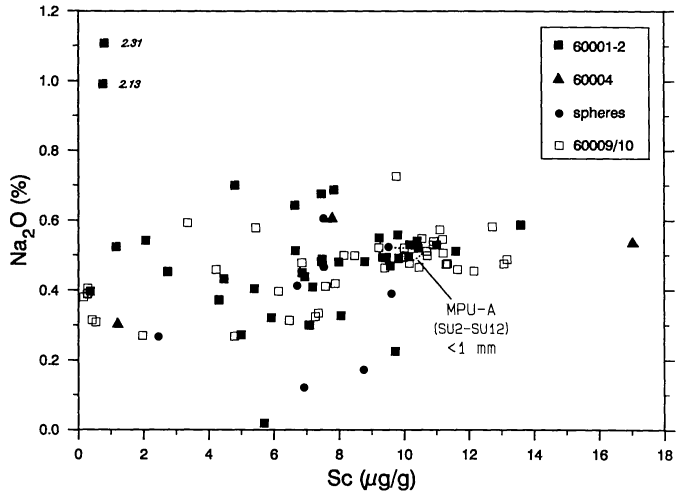

Fig. 20. Variation of Na_2O and Sc concentrations in >1-mm particles and spheres from 60001-7 (like Fig. 19).

Na_2O concentrations, 1.0% and 1.1%. Both are whitish particles consisting almost entirely of plagioclase. Particle 2.13 contains no visible mafic minerals and only a trace of ilmenite. The plagioclase crystals are medium grained and most are recrystallized. Particle 2.31 contains minor (~5%) orthopyroxene and a trace of ilmenite; the plagioclase is weakly shocked. Based on the INAA data, plagioclase in these particles is An_{90-91} (Fig. 21), distinctly more albitic than the An_{96-97} typical of ferroan anorthosite. For comparison, one of the 60002 particles (particle 2.25) is a large fragment of typical ferroan anorthosite (An_{96}) that is similar in composition to the six small particles studied from 60009/10 (Figs. 5b and 6). (INAA results for the three particles are listed sequentially in Table A5.) The sodic particles are considerably enriched in REE, including Eu, compared with ferroan anorthosite (Figs. 21 and 22). They are also enriched in Sr and Ba. Although K concentrations were not determined, the Ba enrichment suggests a larger component of orthoclase than is found in typical ferroan anorthosite.

Plagioclase as sodic as that in particles 2.13 and 2.31 is unusual for Apollo 16 rocks. *James et al.* (1989) argue that ferroan anorthosites can be subdivided into four subsets, including an "anorthositic, sodic" subset. "Type specimens" of this subgroup are rake samples from the rim of North Ray Crater with plagioclase of $An_{94.5-95}$ composition; this is considerably less sodic than the An_{90-91} plagioclase in particles 2.13 and 2.31. Petrologically, the sodic plagioclase grains in 60002 are of special interest because they are intermediate in composition between ferroan anorthosite and alkali anorthosite. Alkali anorthosite is usually regarded as a subset of the magnesian suite of lunar plutonic rocks (*Warren et al.*, 1983a,b). For the present discussion, however, the particles are important only because they have high Na_2O concentrations and occurred in 60002. Thus I defer a thorough petrographic description and speculation of their origin to a more appropriate format. As no large rocks dominated by plagioclase of this composition are known from Apollo 16, I refer to the particles as "sodic plagioclase" and not alkali anorthosite.

6. 60001-7 DISCUSSION

The compositional profiles obtained here reveal four distinctive stratigraphic features in the deep drill core: (1) an anorthosite-rich unit in 60007 (MPU-C), (2) a small amount of mare material distributed throughout 60003 and 60004 (MPU-B), (3) a layer of siderophile-element enrichment at the top of 60002 (bottom of MPU-B), and (4) relatively high concentrations of Na in 60001 and 60002 (MPU-A). To facilitate discussion of these features, the 60001-7 data were subjected to the mixing model described in section 4.4. The modeling was done in the same way as for the 60009/10 core, except that data for Sr and Zr were included (section 2.2). Results for the average core soil, excluding the samples from MPU-A, are presented in Table 4 ["MPU-(B,C,D)"]. As with 60009/10, the best-fit model composition ("calc.") is a very good match to the average composition ("obs."). Depth profiles for the five model components are presented in Fig. 23.

6.1. Anorthosite in MPU-C

The mixing-model results indicate that MPU-C is similar to the plagioclase-rich units at 43 and 54 cm depth in 60009/10 in having a high concentration of anorthosite, and this is confirmed by the petrographic data (section 5.1.1). The model indicates 47% anorthosite component for the most feldspathic sample in 60001-7 at 18 cm depth (Fig. 23) compared with 59% at 43 cm depth and 75% at 54 cm depth in 60009 (Fig. 9). *Heymann et al.* (1978) conclude that the anorthositic

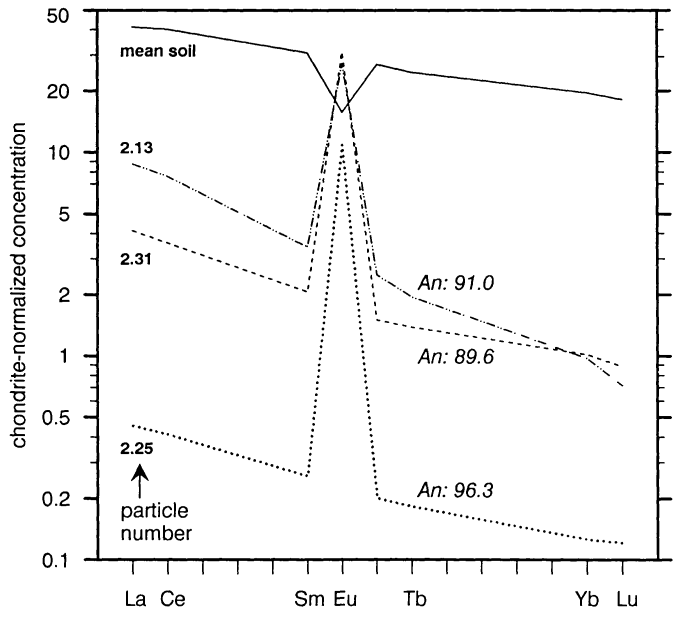

Fig. 21. Concentrations of rare earth elements in plagioclase particles from 60002 normalized to concentrations in volatile-free CI chondrites (Table 3). The anorthite concentrations of the plagioclases were calculated from bulk Na_2O and CaO concentrations.

"horizons" in the two cores are "almost certainly the same." Considering the ubiquity of anorthosite at the Apollo 16 site, however, there is no certainty that the two cores sampled the same stratigraphically contiguous unit of anorthosite-rich material. As the cores were taken only about 35-40 m apart, the *source* of the anorthosite is likely to be the same, however. No surface or trench soils collected in the vicinity of the lunar module (Stations LM, 1, and 2) are as feldspathic as the most feldspathic soils in 60007, although 61221, taken from a trench on the rim of Plum Crater at Station 1, is only slightly more mafic (Fig. 14).

6.2. Sodium Enrichment in MPU-A

The soil from MPU-A (60001 and bottom two-thirds of 60002) is unusual in several ways. It is relatively immature (coarse grained, low I_s/FeO; Fig. 12) compared with soil higher in the core (finer grained, high I_s/FeO). *Vaniman et al.* (1976) note several distinct petrographic features. In addition to an abundance of large, anorthosite "clasts," the MPU-A soil contains a large amount of yellow glass and a scarcity of green glass compared with other units. The single sample of soil from MPU-A studied by *Russ* (1973) has suffered the largest neutron dose of any Apollo 16 soil measured. The $^4He/^{20}Ne$ ratios are lower and $^{40}Ar/^{36}Ar$ ratios are higher in the MPU-A fines than for other soils in the core and all surface and trench soils from Apollo 16 except trench soil 61221 (*Bogard and Hirsch,* 1975; *Heymann et al.,* 1978). [Like the MPU-A fines, trench soil 61221 is also enriched in Na (Figs. 22 and 24); however, the lower Sc and Sm concentrations indicate that 61221 is less mafic than the MPU-A soil (Fig. 14).] *Bogard and Hirsch* (1975) conclude that the MPU-A soil is old and that its "solar-derived gases and excess ^{40}Ar were implanted $\geq 10^9$ yr ago."

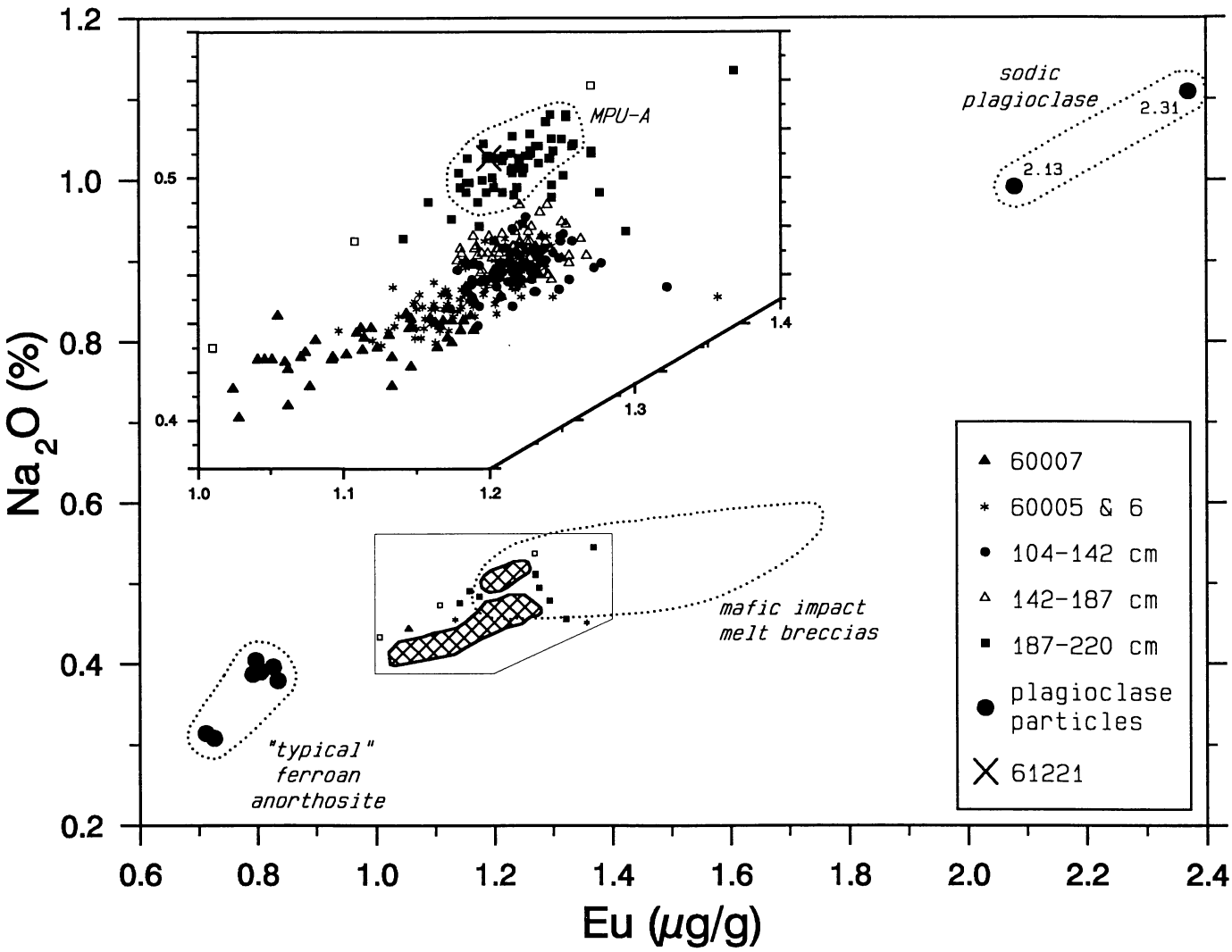

Fig. 22. Variation of Na_2O and Eu concentrations in <1-mm fines from 60001-7 (expanded in upper left corner) compared with >1-mm particles of plagioclase/anorthosite and impact-melt breccias. The "typical" ferroan anorthosite field includes the six particles from 60009/10 (Figs. 5b and 6) and particle 6.25 from 60002. Soils from MPU-A (60001 and 60002) are distinctly enriched in Na_2O, but not Eu, compared with other soils from the core. Although somewhat counter-intuitive, ferroan anorthosite has the lowest concentrations of Na_2O and Eu among common Apollo 16 materials.

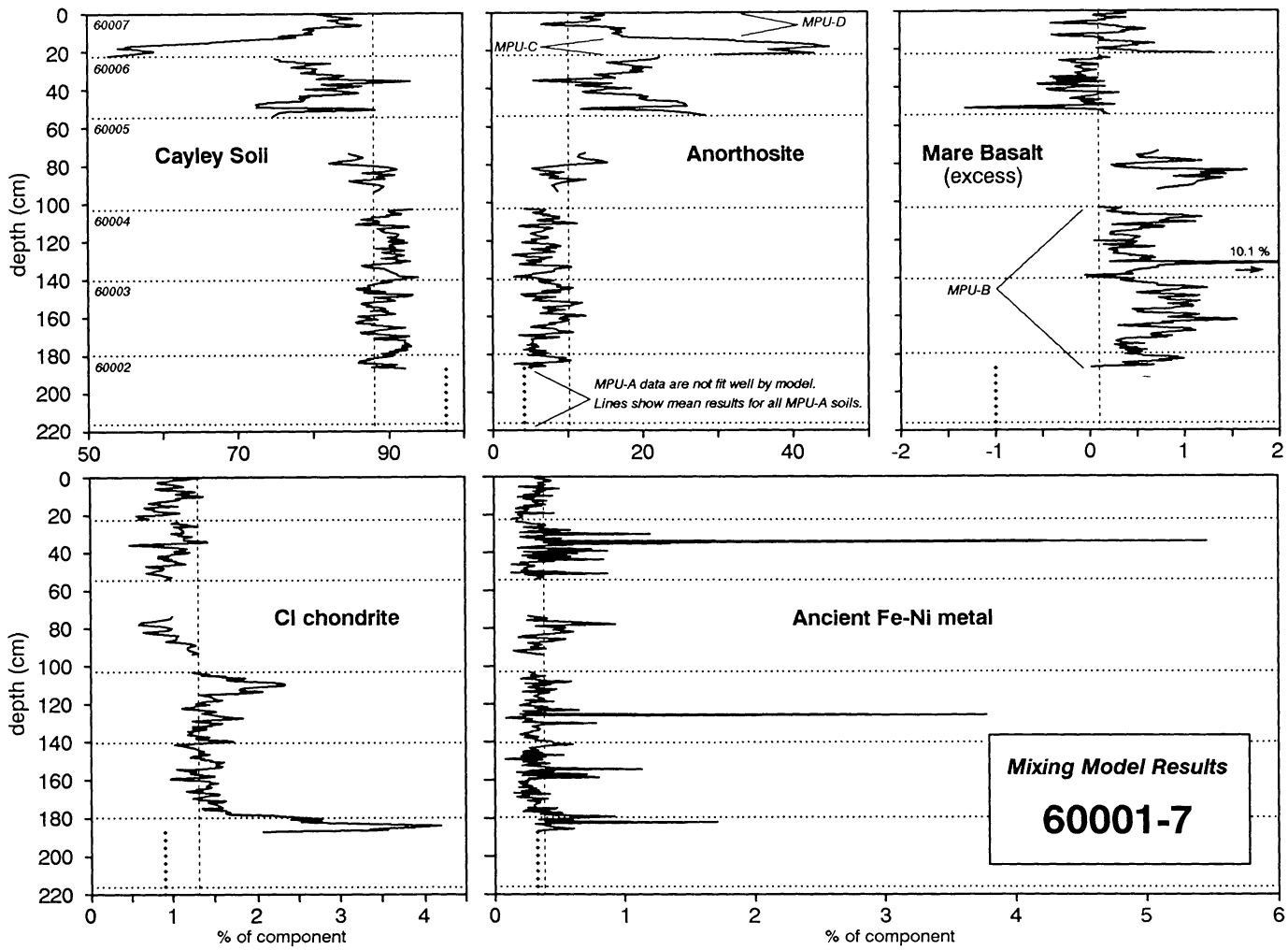

Fig. 23. Mixing model results for <1-mm fines from 60001-7 (see Fig. 9). Samples with anomalously high Sm/Sc ratios are excluded (Fig. 13). None of the soils from MPU-A were adequately fit by the model, primarily as a result of their high Na concentrations. The inadequate, but best-fit, model results for the mean composition of these soils are indicated by the vertical dotted line.

The simple mixing model, which is successful for the 60009/10 soils and soils from other units in 60001-7, does not account for the composition of the MPU-A soils, i.e., the MPU-A soils are not a simple mixture of typical Cayley soils and ferroan anorthosite (± mare basalt). In Fig. 23, the best-fit model results for the mean composition of all MPU-A soils is plotted (vertical dotted line), but because of the inadequacy of the model, these results are not quantitatively comparable with those for soils above this unit. When components representing the sodic plagioclase particles and mafic, ITE-rich, impact-melt breccias are included in the model (Table 3), the fit is improved but is still not adequate. Addition of a sufficient amount of sodic plagioclase, such as particles 2.13 and 2.31, to account for the observed Na enrichment causes the Eu concentration of the best-fit mixture to be considerably larger than actually observed (Table 4); no combination of components accounts for both the Na enrichment and the constancy of Eu across the boundary between MPU-A and MPU-B (Figs. 12 and 22). Thus, either (1) the model is adequate, but the Na-rich component of the MPU-A soils has not been identified or (2) the model does not describe the MPU-A soils.

For two reasons I favor conclusion 2, i.e., that the Cayley soil component is only a minor component of the MPU-A soil (despite the compositional similarity) and, consequently, that the MPU-A soil is of a different provenance than other soils in the core. First, it is unlikely that simple addition of an unidentified component to typical Cayley soil could account for the composition of the MPU-A soil because it is difficult to conceive of even a hypothetical Na-rich component (except, perhaps, for a vapor phase condensate) that would increase the Na_2O concentration by a factor of 1.08 (on the average) and not affect the other analyzed elements to any significant extent. Second, most other Apollo 16 soils with similarly high concentrations of Sc and Sm are relatively mature and, consequently, fine grained; the MPU-A soil is relatively immature and coarse grained. This suggests that it is not a well-mixed regolith of many lithologies like the Cayley soil

component, but that it is dominated by a single lithology (in the way the immature soil from 54 cm depth in 60009/10 is dominated by anorthosite), which has a composition similar to the soil. Among the coarse-grained soil particles from MPU-A (>1 mm) are several that are very similar in composition to the <1-mm fines (section 5.2.3 and Figs. 19 and 20). Thus, both the fines and particles may derive in large part from one (or several lithologically similar) local rock(s). This model is similar to that of *Heymann et al.* (1978), who suggest that the MPU-A fines derived in large part by filleting of boulders at the bottom of a secondary crater.

If all the >1-mm particles with soil-like compositions were impact-melt breccias, for example, then that would be strong evidence that the MPU-A soils derive mainly from comminution of a single lithology. The actual data are not so conclusive, of course. Of the eight particles examined with soil-like compositions, four are regolith breccias and one of the remaining four is a glassy-matrix breccia that may be lithified regolith (section 5.2.3). Thus the data are reasonably consistent with a model such as that of *Basu and McKay* (1989) in which the MPU-A soils derive mainly from pulverization of large regolith breccias. The possibility also exists, however, that the compositional similarity between the <1-mm fines and the >1-mm particles results because the particles derive from the lithification of fines and not because the fines derive from comminution of larger rocks. As soil matures with exposure to micrometeorite impacts, the grain size generally decreases because the rate of destruction exceeds the rate of construction of agglutinate particles (*McKay et al.*, 1974). Two of the soil-like particles from MPU-A are agglutinates and these may well have been formed directly from the MPU-A fines. (Might they instead have been formed by micrometeorite impact into a regolith-breccia boulder?) However, the other four do not appear to be the products of near-surface induration by small impacts. These particles are almost certainly fragments of larger rocks that were produced by lithification of a preexisting regolith by a large impact.

There are other similarities between the MPU-A soils and some Apollo 16 regolith breccias. Like the MPU-A fines, the ancient Apollo 16 regolith breccias have high $^{40}Ar/^{36}Ar$ ratios, although the ratios in many of the breccias are much greater than those of MPU-A fines (*McKay et al.*, 1986; *Heymann et al.*, 1978). Also, the Na_2O concentration of average MPU-A soil (and 61221), although unusual compared with soil from higher units in the core and to any typical surface soil (e.g., 60601), is typical of that for Apollo 16 regolith breccias (Fig. 24). In fact, with respect to the large range of Na_2O concentrations observed in Apollo 16 regolith breccias, fines from above MPU-A in 60001-7 (as well as 60601 and 60009/10) are unusual in having *low* Na_2O concentrations. These features suggest that the Cayley soils are distinct in time or provenance from MPU-A soils, which in turn may be related to the ancient regolith breccias. However, that relationship, if any, is not straightforward. It is clear from Fig. 24 that both the MPU-A fines and the regolith-breccia particles from MPU-A are more mafic (higher Sc concentration) than the suite of ancient regolith breccias (*McKay et al.*, 1986) and, in this regard, are more similar to the Cayley soils. If the Cayley soils (present surface soils at the LM Station) are genetically related

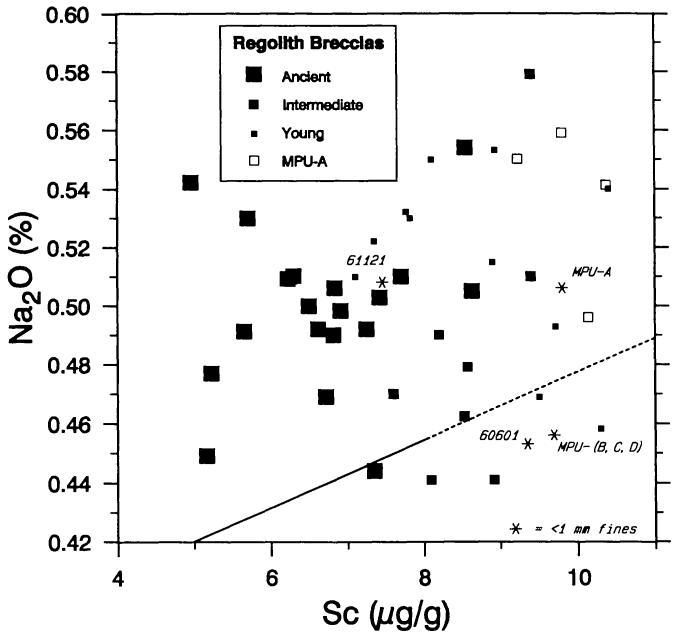

Fig. 24. Variation of Na_2O and Sc concentrations in Apollo 16 regolith breccias and some <1-mm fines. The open squares are for the >1-mm particles from MPU-A (60001 and 60002) discussed in section 5.2.3 and 6.2. The filled squares are for large samples from various stations at Apollo 16. "Ancient" regolith breccias are those with $^{40}Ar/^{36}Ar > 12$ and $I_s/FeO < 1$; "young" = $^{40}Ar/^{36}Ar < 5$ or $I_s/FeO > 5$; intermediate = all others (after *McKay et al.*, 1986). The solid line is the mixing line for the plagioclase-rich soils between 36 and 57 cm depth in 60009/10 (Fig. 6); the dashed portion represents extrapolation of the line to higher Sc concentrations. The plot shows that (1) Na_2O concentrations in regolith breccias have a large range and do not correlate with "ancientness," (2) regolith breccia particles and <1-mm fines from 60002 ("MPU-A") have Na_2O concentrations typical of the large regolith breccias, but are richer in Sc on the average, and (3) other LM-Station soils (60601), the line representing 60009/10, and all soil above MPU-A in 60001-7 ["MPU-(B,C,D)"] have Na_2O concentrations at the low end of the range for the regolith breccias.

to the ancient regolith breccias, which they may not be, then perhaps the MPU-A soil is some intermediate relative in that relationship.

In summary, the MPU-A soils appear to represent an old regolith that is probably composed of lithologies generally similar to, yet distinct from, those composing the Cayley soils presently at the surface. The average plagioclase composition of the source lithologies was slightly more sodic than those of the Cayley soil component, and other minor compositional differences as well as petrographic differences also occur. Some large impact event lithified the soil, creating regolith breccia such as the >1-mm particles of section 5.2.3. At that point, either of two scenarios can explain the data. In the first scenario, which is a variation of the model of *Heymann et al.* (1978), an impact excavated the breccia and deposited it as relatively coarse-grained debris at the 60001-7 site, possibly in a secondary crater. Exposure to micrometeorite impacts at

the surface reduced the average particle size of this material, filling in low areas between the larger boulders. *Gose and Morris* (1977) argue that the boundary between MPU-A and MPU-B cannot represent a surface that was exposed for any substantial length of time because I_s/FeO remains low and rather constant throughout MPU-A instead of decreasing with depth below the boundary (Fig. 12), as expected from *in situ* maturation. However, the observed I_s/FeO profile could be generated at the surface if MPU-A grew rapidly by degradation of boulders. This model requires that MPU-B was deposited on top of MPU-A while the boulders were still sufficiently large to be producing fillets, in which case the boulders are still buried at the site. In the second scenario, the regolith breccia was excavated and exposed at the surface at a different location. Some maturation of the soil occurred at this time, perhaps with input of other material. A subsequent impact deposited this regolith as MPU-A at the 60001-7 site in such a way to homogenize any I_s/FeO variation with depth that may have existed. MPU-B and MPU-C may have been deposited by the same impact (section 6.4).

What is the significance of the two sodic plagioclase particles containing plagioclase with An_{90} compositions? The two particles were recovered 10 cm apart in 60002 and I have not observed similar particles among almost 200 soil particles studied from Apollo 16 soils (mostly surface). The topmost sample of <1-mm fines from 60001 is anomalously enriched in both Na and Eu and this is entirely consistent with plagioclase such as particles 2.13 and 2.31. However, petrographic studies have not reported a large fraction of An_{90} plagioclase in MPU-A compared with other units of the core (*Vaniman et al.,* 1976; *Meyer et al.,* 1975). Thus, while the two particles of An_{90} plagioclase are not sampling anomalies, neither can they be volumetrically important components of these soils. *Vaniman et al.* (1976) note, however, that there is a distinct difference in the nature of the plagioclase in MPU-A. Compositions of monomineralic feldspar grains in MPU-A scatter over the same range of compositions observed in other units (An_{90-98}), but the cluster of compositions observed in other units at An_{96-97} does not occur, resulting in a slightly lower average anorthite concentration for MPU-A (An_{95-96}). Also, in other units plagioclase single crystals are "typically unstrained, unsheared and lack polygonal or other recrystallization textures" whereas feldspar fragments from MPU-A were "extensively modified by shear and recrystallization features." Plagioclase such as this is a principal clast type in some of the regolith breccia particles from MPU-A (section 5.2.3). Thus, the Na enrichment in the <1-mm fines from MPU-A almost certainly results from lithologies containing plagioclase more sodic on the average than that from other units in the core, but particles 2.13 and 2.31 are not good representatives of that plagioclase. The lithology from which such sodic plagioclase derives is not known.

6.3. Mare Basalt in MPU-B

The mixing model indicates that soil at the top of 60001-7 (MPU-C and MPU-D), like the soil in 60009/10, contains on the average no mare basalt component in excess of that which may be carried by the Cayley soil component (Fig. 23). However, the Sc enrichment and low La/Sm ratio in MPU-B requires a model component of about 0.5% to 1.5% mare basalt. This component is distributed rather uniformly through the thick unit, although it is slightly more concentrated between 142 and 172 cm depth. The model also indicates that the 60005 soils contain a similar concentration of mare basalt component. Although the soils have the chemical signature of mare material, compositional data cannot be used to distinguish whether the material occurs as fragments of basalt, pyroclastic glass, or some type of impact product. Clearly, some discrete fragments of mare basalt occur; a number of these have been recovered and studied from 60003 (*Delano,* 1975) and a fragment of mare basalt is the likely cause of the anomalous sample at 132 cm depth (section 5.1.4). However, the distribution pattern suggests that most of the mare material is fine grained, thus the mare glass fragments observed in petrologic studies (*Naney et al.,* 1976; *Meyer et al.,* 1975; *Meyer and McCallister,* 1976) probably carry much of the chemical signature of mare basalt.

The enrichment in mare basalt component in MPU-B is reminiscent of the 64001/2 double drive tube at Station 4 on Stone Mountain, 4 km to the south of the LM/ALSEP site (Fig. 1). In that core, all material between 48 and 26 cm depth (possibly higher, as the upper tube was not studied at high resolution) is enriched in mare material by an average of about 1.5% compared with soil below that (to the bottom of the core at 60 cm depth; Fig. 25) (*Korotev et al.,* 1984). The unenriched unit in 64001 is "normal" and, in fact, is very similar in composition to the MPU-D soil at the top of 60007 and to 60601 (section 3.1). Within the unit enriched in mare material in 64001 are two or possibly three thin bands (1-1.5 cm wide) containing higher concentrations of mare material (i.e., high Sc and low La/Sm; Fig. 25). The band at 42 cm depth contains up to 12% mare material that apparently occurs in the form of small particles of impact glass or regolith breccias (J. W. Delano and A. Basu, personal communication, 1990). No similar bands of extreme enrichment of mare material occur in 60001-7. None of the surface and trench soils from Apollo 16 are similar to the units enriched in mare material found in 64001 and 60001-7.

6.4. Siderophile Elements in MPU-B

The mixing model results for 60001-7 reflect the arguments made in section 5.1.7 that the siderophile-element enrichment at 177-187 cm depth derives primarily from a layer of chondritic material, not Fe-Ni metal such as found in mafic impact-melt breccias (Fig. 23). At the peak of the enrichment, there is a 4% component (CI equivalent) of chondritic material, compared with about 1% for most of the length of the core. The model results also suggest a smaller chondrite-rich layer at the top of 60003, between about 105 and 113 cm depth. (This is somewhat more evident in the smoothed model results of Fig. 23 than in the raw data of Figs. 12 and 17.) The entire MPU-B section (103-187 cm depth) is enriched in the CI component compared with other units of the core and to the 60009/10 soils (Fig. 9).

The model does, in fact, indicate a slight increase in the average concentration of ancient Fe-Ni metal component between 177 cm and 187 cm depth, but I suspect that this

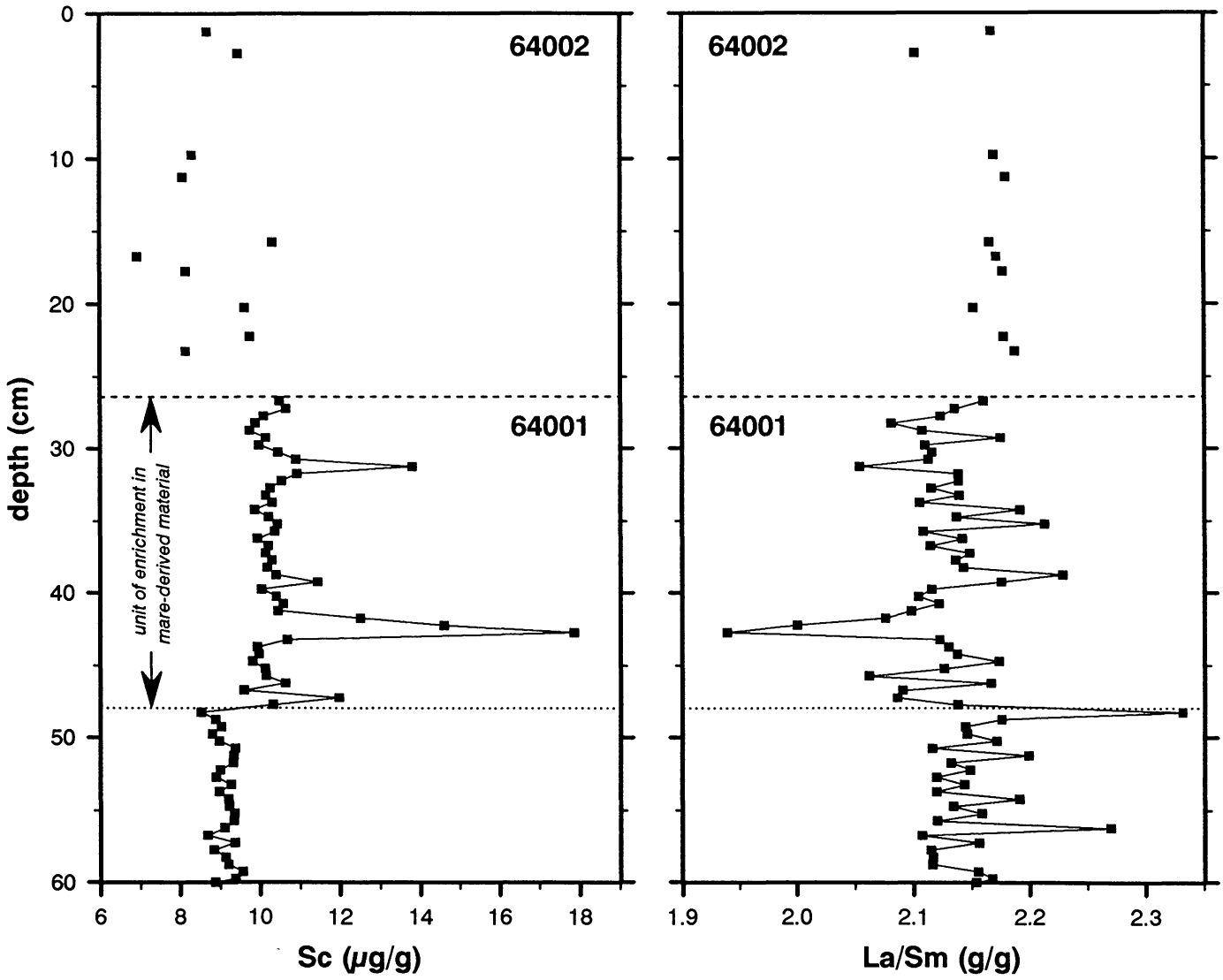

Fig. 25. Depth profiles for Sc and La/Sm in the 64001/2 double-drive tube from Station 4 (*Korotev,* 1982; *Korotev et al.,* 1984; Korotev, unpublished data, 1990). Only 10 samples from 64002 were studied; the dashed lines mark the boundary between the core tubes. The dotted line represents the boundary between the unit enriched in mare material and "normal" soil below. Within the enriched unit, thin bands of soil even more enriched in mare-derived material occur at 31, 42, and possibly 47 cm depth.

results more from a failure of the model to distinguish between the two siderophile-element-rich components than it does from an actual increase in the fraction of ancient Fe-Ni metal. It is important to recognize that the ancient Fe-Ni metal component of the model is *not* just any Ni-bearing, metallic iron (such as that in ordinary chondrites), but metal such as that found in mafic impact-melt breccias with the characteristic siderophile-element signature of the component in Table 3.

Another curious aspect of MPU-B is that all the samples with anomalously high Au concentrations (e.g., Au/Ir ratios exceeding ~1; Fig. 12 and section 5.1.6) occur within this unit (except for one sample at the very top of MPU-A at 188 cm depth and a few samples with marginally high Au/Ir ratios in 60005). Although Au is a notorious contaminant, I suspect that these anomalously high Au concentrations are not a result of contamination because I can think of no reason that Au contamination would be restricted to samples from this region of the core during handling in our laboratory. As discussed in section 2.2, the samples were analyzed in three irradiations. Samples between 84 and 160 cm depth were prepared for analysis in May 1989 and samples between 160 cm depth and the bottom of the core were prepared in July 1989. Gold-rich samples occur in both batches, but only in those samples from MPU-B. Within each batch, samples were prepared in random order with respect to stratigraphic position. If the anomalously high Au concentrations in some samples are not the result of terrestrial contamination, then they are probably the result of

some vapor-deposition process, possibly associated with volatilization during the impact event causing the siderophile-element enrichments at the bottom (and top?) of the unit.

The constancy of lithophile-element concentrations through MPU-B plus the enrichment of this soil in both siderophile elements and mare material confirms the results of earlier studies that MPU-B represents a thick unit of related fines that probably all derive from the same source. Much of the early work on the deep drill core addressed the issue of how many events were required to deposit the various units, whether MPU-B contained any subunits, and, in particular, whether the boundary between MPU-A and MPU-B (187 cm depth) represents an old surface (*Russ,* 1973; *Gose and Morris,* 1977; *Heymann et al.,* 1978). Unfortunately, compositional data do not provide chronological constraints. *Gose and Morris* (1977) observe that the simplest interpretation of their data is that all soil below MPU-D (i.e., below ~13 cm depth) was deposited in a single event, but caution that this soil may have been deposited by "a series of closely spaced events." The data obtained here cannot be used to distinguish between these alternatives. Compositional variations with depth such as those observed in 60001-7 (or 60009/10) could probably occur even if the entire core had been emplaced in a single impact event, given an appropriately layered target. Thus, although the data indicate a major compositional discontinuity at 187 cm depth and a minor discontinuity at 145 cm depth (section 5.1.3), they do not require that these discontinuities represent old surfaces.

If MPU-A and MPU-B were both deposited in a single impact event, as preferred by *Gose and Morris* (1977), the data obtained here indicate only that a sharp boundary and a meteorite-rich layer present in the target material were preserved during deposition. If, however, MPU-B were deposited later than MPU-A, then it becomes useful to speculate on the nature of the deposition events. Either of the models for MPU-A discussed above is adequate. The observation that the bottom of the MPU-B layer is rich in siderophile elements constrains the mechanism of emplacement of that unit. The band of siderophile-element enrichment is sharply discontinuous below and grades more gradually into the overlying soil (Fig. 17). It might be possible to generate such a feature by some type of direct, but heterogeneous, deposition of fine material. For example, the model of *Heymann et al.* (1978) provides one possible sequence of events: (1) An impact of an ordinary chondrite excavated a crater and some fine-grained, glassy debris (section 5.1.7) from the projectile was concentrated on the walls of the crater (fall back?), (2) MPU-A was deposited at the bottom of the crater, and (3) MPU-B was deposited on top of MPU-A by overturning and slumping of the crater walls in such a way that the meteorite-rich material was concentrated at the bottom. However, the feature could also be explained if (1) a meteorite-rich breccia or clod, such as regolith breccia 63507 (section 5.1.7), was deposited on the MPU-A surface (along with other debris), (2) the breccia was eroded by subsequent impacts, and (3) the core passed through the fillet. Unfortunately, a single one-dimensional regolith sample is not sufficient to constrain what is undoubtedly a complicated stratigraphic scenario.

7. SUMMARY AND CONCLUSIONS

Fines from the 60009/10 double drive tube are highly variable in composition. At one extreme is a layer of soil between 18 and 21 cm depth that has the greatest concentrations of ITEs and elements associated with mafic mineral phases (Fe, Sc, Cr). Relatively mafic and ITE-rich soils such as these are common at Apollo 16; soils of generally similar composition occur both as surface and trench samples at Stations 5 and 6, about 3 km to the south, as well as in other cores (60001-7 and 64001). Such soils appear to have an affinity with the Cayley Plains as their composition is similar to that inferred for the Cayley Plains west of the landing site based on orbital geochemical data. At the other extreme are soils between 52 and 55 cm depth, which have very low concentrations of ITEs, Fe, Sc, and Cr as a result of a large component of ferroan anorthosite that occurs primarily as coarse-grained single crystals of plagioclase. None of the approximately 40 samples of Apollo 16 surface and trench soils is as rich in plagioclase as the most plagioclase-rich soil in 60009/10. Thus, the vertical variation in composition within the 0.6-m length of this core exceeds that of soils collected at the surface of the site over 8 km of lateral traverse.

To a good first approximation, the variation in lithophile-element concentrations among soils in 60009/10 can be modeled as binary mixing between an anorthosite component and a "Cayley soil component." The anorthosite component is ferroan anorthosite containing ~99% plagioclase and not some more mafic variety. The Cayley soil component is represented by the most mafic, ITE-rich soils. The Cayley soil component is itself a mixture of various subcomponents such as impact-melt breccias, fragmental breccias, regolith breccias, granulitic breccias, and mare material (basalt and glass), each with a range of compositions. The linearity of mixing lines on two-element concentration plots argues that the relative abundances of these various subcomponents are sufficiently uniform from sample to sample and from region to region in the core that the mixture behaves effectively as a single component. Although the soils are complicated mixtures of many components, the last major mixing event they record is that between anorthosite with a very high plagioclase content and a previously homogenized mixture of more mafic components.

The scatter about the mixing lines shows, however, that the various subcomponents of the Cayley soil component, although well mixed, are not perfectly mixed. Minor variation in the plagioclase composition of the anorthosite also causes scatter about the mixing lines in plots involving Na, Ca, and Eu. These nonuniformities occur at two levels. At a trivial level, an individual small subsample of soil may contain a volumetrically significant amount (perhaps a single large grain) of some compositionally distinct component that draws the sample off the binary mixing line. This is essentially a sampling problem, but one that is common among the 50-mg samples analyzed here. At a more geologically interesting level, a set of stratigraphically consecutive samples may plot off the mixing line because they contain a higher (or lower) proportion than average of some compositionally distinct lithology. For

example, the six samples between 18 and 21 cm depth in 60009/10 contain a greater-than-average proportion of poikilitic impact-melt breccias, which causes these samples to plot slightly on the high-Sm side of the mixing line on a Sm vs. Sc plot. Although deviations such as this are important because they may suggest a unique source or provenance for a particular layer of soil, they have a minor effect on overall composition compared with the effect associated with the variation in the concentration of anorthosite. The ratio of anorthosite to Cayley soil component is large, ranging from 75/25 to 0/100 in the 60009/10 soils. Because the plagioclase concentration of the ferroan anorthosite component of 60009/10 is very high (~99%), the anorthosites of similarly high plagioclase concentration found as hand specimens at Apollo 16 are probably typical of their source and not the result of sampling bias that discriminated against more mafic samples. Nearly all the large samples of ferroan anorthosite returned from the Moon are from Apollo 16; such plagioclase-rich rocks may be atypical samples of the lunar crust.

The 60001-7 drill core was collected about 37 m away from the 60009/10 drive tube. Data presented here show that the contents of core section 60006, which was only 80% full when opened, was physically disturbed and partially mixed after it was disconnected from the adjacent core sections. Because the 60005 section was also only partially full, the core samples retain no stratigraphic information between about 22 and 103 cm depth. It is possible that soil in the 60007 section (surface to 22 cm depth) has also been disturbed and that the 7-cm-wide contact it contains, represented by the gradually systematic variation of composition and other parameters with depth observed in samples between about 10 and 17 cm, may actually be sharper than this on the lunar surface.

Soils from the top half of the core (60005-7) generally follow the mixing trend defined by the 60009/10 soils, indicating that the anorthosite component of both cores contains ~99% plagioclase. A unit rich in anorthosite occurs at about 20 cm depth. Although this unit is not as feldspathic as the two feldspathic layers in 60009/10, it is still more feldspathic (higher Ca, lower Sc and Fe concentrations) than any surface or trench soil from Apollo 16, including 61221 and the North Ray Crater soils. The composition corresponds to about 55% Cayley soil component and 45% anorthosite component. This unit may be related to the anorthositic units in 60009/10, but there is no way to know whether a single stratigraphically continuous layer was sampled by both cores. No other unit of compositionally distinct soil in 60001-7 correlates with any of those observed in 60009/10, except that the soils at the top of both cores are similar to each other.

Soils from the bottom half of the deep drill core (60001-4) also generally follow the Cayley soil-anorthosite mixing trend defined by the 60009/10 soils, but with some important deviations. Samples between 103 and 187 cm depth (mostly 60003 and 60004) are similar to typical Cayley soils in having a low proportion of anorthosite component, but are different from soils of generally similar composition from 60009/10 in being slightly enriched in Sc as a result of a 1 ± 1% component of mare material (crystalline basalt and/or glass) in excess of that which may be present in typical Cayley soil. (One sample of 60004 analyzed here contains 10% mare basalt.) The presence of mare material is indicated by higher Sc concentrations and lower La/Sm ratios in these soils. Although the mare material causes distinct deviations from the binary mixing line in the high-Sc direction on two-element plots involving Sc, it is of minor importance volumetrically compared with the large variation in the abundance of anorthosite.

A significant compositional discontinuity occurs at 187 cm depth in the deep-drill core. Compared to the soil between 103 and 187 cm depth (60003/4), the immature soils between 187 cm depth and the bottom of the core at 220 cm depth (mostly 60001/2) are enriched in Na by a factor of 1.08, probably as a result of a slightly lower average anorthite concentration of the plagioclase. They also have slightly higher concentrations of ITEs and normal concentrations of Sc (no mare component). Although generally similar to the Cayley soils in composition, the 60001/2 fines cannot be modeled as Cayley soil plus (or minus) anorthosite and small proportions of lithologies observed as >1-mm particles in 60002. The 60001/2 soils are of a different provenance than the Cayley soils, a conclusion supported by petrographic data. Among >1-mm particles examined from 60001 and 60002 are a number of regolith breccias with compositions similar to those of the <1-mm fines. Both the fines and some of the particles from 60001/2 probably derive in large part from comminution of larger regolith breccias.

Siderophile elements in <1-mm fines from both cores are carried by two components, both ultimately of meteoritic origin. One is a component of chondritic meteorite. The other is "ancient" Fe-Ni metal such as that found in mafic impact-melt breccias that were formed about 3.9 Ga ago. Typical soils from either core have about 1% chondritic meteorite component (volatile-free CI equivalent) and about 0.3% "ancient" Fe-Ni metal component. Concentrations of Fe-Ni metal are highly variable from sample to sample and concentrations as high as 5% occur in some 50-mg samples of <1-mm fines analyzed here as a result of occasional large metal grains. There is no systematic variation in the Fe-Ni metal component with depth except that the lowest concentrations occur in the most anorthositic soils. This is because the metal is associated with the mafic impact-melt breccias, which are a principal subcomponent of the Cayley component of the soils. The mafic impact-melt breccias are also a principal carrier of mafic silicates and the principal carriers of ITEs in the soils. As a consequence of these associations, magnetic separates made in earlier studies of 60009/10 soils were enriched in ITEs, siderophile elements, and elements associated with mafic silicates (Sc, Cr) because they were enriched in mafic impact-melt breccias at the expense of ferroan anorthosite.

The unit of soil in the deep-drill core between 103 cm and 187 cm depth that is enriched in mare material is also enriched slightly in siderophile elements compared with other units in the core. At the very bottom of this unit, however, is a zone (177-187 cm depth) that is considerably enriched in siderophile elements. Ratios among Cr, Fe^0, and siderophile elements in this zone are not consistent with Fe-Ni metal like that from mafic melt breccias, but are generally consistent with

an H chondrite in which the metal/silicate ratio is ~40/60. At the peak of this zone, siderophile-element concentrations are equivalent to a ~4% CI component. The enrichments terminate sharply at the bottom of the zone, but diminish gradually upward. A zone of slight enrichment in siderophile elements also appears in 60009/10 at 12-17 cm depth. This zone has about 1.8% CI component at its maximum compared with the core average of 1.0%.

The observations made here that compositional variations with depth over distances of a few centimeters are large compared with variations at the surface over distances of kilometers have important consequences for interpretation of data obtained remotely from orbit (e.g., *Clark et al.,* 1990), which is only obtained from the upper few micrometers to centimeters of regolith.

APPENDIX

A1. Miscellaneous Observations on Previous Studies

A1.1. SU2 in 60010. Samples from SU2 in 60010 were analyzed by INAA by both *Blanchard and Brannon* (1977) and *Ali and Ehmann* (1977). Both of these groups studied splits of parent sample 60010,89 at 20-20.5 cm depth from the first dissection column, but the two groups obtained different results. *Blanchard and Brannon* (1977) analyzed three samples of subsplit 60010,3107: two submillimeter grain-size fractions and a sample of unsieved soil. The 90-150-μm and <20-μm grain-size fractions are both similar in composition to the seven samples of <1-mm fines from SU2 analyzed here in having concentrations of Sc, Sm, and related elements at the high end of the range observed among the core samples. However, the unsieved sample is dissimilar to any of the nearly 600 samples of <1-mm fines from Apollo 16 analyzed in this laboratory, being rich in both Sc and ITEs (Sc: 13.2 μg/g, Sm: 8.5 μg/g). These anomalies are probably attributable to the presence of a single large mineral or lithic grain in the small sample analyzed (mass not reported, but probably 20-50 mg), although it is curious that the sample plots on the extension of the mixing line of Fig. 4 (not shown). Sample 60010,3107 is an immature soil with a bimodal grain-size distribution (*McKay et al.,* 1977), so anomalies due to coarse-grained material of unusual composition are likely (e.g., *Morris et al.,* 1989; *Korotev,* 1989). Thus, I believe that the subsample analyzed by *Blanchard and Brannon* (1977) was anomalous.

Unexpectedly, the split from the same sample studied of *Ali and Ehmann* (1977) (60010,191) is not similar to any of those studied here or by *Blanchard and Brannon* (1977) from SU2. The reported composition is generally similar to that of the average core soil (e.g., Sc: 8.3 μg/g, Sm: 5.7 μg/g). A large fragment of anorthosite in the analyzed sample could account for this difference.

A1.2. Incorrect depth for 60010,40. Sample 60010,40 of *Ali and Ehmann* (1977) (section 3.1.5) is plotted at an incorrect depth on all their figures (at 3.5 cm depth instead of 0.35 cm). The split was obtained from parent sample 60010,11 (0.3-0.4 cm), which was one of a set of special samples at the top of the core taken at 1 mm intervals instead of the usual 5 mm intervals (*Fruland et al.,* 1982, Table 3.3).

A1.3. Olivine quench rock. *Vaniman et al.* (1976) describe, in their discussion of hard-to-categorize lithologies observed in 60001-7, an "olivine quench rock," although they do not say at what depth it was found. The fragment may be rich in olivine because it contains a very high proportion of meteoritic silicates. The texture of this rock (Fig. 5 of *Vaniman et al.,* 1976) is similar to that of two olivine-rich glassy particles from 65502 containing over 50% chondritic material, one of which is a sphere [compositional discussion in *Korotev* (1983) and subsequent petrographic examination].

A2. Sc-Sm Mixing Line for 60009/10

It is not clear, at least to the author, what regression model is most appropriate for fitting a line to the data of Fig. 4. The choice is important to the extent it effects (1) interpretation of the line as a mixing line and (2) extrapolation of the line in the low-Sc direction to obtain a composition for the low-Sc mixing component (section 4.1.1). Most of the scatter about the line is sampling scatter, not analytical scatter, because both elements are determined with high precision. Simple linear regression (e.g., Sm against Sc) is inappropriate because it assumes that all the "uncertainty" (analytical or sampling) is with one element or the other, and this is not true. For example, simple regression of Sm against Sc ($Sm = 0.6416 \cdot Sc - 0.007$) leads to a line that nearly intersects the origin, but which is "too horizontal." I have chosen, somewhat arbitrarily, to use the regression method of *York* (1969) with 2% of the concentration value of each element used as the "uncertainty" (any constant percentage leads to the same result). This yields the equation $Sm = Sc \cdot 0.6756 - 0.269$, which has a Sc intercept at 0.40 μg/g Sc. This line is used throughout this work as a reference line for comparing results for other samples. In Figs. 4, 5, 13, 14, 18, and 19, the solid portion of the line is bounded by the (Sc,Sm) points (2.82,1.636) and (10.62,6.906), which are points on the regression line at the lowest and highest Sc concentrations observed in the <1-mm fines from 60009/10.

Acknowledgments. I greatly appreciate the expertise and assistance of B. L. Jolliff in preparation and petrographic examination of the thin sections. I thank C. Satterwhite, K. Willis, and L. Watts of the JSC curatorial staff for their efforts in providing the large number of samples discussed here and the personnel of the University of Missouri Research Reactor for their skill in irradiating them. The paper has benefited by the comments and reviews of L. A. Haskin, D. J. Lindstrom, S. B. Simon, and especially A. Basu; the author appreciates their stamina. This research was supported by NASA grant NAG 9-56 to L. A. Haskin and a DOE reactor-sharing grant to the University of Missouri Research Reactor.

REFERENCES

Ali M. Z. and Ehmann W. D. (1976) Chemical characterization of lunar core 60009. *Proc. Lunar Sci. Conf. 7th,* pp. 241-258.

Ali M. Z. and Ehmann W. D. (1977) Chemical characterization of lunar core 60010. *Proc. Lunar Sci. Conf. 8th,* pp. 2967-2981.

Allton J. H. and Waltz S. R. (1980) Depth scales for Apollo 15, 16, and 17 drill cores. *Proc. Apollo 11 Lunar Sci. Conf.,* pp. 1463-1477.

Allton J., Waltz S., and Dardano C. (1981) *Table of Sample Depths for Apollo 15, 16, and 17 Drill Cores.* Curatorial Branch Publ. No. 56, NASA Johnson Space Center, Houston.

Anders E. and Grevesse N. (1989) Abundances of the elements: Meteoritic and solar. *Geochim. Cosmochim. Acta, 53,* 197-214.

Anders E., Ganapathy R., Krähenbühl U., and Morgan J.W. (1973) Meteoritic material on the Moon. *Moon, 8,* 3-24.

Basu A. and McKay D. S. (1989) Regolith breccias as precursors of present day regolith on the Moon (abstract). In *Lunar and Planetary Science XIX,* pp. 50-51. Lunar and Planetary Institute, Houston.

Beatty D. W., Hill S. M. R., Albee A. L., Ma M.-S., and Schmitt R. A. (1979) The petrology and chemistry of basaltic fragments from Apollo 11 soil, part I. *Proc. Lunar Planet. Sci. Conf. 10th,* pp. 41-75.

Bischoff A., Palme H., Weber H.W., Stöffler D., Braun O., Spettel B., Begemann F., Wänke H., and Ostertag R. (1987) Petrography, shock history, chemical composition and noble gas content of the lunar meteorites Yamato-82192 and -82193. *Mem. Natl. Inst. Polar Res., Spec. Issue 46,* pp. 21-42. Natl. Inst. of Polar Res., Tokyo.

Blanchard D. P. and Brannon J. C. (1977) Effects on composition of maturation in a well documented, isochemical suite of soils from drive tube 60009/10 (abstract). In *Lunar Science VIII,* pp. 121-123. The Lunar Science Institute, Houston.

Blanchard D. P., Korotev R. L., Brannon J. C., Jacobs J. W., Haskin L. A., Reid A. M., Donaldson C. H., and Brown R. W. (1975) A geochemical and petrographic study of 1-2 mm fines from Apollo 17. *Proc. Lunar Sci. Conf. 6th,* pp. 2321-2341.

Blanchard D. P., Jacobs J. W., Brannon J. C., and Brown R. W. (1976) Drive tube 60009: A chemical study of magnetic separates of size fractions from five strata. *Proc. Lunar Sci. Conf. 7th,* pp. 281-294.

Bogard D. D. and Hirsch W. C. (1975) Noble gas studies on grain size separates of Apollo 15 and 16 deep drill cores. *Proc. Lunar Sci. Conf. 6th,* pp. 2057-2083.

Boynton W. V., Baedecker P. A., Chou C.-L., Robinson K. L., and Wasson J. T. (1975) Mixing and transport of lunar surface materials: Evidence obtained by the determination of lithophile, siderophile, and volatile elements. *Proc. Lunar Sci. Conf. 6th,* pp. 2241-2259.

Boynton W. V., Chou C.-L., Robinson K. L., Warren P. H., and Wasson J. T. (1976) Lithophiles, siderophiles, and volatiles in Apollo 16 soils and rocks. *Proc. Lunar Sci. Conf. 7th,* pp. 727-742.

Carrier W. D. III (1974) Apollo drill core depth relationships. *Moon, 10,* 183-194.

Clark P. E., Hawke B. R., and Basu A. (1990) The relationship between orbital, Earth-based, and sample data for lunar landing sites. *Proc. Lunar Planet. Sci. Conf. 20th,* pp. 147-160.

Delano J. W. (1975) Petrology of the Apollo 16 mare component: Mare Nectaris. *Proc. Lunar Sci. Conf. 6th,* pp. 15-47.

Dowty E., Keil K., and Prinz M. (1974) Igneous rocks from Apollo 16 rake samples. *Proc. Lunar Sci. Conf. 5th,* pp. 431-445.

Duke M. B. and Nagle J. S. (1976) *Lunar Core Catalog* (and Supplements). JSC Publ. No. 09252, NASA Johnson Space Center, Houston.

Ehmann W. D., Ali M. Z., and Hossain T. I. M. (1977) Chemical characterization of lunar core 60003 (abstract). In *Lunar Science VII,* pp. 275-276. The Lunar Science Institute, Houston.

Fruland R. M. and Reimold J. N. (1981) *Introduction to the Core Samples from the Apollo 16 Landing Site.* Curatorial Branch Publ. No. 58, JSC Publ. No. 17659, NASA Johnson Space Center, Houston. 50 pp.

Fruland R. M., Nagle J. S., and Allton J. H. (1982) *Catalog of the Apollo 16 Lunar Core 60009/60010.* JSC Publ. No. 17172, NASA Johnson Space Center, Houston. 155 pp.

Ganapathy R., Morgan J. W., Higuchi H., Anders E., and Anderson A. T. (1974) Meteoritic and volatile elements in Apollo 16 rocks and in separated phases from 14306. *Proc. Lunar Sci. Conf. 5th,* pp. 1659-1681.

Gibbons R. V., Hörz F., and Schall R. B. (1976) The chemistry of some individual lunar soil agglutinates. *Proc. Lunar Sci. Conf. 8th,* pp. 405-422.

Goldstein J. I. and Axon H. J. (1973) Composition, structure, and thermal history of metallic particles from 3 Apollo 16 soils, 65701, 68501, and 63501. *Proc. Lunar Sci. Conf. 4th,* pp. 751-775.

Goldstein J. I., Axon H. J., and Agrell S. O. (1975) The grape cluster, metal particle 63344,1. *Earth Planet. Sci. Lett., 28,* 217-224.

Goodrich C. A. and Keil K. (1987) Mare basalts and other clasts in Yamato lunar meteorites Y-791197, -82192 and -82193. *Mem. Natl. Inst. Polar Res., Spec. Issue 46,* pp. 56-70. Natl. Inst. of Polar Res., Tokyo.

Gose W. A. and Morris R. V. (1977) Depositional history of the Apollo 16 deep drill core. *Proc. Lunar Sci. Conf. 8th,* pp. 2909-2928.

Govindaraju K. (1980) Report (1980) on three GIT-IWG rock reference samples: Anorthosite from Greenland, AN-G; Basalte d'Essey-la-Côte, BE-N; Granite de Beauvoir, MA-N. *Geostandards Newslett., 4,* 49-138.

Hansen E. C., Steele I. M., and Smith J. V. (1979) Lunar highland rocks: Element partitioning among minerals I: Electron microprobe analyses of Na, Mg, K and Fe in plagioclase; *mg* partitioning with orthopyroxene. *Proc. Lunar Planet. Sci. Conf. 10th,* pp. 627-638.

Haskin L. A. and Lindstrom D. J. (1988) On identifying parent plutonic rocks from lunar breccia and soil fragments. *Proc. Lunar Planet. Sci. Conf. 18th,* pp. 1-9.

Haskin L. A., Helmke P. A., Blanchard D. P., Jacobs J. W., and Telander K. (1973) Major and trace element abundances in samples from the lunar highlands. *Proc. Lunar Sci. Conf. 4th,* pp. 1275-1296.

Haskin L. A., Lindstrom M. M., Salpas P. A., and Lindstrom D. J. (1981) On compositional variations among lunar anorthosites. *Proc. Lunar Planet. Sci. 12B,* pp. 41-66.

Hertogen J., Janssens H., Takahashi H., Palme H., and Anders E. (1977) Lunar basins and craters: Evidence for systematic compositional changes of the bombarding population. *Proc. Lunar Sci. Conf. 8th,* pp. 17-45.

Heymann D., Jordan J. L., Walker A., Dziczkaniec M., Ray J., and Palma R. (1978) Inert gas measurements in the Apollo-16 drill core and an evaluation of the stratigraphy and depositional history of this core. *Proc. Lunar Planet. Sci. Conf. 9th,* pp. 1885-1912.

Hörz F., Cintala M. J., See T. H., Cardenas F., and Thompson T. D. (1984) Grain size evolution and fractionation trends in an experimental regolith. *Proc. Lunar Planet. Sci. Conf. 15th,* in *J. Geophys. Res., 90,* C183-C196.

Housley R. M., Cirlin E. H., Paton N. E., and Goldberg I. B. (1974) Solar wind and micrometeorite alteration of the lunar regolith. *Proc. Lunar Sci. Conf. 5th,* pp. 2623-2642.

Hu H.-N. and Taylor L. A. (1977) Lack of chemical fractionation in major and minor elements during agglutinate formation. *Proc. Lunar Sci. Conf. 8th,* pp. 3645-3656.

James O. B., Lindstrom M. M., and Flohr M. K. (1989) Ferroan anorthosite from lunar breccia 64435: Implications for the origin and history of lunar ferroan anorthosites. *Proc. Lunar Planet. Sci. Conf. 19th,* pp. 219-243.

Jolliff B. L. (1990) General petrography and bulk composition of lunar meteorite MAC88105 (abstract). In *Lunar and Planetary Science XXI,* pp. 573-574. Lunar and Planetary Institute, Houston.

Korotev R. L. (1976) Geochemistry of grain-size fractions of soils from the Taurus-Littrow valley floor. *Proc. Lunar Sci. Conf. 7th,* pp. 695-726.

Korotev R. L. (1981) Compositional trends in Apollo 16 soils. *Proc. Lunar Planet. Sci. 12B,* pp. 577-605.

Korotev R. L. (1982) Comparative geochemistry of Apollo 16 surface soils and samples from cores 64002 and 60002 through 60007.

Proc. Lunar Planet. Sci. Conf. 13th, in *J. Geophys. Res., 87,* A269-A278.

Korotev R. L. (1983) Geochemical study of individual 1-2 mm particles from Apollo 16 soil 65502 (abstract). In *Lunar and Planetary Science XIV,* pp. 397-398. Lunar and Planetary Institute, Houston.

Korotev R. L. (1987a) National Bureau of Standards coal flyash (SRM 1633a) as a multielement standard for instrumental neutron activation analysis. *J. Radioanal. Nucl. Chem., 110,* 159-177.

Korotev R. L. (1987b) The nature of the meteoritic components of Apollo 16 soil, as inferred from correlations of iron, cobalt, iridium, and gold with nickel. *Proc. Lunar Planet. Sci. Conf. 17th,* in *J. Geophys. Res., 92,* E447-E461.

Korotev R. L. (1987c) The meteoritic component of Apollo 16 noritic impact melt breccias. *Proc. Lunar Planet. Sci. Conf. 17th,* in *J. Geophys. Res., 92,* E491-E512.

Korotev R. L. (1987d) Mixing levels, the Apennine Front soil component, and compositional trends in Apollo 15 soils. *Proc. Lunar Planet. Sci. Conf. 17th,* in *J. Geophys. Res., 92,* E411-E431.

Korotev R. L. (1989) Geochemistry of grain-size fractions of Luna 24 soil: Comments on "The lunar regolith: Chemistry and petrology of Luna 24 grain size fractions" by J. C. Laul, O. D. Rode, S. B. Simon, and J. J. Papike. *Geochim. Cosmochim. Acta, 53,* 3061-3065.

Korotev R. L. (1990a) Cobalt and nickel concentrations in the "komatiite component" of Apollo 16 polymict samples. *Earth Planet. Sci. Lett., 96,* 481-489.

Korotev R. L. (1990b) Are Apollo 16 soils foreign to the Apollo 16 site? (abstract). In *Lunar and Planetary Science XXI,* pp. 657-658. Lunar and Planetary Institute, Houston.

Korotev R. L. and Haskin L. A. (1988) Europium mass balance in polymict samples and implications for plutonic rocks of the lunar crust. *Geochim. Cosmochim. Acta, 52,* 1795-1813.

Korotev R. L., Lindstrom M. M., Lindstrom D. J., and Haskin L. A. (1983) Antarctic meteorite ALHA81005—Not just another lunar anorthositic norite. *Geophys. Res. Lett., 10,* 829-832.

Korotev R. L., Morris R. V., and Lauer H. V. Jr. (1984) Stratigraphy and geochemistry of the Stone Mountain core (64001/2). *Proc. Lunar Planet. Sci. Conf. 15th,* in *J. Geophys. Res., 89,* C143-C160.

Lindstrom D. J. and Korotev R. L. (1982) TEABAGS: Computer programs for instrumental neutron activation analysis. *J. Radioanal. Chem., 70,* 439-458.

Lindstrom M. M., Knapp S. A., Shervais J. W., and Taylor L. A. (1984) Magnesian anorthosites and associated troctolites and dunite in Apollo 14 breccias. *Proc. Lunar Planet. Sci. Conf. 15th,* in *J. Geophys. Res., 89,* C41-C49.

McKay D. S. and Wentworth S. J. (1990) Natural reduction of lunar iron oxide (abstract). In *Lunar and Planetary Science XXI,* pp. 769-770. Lunar and Planetary Institute, Houston.

McKay D. S., Heiken G. H., Taylor R. M., Clanton U. S., Morrison D. A., and Ladle G. H. (1972) Apollo 14 soils: Size distribution and particle types. *Proc. Lunar Sci. Conf. 3rd,* pp. 983-994.

McKay D. S., Fruland R. M., and Heiken G. H. (1974) Grain size and the evolution of lunar soil. *Proc. Lunar Sci. Conf. 5th,* pp. 887-906.

McKay D. S., Morris R. V., Dungan M. A., Fruland R. M., and Fuhrman R. (1976) Comparative studies of grain size separates of 60009. *Proc. Lunar Sci. Conf. 7th,* pp. 295-313.

McKay D. S., Dungan M. A., Morris R. V., and Fruland R. M. (1977) Grain size, petrographic, and FMR studies of double core 60009/10: A study of soil evolution. *Proc. Lunar Sci. Conf. 8th,* pp. 2929-2952.

McKay D. S., Bogard D. D., Morris R. V., Korotev R. L., Johnson P., and Wentworth S. J. (1986) Apollo 16 regolith breccias: Characterization and evidence for early formation in the mega-regolith. *Proc. Lunar Planet. Sci. Conf. 16th,* in *J. Geophys. Res., 91,* D277-D303.

Metzger A. E., Etchegaray-Ramirez M. I., and Haines E. L. (1981) Thorium concentrations in the lunar surface: V. Deconvolution of the central highlands region. *Proc. Lunar Planet. Sci. 12B,* pp. 751-766.

Meyer H. O. A. and McCallister R. H. (1976) Mineral, lithic, and glass clasts <1 mm size in Apollo 16 core section 60003. *Proc. Lunar Sci. Conf. 7th,* pp. 185-198.

Meyer H. O. A. and Tsai H.-M. (1975) Lunar glass compositions: Apollo 16 core sections 60002 and 60004. *Earth Planet. Sci. Lett., 28,* 234-240.

Meyer H. O. A., McCallister R. H., and Tsai H.-M. (1975) Mineralogy and petrology of <1 mm fines from Apollo 16 core sections 60002 and 60004. *Proc. Lunar Sci. Conf. 8th,* pp. 595-614.

Morris R. V. (1976) Surface exposure indices of lunar soils: A comparative FMR study. *Proc. Lunar Sci. Conf. 7th,* pp. 315-335.

Morris R. V. (1980) Origins and size distribution of metallic iron particles in the lunar regolith. *Proc. Lunar Planet. Sci. Conf. 11th,* pp. 1697-1712.

Morris R. V., Gibbons R. V., and Hörz F. (1975) FMR thermomagnetic studies up to 900° of lunar soils and potential magnetic analogs. *Geophys. Res. Lett., 2,* 461-464.

Morris R. V., See T. H., and Hörz F. (1986) Composition of the Cayley formation at Apollo 16 as inferred from impact melt splashes. *Proc. Lunar Planet. Sci. Conf. 17th,* in *J. Geophys. Res., 92,* E21-E42.

Morris R. V., Korotev R. L., and Lauer H. V. Jr. (1989) Maturity and geochemistry of the Van Serg core (79001/2) with implications for micrometeorite composition. *Proc. Lunar Planet. Sci. Conf. 19th,* pp. 269-284.

Muehlberger W. R. (1981) C. Apollo 16 traverse planning and field procedures. In *Geology of the Apollo 16 Area, Central Lunar Highlands* (G. E. Ulrich, C. A. Hodges, and W. R. Muehlberger, eds.), pp. 21-44. U.S. Geol. Surv. Prof. Pap. 1048.

Nagle J. S., Duke M. B., Heiken G., Fryxell R., and Waltz S. R. (1975) Preliminary stratigraphy of the Apollo 16 deep drill string (abstract). In *Lunar Science VI,* pp. 593-594. The Lunar Science Institute, Houston.

Naney M. T., Crowl D. M., and Papike J. J. (1976) The Apollo 16 drill core: Statistical analysis of glass chemistry and the characterization of a high alumina—silica poor (HASP) glass. *Proc. Lunar Sci. Conf. 7th,* pp. 155-184.

Nava D. F., Lindstrom M. M., Schuhmann P. J., Lindstrom D. J., and Philpotts J. A. (1976) The remarkable chemical uniformity of Apollo 16 layered deep drill core section 60002. *Proc. Lunar Sci. Conf. 7th,* pp. 133-139.

Ostertag R., Stöffler D., Bischoff A., Palme H., Schultz L., Spettel B., Weber H., Weckwerth G., and Wänke H. (1986) Lunar meteorite Yamato-791197: Petrography, shock history and chemical composition. *Mem. Natl. Inst. Polar Res., Spec. Issue 41,* pp. 17-44. Natl. Inst. of Polar Res., Tokyo.

Palme H., Spettel B., Wänke H., Bischoff A., and Stöffler D. (1984) Early differentiation of the Moon: Evidence from trace elements in plagioclase. *Proc. Lunar Planet. Sci. Conf. 15th,* in *J. Geophys. Res., 89,* C3-C15.

Papike J. J., Simon S. B., White C., and Laul J. C. (1981) The relationship of the lunar regolith <10 μm fraction and agglutinates. Part I: A model for agglutinate formation and some indirect supportive evidence. *Proc. Lunar Planet. Sci. 12B,* pp. 409-420.

Pearce G. W., Gose W. A., and Strangway D. W. (1973) Magnetic studies on Apollo 15 and 16 lunar samples. *Proc. Lunar Sci. Conf. 4th,* pp. 3045-3076.

Rambaldi E. R. (1977) Trace element content of metals from H- and LL-group chondrites. *Earth Planet. Sci. Lett., 36,* 347-358.

Rhodes J. M., Adams J. B., Blanchard D. P., Charette M. P., Rodgers K. V., Jacobs J. W., Brannon J. C., and Haskin L. A. (1975) Chemistry of agglutinate fractions in lunar soils. *Proc. Lunar Sci. Conf. 6th,* pp. 2291-2307.

Russ G. P. III (1973) Apollo 16 neutron stratigraphy. *Earth Planet. Sci. Lett., 17,* 275-289.

Schaber G. G. (1981) D1. Field geology of the Apollo 16 central region. In *Geology of the Apollo 16 Area, Central Lunar Highlands* (G. E. Ulrich, C. A. Hodges, and W. R. Muehlberger, eds.), pp. 21-44. U.S. Geol. Surv. Prof. Pap. 1048.

Simon S. B., Papike J. J., and Vaniman D. T. (1978) The Apollo 16 drive tube 60009/60010. Part 1: Modal petrology. *Proc. Lunar Planet. Sci. Conf. 9th,* pp. 1813-1826.

Simonds C. H., Warner J. L., and Phinney W. C. (1973) Petrology of Apollo 16 poikilitic rocks. *Proc. Lunar Sci. Conf. 4th,* pp. 613-632.

Stöffler D., Knöll H.-D., Marvin U. B., Simonds C. H., and Warren P. H. (1980) Recommended classification and nomenclature of lunar highland rocks—a committee report. In *Proceedings of the Conference on the Lunar Highlands Crust* (J. J. Papike and R. B. Merrill, eds), pp. 51-70. Pergamon, New York.

Takeda H., Kojima H., Nishio F., Yanai K., Lindstrom M. M., and Yamato Lunar Meteorite Consortioum Group (1989) Preliminary report on the Yamato-86032 lunar meteorite: I. Recovery, sample descriptions, mineralogy and petrography. In *Proceedings of the Fourteenth Symposium on Antarctic Meteorites,* pp. 3-14. Natl. Inst. of Polar Res., Tokyo.

Vaniman D. T. and Papike J. J. (1980) Lunar highlands melt rocks: Chemistry, petrology, and silicate mineralogy. In *Proceedings of the Conference on the Lunar Highlands Crust* (J. J. Papike and R. B. Merrill, eds.), pp. 271-337. Pergamon, New York.

Vaniman D. T., Lellis S. F., Papike J. J., and Cameron K. L. (1976) The Apollo 16 drill core: Modal petrology and characterization of the mineral and lithic component. *Proc. Lunar Sci. Conf. 7th,* pp. 199-239.

Vaniman D. T., Papike J. J., and Schweitzer E. L. (1978) The Apollo 16 drive tube 60009/60010. Part II: Petrology and major element partitioning among regolith components. *Proc. Lunar Planet. Sci. Conf. 9th,* pp. 1827-1860.

Via W. N. and Taylor L. A. (1976) Chemical aspects of agglutinate formation: Relationships between agglutinate composition and the composition of the bulk soil. *Proc. Lunar Sci. Conf. 7th,* pp. 393-403.

Warner J. L., Simonds C. H., and Phinney W. C. (1976) Genetic distinction between anorthosites and Mg-rich plutonic rocks: New data from 76255 (abstract). In *Lunar Science VII,* pp. 916-917. The Lunar Science Institute, Houston.

Warren P. H. (1985) The magma ocean concept and lunar evolution. *Annu. Rev. Earth Planet. Sci., 13,* 201-240.

Warren P. H. (1990) Lunar anorthosites and the magma-ocean plagioclase-flotation hypothesis: Importance of FeO enrichment in the parent magma. *Am. Mineral., 75,* 46-58.

Warren P. H. and Wasson J. T. (1977) Pristine nonmare rocks and the nature of the lunar crust. *Proc. Lunar Sci. Conf. 8th,* pp. 2215-2235.

Warren P. H. and Wasson J. T. (1979) The compositional-petrographic search for pristine nonmare rocks: Third foray. *Proc. Lunar Planet. Sci. Conf. 10th,* pp. 583-610.

Warren P. H. and Wasson J. T. (1981) Foraging westward for pristine rocks: Complications for petrogenetic models. *Proc. Lunar Planet. Sci. 12B,* pp. 21-40.

Warren P. H., Taylor G., Keil K., Kallemeyn G. W., Rosener P. S., and Wasson J. T. (1983a) Sixth foray for pristine nonmare rocks and as assessment of the diversity of lunar anorthosites. *Proc. Lunar Planet. Sci. Conf. 13th,* in *J. Geophys. Res., 88,* A615-A630.

Warren P. H., Taylor G., Keil K., Kallemeyn G. W., Shirley D. N., and Wasson J. T. (1983b) Seventh foray: Whitlockite-rich lithologies, a diopside-bearing troctolitic anorthosite, ferroan anorthosite, and KREEP. *Proc. Lunar Planet. Sci. Conf. 14th,* in *J. Geophys. Res., 89,* B151-B164.

Warren P. H., Jerde E. A., and Kallemeyn G. W. (1990) Pristine Moon rocks: An alkali anorthosite with coarse augite exsolution from plagioclase, a magnesian harzburgite, and other oddities. *Proc. Lunar Planet. Sci. Conf. 20th,* pp. 31-59.

Wasson J. T. (1985) *Meteorites.* Freeman, New York. 267 pp.

Wasson J. T. and Kallemeyn G. W. (1988) Composition of chondrites. *Philos. Trans. R. Soc. London, A325,* 535-544.

Wlotzka F., Spettel B., and Wänke H. (1973) On the composition of metal from Apollo 16 fines and the meteorite component. *Proc. Lunar Sci. Conf. 4th,* pp. 1483-1491.

York D. (1969) Least squares fitting of a straight line with correlated errors. *Earth Planet. Sci. Lett., 5,* 320-324.

TABLE A1. INAA results for <1-mm fines from double drive tube 60009/10.

Depth (cm)	Parent Split	Note	SU	Na_2O %	CaO %	Sc μg/g	Cr μg/g	FeO %	Co μg/g	Ni μg/g	Ba μg/g	La μg/g	Sm μg/g	Eu μg/g	Tb μg/g	Yb μg/g	Lu μg/g	Hf μg/g	Ta μg/g	Ir ng/g	Au ng/g	Th μg/g	U μg/g
60010																							
0.05	5		7	0.448	15.2	9.33	786	5.33	34.7	600	130	12.33	5.76	1.15	1.05	4.08	0.554	4.26	0.47	24.	12.5	1.93	0.47
0.25	9		7	0.454	15.6	9.38	805	5.30	24.2	410	133	13.92	6.45	1.17	1.15	4.34	0.616	4.57	0.50	12.	8.7	2.49	0.65
0.75	2105	J	7	0.451	15.2	9.30	765	5.67	38.3	620	124	12.72	5.86	1.20	1.11	4.13	0.570	4.84	0.51	17.	10.3	2.10	0.44
1.25	2103		7	0.461	15.0	9.47	785	5.43	30.3	460	139	12.61	5.89	1.18	1.19	4.23	0.574	4.51	0.55	11.	8.5	2.29	0.50
1.75	2101		7	0.449	15.2	9.93	766	5.50	28.1	400	136	12.77	5.93	1.18	1.20	4.22	0.585	4.54	0.59	17.	6.3	2.16	0.54
2.25	2099		7	0.447	15.4	9.23	756	5.33	29.1	550	145	12.69	5.87	1.16	1.07	4.10	0.571	4.27	0.51	14.	6.5	2.04	0.58
2.75	2097		7	0.444	15.8	9.24	760	5.30	27.8	480	149	13.58	6.22	1.16	1.18	4.22	0.595	4.48	0.48	15.	7.9	2.35	0.55
3.25	2095		7	0.447	15.6	9.31	783	5.39	31.3	450	138	12.40	5.72	1.18	1.13	4.03	0.554	4.58	0.53	20.	8.7	2.14	0.59
3.75	2093	J	7	0.444	15.8	10.07	786	5.46	25.4	380	136	12.50	5.83	1.18	1.16	4.18	0.579	4.38	0.49	12.	5.3	2.06	0.62
4.25	2091		7	0.444	15.1	9.65	782	5.26	25.8	370	123	12.32	5.73	1.13	1.07	3.97	0.558	4.15	0.45	9.	7.5	2.16	0.55
4.75	2089		6	0.457	15.2	9.38	749	5.23	26.6	430	127	11.86	5.53	1.16	1.02	3.98	0.554	4.34	0.50	13.	7.4	2.22	0.54
5.25	2087		6	0.453	15.8	8.96	721	5.12	28.6	450	124	11.76	5.45	1.14	1.05	3.86	0.524	4.07	0.52	13.	8.6	1.98	0.48
5.75	2085		6	0.457	15.6	8.90	734	5.12	26.6	390	132	12.65	5.84	1.16	1.08	4.10	0.579	4.49	0.47	14.	7.3	2.32	0.53
6.25	2083		6	0.455	16.1	9.25	746	5.24	27.4	350	144	13.11	6.07	1.18	1.16	4.24	0.587	4.75	0.54	13.	5.8	2.15	0.60
6.75	2081		6	0.446	15.4	9.06	727	5.13	27.2	350	145	12.34	5.77	1.14	1.07	4.17	0.566	4.35	0.54	13.	6.6	2.25	0.46
7.25	2079		6	0.476	15.5	9.24	766	5.29	28.2	460	133	13.18	6.08	1.23	1.18	4.32	0.586	4.60	0.54	14.	8.6	2.39	0.51
7.75	2077		6	0.485	15.3	9.42	744	5.39	28.6	390	157	14.31	6.53	1.21	1.22	4.61	0.663	5.59	0.64	13.	7.2	2.78	0.71
8.25	2075		5	0.472	15.7	9.33	764	5.28	25.1	360	143	12.69	5.90	1.17	1.13	4.12	0.578	4.50	0.53	10.	6.4	2.24	0.48
8.75	2073		5	0.447	15.7	9.36	752	5.31	29.3	480	135	12.24	5.66	1.18	1.10	3.96	0.544	4.24	0.49	21.	5.8	1.90	0.34
9.25	2071		5	0.456	15.1	9.35	777	5.25	24.9	420	134	12.68	5.93	1.21	1.12	4.17	0.579	4.55	0.55	10.	5.3	2.25	0.47
9.75	2069		5	0.451	15.3	9.13	762	5.31	28.8	410	141	13.37	6.16	1.17	1.11	4.21	0.585	4.49	0.53	12.	8.0	2.20	0.51
10.25	2067		5	0.441	16.0	9.34	752	5.27	29.2	410	140	12.67	5.87	1.14	1.06	4.12	0.575	4.51	0.48	11.	7.3	2.10	0.51
10.75	2065		5	0.444	15.5	9.33	737	5.25	30.5	380	162	12.22	5.72	1.10	1.07	4.09	0.571	4.43	0.47	16.	8.4	2.05	0.40
11.25	2063	J	5	0.452	15.3	9.38	778	5.42	30.7	460	178	13.44	6.24	1.16	1.19	4.38	0.602	4.91	0.56	14.	8.7	2.45	0.62
11.75	2061		5	0.439	15.9	9.20	747	5.27	29.9	380	134	12.39	5.74	1.17	1.06	4.04	0.560	4.27	0.46	11.	6.8	2.04	0.58
12.25	2059		5	0.455	15.4	9.43	777	5.83	44.1	660	138	12.64	5.85	1.19	1.15	4.10	0.574	4.60	0.51	21.	12.1	2.31	0.54
12.75	2057		5	0.461	15.0	9.62	784	5.32	24.7	350	143	13.32	6.23	1.20	1.18	4.36	0.588	4.59	0.50	12.	5.7	2.24	0.59
13.25	2055		4	0.469	15.0	9.18	741	6.18	60.7	810	126	11.97	5.59	1.22	1.07	4.01	0.548	4.12	0.52	36.	14.8	2.23	0.50
13.75	2053		4	0.480	15.1	9.18	739	5.40	44.0	600	146	11.93	5.57	1.19	0.98	3.94	0.558	4.26	0.46	17.	8.8	2.34	0.47
14.25	2051	J	4	0.465	15.3	8.78	715	4.99	24.5	380	124	11.48	5.34	1.14	1.04	3.71	0.522	4.17	0.49	11.	4.3	2.10	0.52
14.75	2049		4	0.453	15.9	8.15	657	5.21	37.9	610	122	10.19	4.77	1.09	0.95	3.38	0.460	3.59	0.30	20.	11.3	1.58	0.46
15.25	2047		3	0.454	15.8	8.37	722	5.78	57.1	940	119	10.75	4.96	1.11	0.93	3.49	0.477	3.83	0.40	28.	19.	1.78	0.43
15.75	2045		3	0.454	16.2	8.20	680	4.79	24.7	430	113	11.04	5.16	1.13	0.97	3.62	0.505	4.01	0.47	10.	6.2	1.85	0.56
16.25	2043		3	0.458	16.5	8.46	701	4.96	27.1	420	121	10.98	5.10	1.14	0.95	3.55	0.488	3.89	0.39	15.	6.5	1.92	0.42
16.75	2041		3	0.451	16.1	7.95	636	4.44	20.8	270	101	9.97	4.68	1.13	0.89	3.27	0.456	3.79	0.38	9.	3.8	1.71	0.35
17.25	2039		3	0.456	15.5	8.41	665	5.23	35.1	570	119	11.23	5.28	1.17	1.02	3.83	0.527	4.23	0.46	16.	10.8	1.85	0.50
17.75	2037		3	0.461	15.3	8.85	735	5.13	23.7	340	136	12.21	5.71	1.17	1.10	4.00	0.559	4.46	0.49	14.	6.1	2.28	0.57
18.25	2035		2	0.488	15.3	10.32	797	5.70	31.6	450	157	14.07	6.69	1.23	1.26	4.87	0.656	5.06	0.60	12.5	8.9	2.72	0.61
18.75	2033		2	0.478	14.9	10.36	816	5.66	25.1	350	162	14.71	6.83	1.21	1.33	4.77	0.663	4.90	0.56	9.5	6.4	2.49	0.58
19.25	2031		2	0.481	15.7	10.40	810	5.54	24.5	360	166	15.01	7.01	1.21	1.37	5.01	0.691	5.28	0.63	10.	5.9	2.50	0.67
19.75	2029		2	0.478	15.0	10.61	825	5.55	23.6	300	156	15.70	7.34	1.23	1.37	5.07	0.695	5.36	0.63	8.0	7.4	2.84	0.66
20.25	2027	J	2	0.480	15.1	10.50	840	5.63	24.2	390	162	14.86	6.90	1.19	1.28	4.95	0.677	5.41	0.60	11.	4.2	2.42	0.63
20.75	2025		2	0.473	15.5	10.62	831	5.57	24.5	330	169	14.60	6.80	1.23	1.37	4.91	0.670	5.35	0.55	10.	5.3	2.64	0.66
21.25	2023		2	0.467	15.6	9.90	797	5.45	25.3	310	149	14.35	6.65	1.18	1.25	4.50	0.616	4.50	0.59	9.	5.7	2.34	0.58
21.75	2021		1	0.453	16.4	7.72	624	4.47	23.5	350	105	10.24	4.76	1.12	0.90	3.43	0.472	3.96	0.44	9.	6.7	1.83	0.48
22.25	2019		1	0.449	16.3	7.16	584	4.15	19.2	280	105	9.72	4.52	1.09	0.85	3.11	0.436	3.82	0.35	10.	4.6	1.89	0.34
22.75	2017		1	0.440	16.5	6.70	546	4.04	22.5	320	104	8.63	4.04	1.07	0.76	2.87	0.386	2.96	0.32	10.	6.8	1.53	0.38
23.25	2015		1	0.437	16.2	7.20	618	4.25	20.1	320	106	9.58	4.48	1.08	0.81	3.14	0.427	3.42	0.40	7.9	5.0	1.65	0.53

TABLE A1. (continued).

Depth (cm)	Parent Split	Note	SU	Na_2O %	CaO %	Sc µg/g	Cr µg/g	FeO %	Co µg/g	Ni µg/g	Ba µg/g	La µg/g	Sm µg/g	Eu µg/g	Tb µg/g	Yb µg/g	Lu µg/g	Hf µg/g	Ta µg/g	Ir ng/g	Au ng/g	Th µg/g	U µg/g
23.75	2013		1	0.440	15.8	7.19	582	4.21	23.9	380	121	11.27	5.20	1.11	0.98	3.35	0.465	3.65	0.40	11.	6.1	1.83	0.50
24.25	2011		1	0.438	15.9	7.36	582	4.29	20.6	370	99	10.10	4.68	1.10	0.92	3.29	0.462	3.56	0.40	10.	5.7	1.60	0.43
24.75	2008	J	1	0.425	15.9	7.37	603	7.00	110.8	1790	116	10.35	4.74	1.07	0.87	3.33	0.474	3.55	0.40	56.	42.	1.99	0.41
25.25	2006		1	0.438	16.2	7.84	625	4.53	22.9	310	116	10.94	5.02	1.11	1.00	3.58	0.486	3.72	0.44	11.	7.0	1.70	0.41
25.75	2204		1	0.440	16.0	7.87	651	4.81	30.2	430	132	12.27	5.65	1.12	1.09	3.96	0.545	4.30	0.45	13.	12.1	2.08	0.37
26.30	2202		1	0.439	16.4	7.62	604	4.31	19.5	270	118	10.88	5.09	1.13	0.94	3.47	0.485	3.91	0.43	7.7	6.3	1.88	0.54
26.95	2000		1	0.435	15.9	7.49	597	4.38	21.9	370	122	10.88	5.02	1.12	0.99	3.59	0.490	3.68	0.44	10.	7.4	1.70	0.49
60009																							
27.50	5		10	0.461	15.7	8.29	667	5.43	43.8	720	126	11.92	5.53	1.18	1.01	3.84	0.527	4.25	0.47	23.	13.9	2.18	0.49
28.05	3000		10	0.459	16.5	8.06	656	4.57	21.5	270	114	11.29	5.24	1.17	0.99	3.79	0.502	4.07	0.43	9.3	3.8	1.85	0.47
28.55	3002		10	0.462	15.5	8.12	658	4.75	24.8	360	122	11.21	5.21	1.15	1.02	3.74	0.503	3.97	0.56	10.	6.0	2.07	0.43
29.10	3005	J	10	0.439	16.7	8.34	662	4.68	22.9	310	121	11.85	5.52	1.14	1.04	3.97	0.535	4.24	0.46	11.5	4.7	2.03	0.43
29.55	3007		10	0.452	16.5	7.78	630	4.42	22.1	360	117	10.65	4.97	1.11	0.94	3.58	0.483	3.92	0.38	10.5	7.1	1.61	0.46
30.05	3009		10	0.458	15.5	8.31	662	4.99	32.8	490	130	11.39	5.34	1.14	1.04	3.84	0.524	4.03	0.46	19.	8.3	2.06	0.57
30.60	3011		10	0.452	15.5	7.80	642	4.82	32.0	430	131	11.13	5.16	1.15	1.07	3.72	0.498	3.87	0.47	15.	8.6	1.81	0.45
31.05	3013		10	0.463	16.0	8.09	657	4.77	28.9	360	131	11.57	5.35	1.13	1.01	3.85	0.510	3.95	0.46	13.	7.2	1.93	0.63
31.10	3015		9	0.451	15.8	8.51	682	4.77	23.3	330	143	11.98	5.56	1.16	1.14	4.01	0.547	4.11	0.45	11.	7.3	2.01	0.58
31.55	3017		9	0.461	16.4	8.07	663	4.71	27.2	440	117	11.05	5.14	1.15	0.90	3.68	0.502	4.00	0.42	12.	6.2	2.02	0.52
32.05	3019		9	0.458	15.7	8.26	671	4.73	24.2	370	113	11.49	5.33	1.18	1.06	3.83	0.524	6.19	0.45	9.7	5.2	2.07	0.49
32.55	3021		9	0.457	16.4	8.14	681	4.76	23.3	360	126	11.05	5.14	1.15	0.94	3.69	0.502	3.98	0.45	12.5	5.6	1.99	0.51
33.05	3023		9	0.470	15.8	8.44	968	5.02	27.8	440	130	11.16	5.24	1.10	1.08	3.77	0.512	4.11	0.47	15.	7.2	1.81	0.58
33.55	3025		9	0.481	15.8	8.50	698	5.05	31.7	550	142	10.96	5.11	1.13	1.01	3.64	0.490	3.78	0.43	16.	8.3	1.97	0.46
34.05	3028		9	0.468	16.3	8.75	722	4.98	25.8	390	137	12.21	5.63	1.17	1.02	4.02	0.547	4.90	0.46	12.	5.6	2.10	0.50
34.55	3030		9	0.463	16.3	8.12	659	4.85	30.0	490	115	10.88	5.02	1.11	1.02	3.68	0.484	3.84	0.43	15.	8.0	1.78	0.44
35.05	3032		9	0.483	16.0	8.26	677	4.91	29.9	460	121	11.69	5.37	1.19	0.97	3.89	0.525	4.07	0.49	14.	6.2	2.07	0.57
35.55	3034		9	0.462	15.8	8.06	656	4.72	24.9	320	122	11.62	5.39	1.14	1.07	3.85	0.523	4.18	0.45	10.	6.2	2.07	0.64
36.05	3036		8	0.446	16.0	7.60	609	4.65	32.2	490	129	12.26	5.67	1.11	1.03	3.82	0.507	3.65	0.41	14.	9.5	2.07	0.59
36.55	3038		8	0.436	16.2	7.27	576	4.04	18.8	260	106	9.68	4.49	1.08	0.97	3.19	0.435	3.28	0.41	7.9	4.0	1.53	0.38
37.05	3041		8	0.430	17.4	6.32	518	3.68	19.3	270	104	8.73	4.02	1.06	0.74	2.88	0.388	3.16	0.36	8.6	4.7	1.57	0.43
37.55	3044		8	0.433	16.9	6.42	527	3.73	18.3	240	94	9.27	4.27	1.08	0.83	3.10	0.411	3.27	0.38	7.6	6.0	1.54	0.41
38.05	3046		8	0.441	16.2	7.62	630	4.49	24.5	350	128	11.00	5.09	1.09	0.90	3.58	0.491	3.81	0.41	11.5	5.4	2.02	0.41
38.55	3048		8	0.447	16.1	7.33	594	4.20	19.8	250	121	10.18	4.71	1.10	0.95	3.35	0.458	3.61	0.43	7.5	4.4	1.85	0.46
39.05	3050		7	0.443	16.2	6.98	569	4.02	17.2	250	123	10.76	4.98	1.11	0.94	3.51	0.482	3.90	0.41	9.4	4.0	1.99	0.37
39.55	3052		7	0.440	16.2	6.83	563	4.13	24.4	360	95	9.16	4.28	1.11	0.83	3.07	0.413	3.31	0.48	14.	7.4	1.75	0.44
40.05	3054		7	0.449	17.1	7.00	561	4.06	21.4	290	107	9.80	4.52	1.07	0.85	3.16	0.431	3.33	0.36	8.7	4.8	1.69	0.44
40.55	3056		7	0.437	16.0	6.82	592	4.25	27.0	380	117	10.34	4.78	1.07	0.95	3.37	0.458	3.52	0.45	14.	6.3	1.67	0.49
41.05	3058		7	0.450	16.5	6.57	534	3.86	17.9	244	103	8.51	3.96	1.09	0.76	2.86	0.379	3.07	0.36	6.9	3.9	1.50	0.38
41.55	3060		7	0.448	16.5	6.18	509	4.36	43.1	680	91	9.12	4.22	1.11	0.85	2.92	0.393	3.01	0.35	17.	17.0	1.50	0.37
42.05	3062		7	0.438	16.8	5.79	477	3.49	17.9	270	86	8.33	3.88	1.07	0.73	2.69	0.371	2.88	0.34	7.5	6.0	1.54	0.32
42.55	3065		7	0.422	17.6	5.33	439	3.12	13.7	220	90	7.49	3.44	1.02	0.67	2.44	0.326	2.59	0.30	7.4	2.6	1.17	0.23
43.05	3067	J	7	0.414	17.1	4.71	376	2.78	11.8	140	72	6.39	2.94	0.98	0.58	2.08	0.286	2.16	0.26	7.2	2.1	0.94	0.35
43.55	3070		7	0.422	17.8	4.86	391	2.86	13.0	170	71	6.44	2.97	0.99	0.57	2.12	0.285	2.21	0.23	6.0	4.2	1.00	0.28
44.05	3072		7	0.436	17.3	6.16	532	3.61	15.9	210	98	9.21	4.20	1.07	0.81	2.96	0.403	3.24	0.33	6.1	4.6	1.42	0.41
44.55	3074		7	0.440	16.8	7.20	585	4.33	26.1	370	116	10.28	4.76	1.10	0.90	3.40	0.461	3.60	0.39	11.	8.2	1.71	0.47
45.05	3076		7	0.456	16.1	7.56	615	4.30	17.8	210	124	10.80	5.04	1.13	0.98	3.56	0.485	3.66	0.47	10.	4.2	1.82	0.52
45.55	3078		7	0.446	16.2	7.43	616	4.59	29.5	460	118	10.59	4.92	1.13	0.96	3.50	0.484	3.72	0.43	10.	8.5	1.68	0.36
46.05	3080		7	0.435	16.9	7.30	632	4.16	17.8	260	103	9.07	4.21	1.07	0.77	3.08	0.411	3.37	0.34	8.0	5.4	1.66	0.38
46.55	3082		7	0.444	16.4	6.99	579	4.11	18.2	260	101	10.16	4.70	1.10	0.96	3.29	0.447	3.32	0.38	7.2	6.3	1.67	0.42

TABLE A1. (continued).

Depth (cm)	Parent Split	Note	SU	Na_2O %	CaO %	Sc μg/g	Cr μg/g	FeO %	Co μg/g	Ni μg/g	Ba μg/g	La μg/g	Sm μg/g	Eu μg/g	Tb μg/g	Yb μg/g	Lu μg/g	Hf μg/g	Ta μg/g	Ir ng/g	Au ng/g	Th μg/g	U μg/g
47.05	3085		7	0.441	16.3	6.79	566	4.38	34.6	520	103	9.23	4.31	1.08	0.84	3.06	0.420	3.22	0.37	16.	11.0	1.66	0.40
47.55	3087		6	0.447	15.9	7.79	629	4.49	23.4	420	128	10.49	4.83	1.12	0.97	3.49	0.473	3.74	0.43	10.5	5.2	1.98	0.37
48.05	3089		6	0.463	16.0	8.51	686	4.92	26.7	354	128	13.40	6.08	1.17	1.18	4.16	0.557	4.25	0.47	11.	7.1	2.07	0.56
48.55	3091	J	5	0.459	15.9	7.82	614	4.41	20.9	300	114	10.07	4.72	1.13	0.93	3.34	0.460	3.60	0.44	11.	5.6	1.70	0.43
49.05	3093		5	0.440	16.8	6.37	530	4.06	26.6	390	93	8.98	4.17	1.08	0.81	2.97	0.417	3.79	0.33	10.	7.6	1.49	0.46
49.55	3095		4	0.445	15.8	7.26	604	4.38	27.5	410	111	10.46	4.84	1.13	0.98	3.36	0.457	3.47	0.38	13.	9.2	1.64	0.56
50.05	3097		4	0.440	15.8	6.57	570	4.56	39.1	560	121	9.99	4.58	1.09	0.88	3.24	0.439	3.37	0.43	13.	11.7	1.75	0.41
50.55	3100		4	0.437	16.4	6.54	591	4.05	20.1	310	112	10.54	4.79	1.10	0.92	3.38	0.456	3.55	0.41	6.9	6.2	1.69	0.53
51.05	3102		4	0.440	16.4	7.21	638	4.52	28.1	480	118	11.66	5.38	1.12	1.01	3.78	0.525	4.05	0.45	6.9	7.1	2.05	0.49
51.55	3104		4	0.445	15.6	7.19	604	4.72	34.5	530	127	10.69	5.01	1.10	0.99	3.45	0.475	3.65	0.44	13.	11.0	1.75	0.53
52.05	3106	D	4	0.430	16.7	6.53	546	4.09	27.3	420	103	9.14	4.24	1.08	0.80	3.04	0.413	3.32	0.36	13.	7.5	1.66	0.37
52.55	3109	D	4	0.436	17.3	5.89	485	3.58	21.0	300	86	7.98	3.71	1.07	0.74	2.65	0.356	2.94	0.32	8.2	5.1	1.27	0.28
52.05	3107	L	3	0.431	17.0	5.27	431	3.10	15.1	215	82	7.10	3.31	1.03	0.63	2.33	0.310	2.43	0.26	5.2	4.7	1.30	0.31
52.55	3110	L	3	0.410	18.3	3.53	275	2.09	8.6	110	47	4.28	2.00	0.96	0.37	1.43	0.191	1.55	0.16	2.7	2.6	0.69	0.18
53.05	3112		3	0.396	17.7	3.77	300	2.43	15.9	230	53	5.11	2.37	0.95	0.45	1.55	0.212	1.54	0.23	4.3	3.1	0.76	0.15
53.55	3114	J	3	0.406	17.8	3.38	264	2.05	6.8	92	52	4.24	1.95	0.96	0.38	1.36	0.185	1.38	0.17	2.1	1.7	0.65	0.16
54.05	3116		3	0.396	17.8	3.38	272	2.13	6.9	67	55	4.53	2.08	0.94	0.39	1.46	0.197	1.50	0.17	2.2	1.2	0.70	0.18
54.55	3118		3	0.385	18.4	2.82	218	1.93	7.4	87	41	3.36	1.55	0.90	0.29	1.10	0.149	1.19	0.13	1.9	1.7	0.52	0.17
55.05	3120		3	0.398	18.3	3.59	296	2.35	14.8	250	56	4.96	2.26	0.96	0.41	1.56	0.214	1.71	0.18	5.9	4.4	0.86	0.19
55.55	3122		2	0.418	18.3	4.29	340	2.62	13.1	155	61	5.87	2.70	1.00	0.50	1.93	0.256	1.94	0.28	5.0	3.3	1.16	0.28
56.05	3124		2	0.431	17.1	5.06	412	2.89	11.9	160	74	6.20	2.90	1.02	0.55	2.05	0.283	2.19	0.27	4.5	3.2	1.09	0.29
56.55	3126		2	0.422	17.3	5.52	450	4.87	73.8	1020	78	6.68	3.07	1.03	0.57	2.18	0.299	2.29	0.28	48.	18.1	1.26	0.28
57.05	3129		2	0.444	16.8	7.38	600	4.24	19.8	300	104	9.50	4.41	1.12	0.80	3.17	0.425	3.38	0.37	11.	8.1	1.77	0.49
57.55	3131		1	0.456	15.9	8.73	712	5.01	25.1	400	123	11.17	5.15	1.16	0.95	3.68	0.511	3.91	0.46	14.	6.0	1.92	0.46
58.05	3133		1	0.468	15.6	9.62	767	5.23	23.7	340	123	12.23	5.76	1.19	1.09	4.13	0.566	4.42	0.47	11.	4.8	2.07	0.45
58.55	3135	J	1	0.473	15.4	9.46	751	5.10	21.2	290	136	12.23	5.73	1.19	1.18	4.14	0.572	4.51	0.55	11.	10.3	1.95	0.53
Mean				0.448	16.1	7.82	639	4.61	26.5	394	118	10.80	5.01	1.12	0.96	3.54	0.485	3.82	0.43	12.3	7.2	1.86	0.46
Minimum				0.385	14.9	2.82	218	1.93	6.8	67	41	3.36	1.55	0.90	0.29	1.10	0.149	1.19	0.13	1.9	1.2	0.52	0.15
Maximum				0.488	18.4	10.62	968	7.00	110.8	1790	178	15.70	7.34	1.23	1.37	5.07	0.695	6.19	0.64	56.	42.	2.84	0.71
±				0.008	0.5	0.08	7	0.05	0.3	40	12	0.15	0.08	0.03	0.05	0.06	0.010	0.12	0.04	2.0	1.0	0.08	0.07

Depth = depth below surface of the center of the sampling interval (*Fruland et al.*, 1982). Note: J = samples from this depth were studied by a consortium at the Johnson Space Center in 1976-1977; D = dark soil; L = light soil. SU = stratigraphic unit (SU) of *Duke and Nagle* (1976). "±" = estimate of analytical precision (one standard deviation).

TABLE A2. INAA results for >1-mm particles from 60009/10 arranged in order of increasing Sc concentration.

Particle Number	Mass mg	Na_2O %	CaO %	Sc μg/g	Cr μg/g	FeO %	Co μg/g	Ni μg/g	Sr μg/g	Zr μg/g	Ba μg/g	La μg/g	Ce μg/g	Sm μg/g	Eu μg/g	Tb μg/g	Yb μg/g	Lu μg/g	Hf μg/g	Ta μg/ g	Ir ng/g	Au ng/g	Th μg/g	U μg/g
20 cm																								
20-L	2.85	0.314	18.5	0.43	17	0.33	0.51	15	155	<15	8	0.210	0.49	0.090	0.712	0.013	0.045	0.0068	<0.5	<0.02	<2.	<2.	0.02	<0.04
20-M	3.41	0.308	18.9	0.54	32	0.38	0.94	<15	159	<15	7	0.238	0.56	0.102	0.726	0.016	0.051	0.0075	0.036	<0.02	<2.	<2.	<0.03	<0.06
20-C	7.75	0.270	18.5	1.97	877	1.43	3.26	7	148	<20	7	0.244	0.70	0.109	0.680	0.025	0.074	0.0106	0.046	0.009	<2.	<2.	0.025	0.04
20-Q	2.47	0.592	17.2	3.36	265	2.20	5.72	<60	230	<40	27	1.03	2.59	0.482	1.30	0.080	0.359	0.051	0.35	0.049	2.5	<1.5	0.104	<0.1
20-E	8.66	0.458	17.6	4.23	284	2.22	4.93	17	176	<30	29	1.00	2.53	0.508	1.01	0.102	0.429	0.064	0.365	0.080	1.0	<2.5	0.111	<0.1
20-N	4.90	0.268	17.4	4.79	335	2.53	4.11	<40	145	<40	<15	0.24	0.64	0.118	0.642	0.029	0.171	0.0266	0.060	<0.02	<3.	<2.	<0.03	<0.1
20-D	11.16	0.477	15.9	6.86	580	4.58	119.0	275	197	151	100	10.9	28.4	5.18	1.15	1.04	3.43	0.471	3.60	0.42	6.4	1.4	1.78	0.55
20-T	2.56	0.324	17.3	7.27	427	3.69	7.45	41	155	<50	17	1.00	2.64	0.566	0.772	0.116	0.519	0.076	0.36	0.055	<3.	<2.	0.13	0.06
20-K	6.79	0.334	15.8	7.37	657	4.68	24.6	300	164	125	100	9.31	24.2	4.56	1.08	0.88	3.02	0.422	3.29	0.42	11.4	5.7	1.50	0.39
20-P	3.77	0.499	16.1	8.15	622	3.94	16.6	230	178	215	142	14.9	39.6	7.16	1.19	1.40	4.44	0.593	5.16	0.63	6.8	2.9	2.68	0.81
20-J	2.19	0.498	15.8	8.48	710	4.99	35.1	460	166	130	101	8.34	21.7	3.97	1.03	0.84	2.78	0.394	3.08	0.37	19.2	6.9	1.55	0.54
20-O	4.69	0.521	13.5	9.22	878	10.75	175.	3500	247	260	182	18.4	48.2	8.80	1.34	1.67	5.73	0.799	6.36	0.75	35.	71.	2.93	0.81
20-S	2.61	0.726	17.7	9.76	285	3.08	3.53	<50	264	<50	29	0.91	2.30	0.649	1.58	0.174	0.85	0.129	0.54	0.027	<3.	<2.	0.10	0.07
20-I	4.88	0.520	13.6	10.0	975	5.74	6.71	55	147	330	233	24.0	63.8	11.4	1.44	2.20	7.53	1.03	8.29	0.98	<3.	<2.	3.95	1.25
20-H	2.99	0.547	13.1	10.6	979	6.40	33.4	590	166	380	273	25.4	67.5	12.2	1.58	2.41	8.24	1.13	9.31	1.08	7.8	15.8	4.26	1.31
20-G	16.05	0.510	13.1	10.7	1036	7.25	46.8	730	180	380	259	27.5	72.	13.0	1.48	2.51	8.50	1.18	9.19	1.04	21.9	14.8	4.26	1.16
20-A	18.99	0.505	13.4	11.2	1145	6.63	15.7	200	148	410	260	28.9	75.	13.4	1.51	2.58	8.85	1.22	9.74	1.10	4.3	3.9	4.77	1.33
20-F	4.96	0.475	14.1	11.3	890	5.85	21.5	280	158	285	184	17.1	44.6	8.15	1.26	1.56	5.70	0.792	5.97	0.73	6.7	4.5	2.89	0.70
20-R	1.11	0.458	14.6	11.7	912	6.02	25.4	330	180	215	153	13.8	36.6	6.85	1.23	1.34	4.65	0.646	5.07	0.61	12.6	5.6	2.53	0.72
20-B	20.62	0.580	15.1	12.7	806	6.39	16.7	230	179	670	399	45.4	118.	21.2	1.81	4.04	12.8	1.76	15.8	1.70	7.0	3.6	6.80	1.62

TABLE A2. (continued).

Particle Number	Mass mg	Na_2O %	CaO %	Sc µg/g	Cr µg/g	FeO %	Co µg/g	Ni µg/g	Sr µg/g	Zr µg/g	Ba µg/g	La µg/g	Ce µg/g	Sm µg/g	Eu µg/g	Tb µg/g	Yb µg/g	Lu µg/g	Hf µg/g	Ta µg/ g	Ir ng/g	Au ng/g	Th µg/g	U µg/g
54 cm																								
54-G	1.78	0.387	18.9	0.27	1.3	0.17	0.22	<20	184	<10	<15	0.146	0.35	0.057	0.792	<0.02	<0.07	0.0034	<0.03	<0.01	<2.	<2.	<0.03	<0.06
54-H	3.82	0.390	18.9	0.29	1.0	0.16	0.32	<10	167	<10	10	0.154	0.33	0.063	0.805	0.006	0.017	0.0028	<0.03	<0.01	<2.	<1.	<0.02	<0.05
54-I	4.66	0.404	19.0	0.29	1.2	0.17	0.28	<10	167	<10	7	0.134	0.34	0.056	0.797	0.010	0.015	0.0028	<0.03	<0.01	<2.	<2.	<0.02	<0.05
54-D	2.86	0.577	17.1	5.45	344	3.32	10.0	77	187	42	48	2.93	7.8	1.49	1.20	0.305	1.03	0.143	1.13	0.16	5.3	<4.	0.42	0.09
54-B	1.52	0.418	15.2	7.88	699	4.63	27.2	450	139	250	153	17.7	46.6	8.34	1.17	1.62	5.46	0.744	6.07	0.65	5.6	9.8	2.73	0.85
54-E	2.21	0.465	13.0	10.5	1046	9.53	119.	1890	190	350	260	24.4	63.7	11.4	1.41	2.27	7.55	1.06	8.28	0.95	78.	34.	4.06	0.97
54-C	2.29	0.529	12.2	10.9	1368	9.78	118.	1880	220	400	270	27.0	71.	13.1	1.47	2.48	8.53	1.19	9.38	1.06	92.	42.	4.35	1.07
54-A	15.39	0.539	12.8	10.9	1142	7.23	39.4	590	150	400	272	27.9	72.	13.0	1.48	2.54	8.54	1.19	9.42	1.04	21.2	12.0	4.29	1.15
54-F	1.59	0.544	13.0	11.2	1129	6.44	7.78	90	145	430	265	27.6	71.	12.8	1.50	2.48	8.43	1.20	9.62	1.06	<7.	<8.	4.47	0.89
54-J	2.34	0.474	11.9	13.1	1229	7.94	33.2	650	157	380	285	27.7	73.	13.1	1.53	2.58	8.71	1.23	9.63	1.13	<10.	17.5	4.83	1.53
58 cm																								
58-I	3.77	0.379	19.7	0.16	1.8	0.16	0.30	<10	172	<30	6	0.164	0.39	0.065	0.835	<0.015	0.016	0.0014	<0.03	<0.02	<2.	<2.	0.018	<0.05
58-D	8.66	0.396	17.5	6.15	427	3.01	6.18	43	164	<30	17	1.16	3.08	0.593	0.865	0.126	0.536	0.077	0.39	0.046	<3.	<3.	0.137	<0.1
58-G	6.42	0.313	15.5	6.48	705	4.89	26.0	270	144	<30	17	1.10	2.86	0.548	0.710	0.128	0.45	0.064	0.35	0.107	10.5	3.9	0.087	<0.15
58-F	1.46	0.463	15.2	9.4	707	4.81	19.6	250	161	155	151	13.1	34.3	6.20	1.19	1.26	4.18	0.567	3.86	0.52	7.8	3.0	2.61	0.60
58-H	4.77	0.493	13.7	10.0	972	6.67	24.8	390	158	390	268	28.6	74.	13.6	1.50	2.56	8.27	1.12	9.51	1.07	3.4	6.4	4.61	1.16
58-E	8.05	0.476	13.3	10.2	1053	7.53	35.7	540	153	330	209	22.9	59.5	10.7	1.29	2.10	7.36	1.01	8.14	0.91	12.3	8.7	4.24	1.08
58-B	14.14	0.498	12.4	10.7	1092	8.28	77.6	1180	198	380	251	26.9	70.	12.6	1.49	2.43	8.31	1.12	9.10	1.00	12.8	23.4	4.25	1.02
58-A	11.02	0.572	13.5	11.1	1134	7.18	33.8	530	152	420	269	28.6	75.	13.3	1.52	2.56	8.80	1.19	9.65	1.07	12.8	11.9	4.55	1.23
58-J	1.90	0.473	15.2	11.3	816	5.39	21.6	290	165	240	166	14.7	38.9	7.10	1.20	1.42	4.90	0.702	5.97	0.61	8.3	<7.	2.46	0.51
58-C	19.86	0.486	12.4	13.2	1268	7.81	42.8	660	156	410	301	31.0	81.	14.4	1.50	2.80	9.68	1.33	10.4	1.25	14.3	14.7	5.27	1.46

Sample depths: 20 cm = 60010,478 (parent 90) at 20.0-20.5 cm depth; 54 cm = 60009,618 (parent 214) at 53.8-54.3 cm depth; 58 cm = 60009,1270 (parent 1154) at 57.8-58.3 cm depth.

TABLE A3. INAA results for <1-mm fines from deep drill core 60001-7.

Depth (cm)	6000X	Parent Split	SU	Na_2O %	CaO %	Sc μg/g	Cr μg/g	FeO %	Co μg/g	Ni μg/g	Sr μg/g	Zr μg/g	Ba μg/g	La μg/g	Sm μg/g	Eu μg/g	Tb μg/g	Yb μg/g	Lu μg/g	Hf μg/g	Ta μg/g	Ir ng/g	Au ng/g	Th μg/g	U μg/g
0.25	7	90	46	0.426	15.3	8.87	733	5.15	29.4	420	155	160	126	12.3	5.67	1.13	1.10	3.96	0.561	4.31	0.50	14.1	8.1	1.94	0.57
0.75	7	88	46	0.441	15.9	9.10	750	5.29	30.4	395	170	125	135	12.4	5.79	1.18	1.14	4.13	0.570	4.29	0.47	15.7	6.9	2.06	0.57
1.25	7	85	46	0.443	16.4	9.28	762	5.26	26.7	360	175	185	141	12.5	5.80	1.19	1.11	3.98	0.570	4.75	0.51	12.9	9.6	2.12	0.42
1.75	7	83	46	0.441	15.8	9.22	751	5.33	29.2	415	155	175	134	12.3	5.74	1.17	1.10	4.03	0.560	4.37	0.54	13.4	9.4	2.04	0.52
2.25	7	80	45	0.451	16.5	9.40	773	5.45	30.8	420	170	165	142	13.0	6.09	1.21	1.16	4.29	0.591	4.69	0.53	13.9	8.5	2.15	0.57
2.75	7	79	45	0.437	15.6	9.13	738	5.21	26.6	370	165	210	143	12.9	6.01	1.19	1.16	4.20	0.586	5.06	0.54	11.1	7.6	2.20	0.48
3.25	7	78	45	0.455	15.3	9.32	762	5.17	24.9	320	155	160	132	12.4	5.73	1.18	1.12	4.02	0.556	4.44	0.50	9.9	6.8	2.12	0.48
3.75	7	76	45	0.441	15.9	9.09	749	5.15	26.4	365	170	140	125	12.0	5.65	1.17	1.05	3.96	0.558	4.32	0.48	12.1	8.1	2.11	0.48
4.25	7	73	45	0.440	15.9	9.34	764	5.35	29.3	430	190	200	145	12.9	6.00	1.16	1.20	4.24	0.582	4.62	0.52	13.4	8.0	2.13	0.43
4.75	7	71	45	0.450	16.0	9.22	778	5.30	27.5	375	175	170	145	12.8	6.00	1.19	1.11	4.21	0.581	4.53	0.49	13.3	11.0	2.14	0.51
5.25	7	69	45	0.414	15.3	8.77	712	4.97	23.7	315	175	165	136	12.0	5.59	1.13	1.07	3.92	0.557	4.21	0.48	11.8	4.8	1.98	0.47
5.75	7	68	45	0.437	15.4	9.53	767	5.33	26.6	380	120	185	136	12.8	5.98	1.18	1.13	4.22	0.593	4.54	0.53	11.5	6.9	2.19	0.53
6.25	7	66	45	0.438	14.7	8.95	736	5.24	29.1	395	170	185	156	13.3	6.18	1.12	1.16	4.25	0.598	4.76	0.54	12.2	9.8	2.23	0.54
6.75	7	64	45	0.434	15.9	9.11	759	5.15	24.6	340	150	170	144	12.5	5.84	1.17	1.12	4.15	0.580	4.40	0.48	10.7	7.2	2.15	0.56
7.25	7	62	45	0.432	16.0	8.99	749	5.27	29.2	385	155	170	143	12.6	5.83	1.17	1.11	4.10	0.582	4.38	0.54	15.1	9.2	2.14	0.52
7.75	7	59	45	0.438	16.1	8.87	736	5.08	27.0	365	185	160	122	11.7	5.43	1.15	1.04	3.84	0.539	4.06	0.49	13.6	7.2	1.92	0.53
8.25	7	57	45	0.422	15.8	8.61	715	5.01	28.9	405	165	180	132	11.7	5.42	1.15	1.02	3.78	0.536	4.31	0.48	16.3	9.9	1.97	0.48
8.75	7	55	45	0.449	16.3	9.08	734	5.15	25.8	310	165	200	136	12.3	5.74	1.19	1.14	4.03	0.571	4.42	0.53	12.3	7.9	2.10	0.49
9.25	7	53	45	0.430	16.0	9.25	761	5.14	23.3	310	165	165	135	12.3	5.74	1.16	1.11	4.05	0.548	4.48	0.48	11.1	8.7	1.97	0.56
9.75	7	51	45	0.438	16.3	9.12	747	5.10	25.2	350	215	145	137	11.9	5.57	1.14	1.06	3.97	0.548	4.10	0.49	12.6	5.9	1.95	0.44
10.25	7	49	45	0.442	16.2	9.17	739	5.42	32.9	500	170	170	144	12.5	5.78	1.15	1.10	4.10	0.563	4.34	0.51	17.1	9.6	2.03	0.47
10.60	7	47	45	0.439	15.7	8.81	718	4.93	23.4	355	155	155	130	11.9	5.51	1.17	1.06	3.88	0.541	4.22	0.50	10.4	4.3	1.97	0.52
10.85	7	45	44	0.442	16.3	8.94	736	5.08	26.0	380	160	205	136	11.9	5.59	1.16	1.05	3.94	0.550	4.59	0.51	10.8	5.8	1.98	0.41
11.25	7	43	44	0.446	15.6	9.04	742	5.11	25.0	350	165	180	130	12.4	5.78	1.17	1.13	4.06	0.578	4.54	0.49	12.5	7.2	2.06	0.44
11.75	7	41	44	0.406	14.6	8.16	669	4.52	20.8	295	175	145	119	10.9	5.03	1.06	0.97	3.56	0.483	3.80	0.46	9.9	6.2	1.77	0.50
12.25	7	39	44	0.427	15.6	8.42	697	4.82	26.2	395	165	140	121	11.3	5.30	1.10	1.03	3.76	0.519	3.98	0.46	13.1	8.3	1.94	0.50
12.75	7	38	43	0.430	15.9	7.87	670	4.72	28.1	390	155	170	130	11.8	5.48	1.12	1.06	3.83	0.532	4.16	0.47	14.0	8.1	1.93	0.52
13.25	7	36	43	0.438	16.1	8.19	655	4.52	20.9	305	160	155	129	11.5	5.40	1.11	1.03	3.90	0.533	4.18	0.46	8.6	6.6	1.97	0.58
13.75	7	34	43	0.429	16.2	7.96	666	4.59	23.4	345	180	155	117	10.6	4.93	1.11	0.94	3.44	0.473	3.68	0.44	10.1	6.9	1.70	0.44
14.25	7	32	43	0.444	16.4	7.66	635	4.42	23.0	285	155	170	125	10.4	4.86	1.14	0.91	3.35	0.470	3.63	0.40	10.3	7.8	1.77	0.39
14.75	7	30	43	0.434	17.0	7.41	622	4.44	27.3	385	165	130	116	10.2	4.77	1.11	0.93	3.37	0.474	3.60	0.43	13.0	8.2	1.64	0.47
15.25	7	29	43	0.436	16.6	7.20	587	4.08	19.5	275	185	165	109	9.5	4.42	1.11	0.87	3.09	0.432	3.39	0.38	8.9	5.2	1.54	0.44
15.60	7	28	43	0.435	16.1	7.49	626	4.50	29.9	400	180	150	116	10.5	4.85	1.13	0.91	3.42	0.464	3.50	0.41	14.9	7.1	1.69	0.36
15.85	7	27	42	0.428	16.5	6.90	562	3.94	20.5	255	165	145	107	9.2	4.25	1.07	0.85	2.99	0.419	3.43	0.36	8.0	6.2	1.52	0.32
16.25	7	25	42	0.433	16.8	6.63	547	3.73	16.8	215	195	120	102	9.0	4.21	1.08	0.80	2.87	0.402	3.12	0.35	6.9	4.2	1.48	0.40
16.75	7	23	42	0.414	16.4	7.01	560	3.91	18.0	240	170	115	102	8.9	4.11	1.08	0.80	2.94	0.413	3.33	0.35	9.1	4.7	1.43	0.37
17.25	7	21	42	0.425	16.8	6.81	568	3.93	18.6	255	200	115	99	8.8	4.12	1.09	0.77	2.81	0.392	2.98	0.35	7.0	5.3	1.44	0.28
17.75	7	19	42	0.425	17.2	6.13	505	3.63	20.5	295	185	135	89	7.9	3.73	1.04	0.73	2.62	0.368	2.96	0.35	9.3	5.0	1.28	0.27
18.25	7	17	42	0.424	17.0	6.55	536	3.83	20.6	280	190	125	95	9.0	4.19	1.06	0.80	2.93	0.400	3.16	0.35	9.9	5.3	1.46	0.34
18.75	7	15	42	0.426	17.1	6.60	526	3.67	17.7	240	180	90	97	8.2	3.82	1.07	0.73	2.64	0.370	2.75	0.34	9.1	4.7	1.34	0.35
19.25	7	13	42	0.425	16.9	6.52	558	4.18	32.0	470	170	140	105	9.1	4.26	1.05	0.81	2.97	0.414	3.23	0.35	17.6	9.9	1.48	0.27
19.75	7	11	42	0.421	16.5	6.74	552	3.82	17.2	235	155	100	105	9.4	4.39	1.06	0.85	3.04	0.424	3.13	0.37	7.1	5.1	1.55	0.33
20.25	7	9	42	0.401	16.2	6.34	533	3.62	16.2	195	185	120	97	8.3	3.92	1.03	0.71	2.75	0.392	2.99	0.35	7.3	4.2	1.46	0.38
20.75	7	8	42	0.426	17.5	6.84	556	3.83	16.4	225	185	125	108	8.9	4.16	1.09	0.80	2.97	0.408	3.20	0.34	6.7	5.8	1.45	0.42
21.25	7	6	42	0.425	16.1	6.62	540	3.74	17.7	245	170	120	101	8.5	4.00	1.05	0.75	2.81	0.386	2.98	0.32	7.2	4.1	1.34	0.40
21.75	7	4	42	0.413	16.2	6.50	531	3.69	17.0	235	170	100	102	8.2	3.83	1.02	0.74	2.70	0.380	2.96	0.32	7.5	5.7	1.37	0.32
22.20	7	2	42	0.443	16.8	6.37	521	3.71	17.0	200	170	115	92	8.1	3.78	1.06	0.73	2.62	0.376	2.93	0.32	6.7	3.0	1.33	0.37

TABLE A3. (continued).

Depth (cm)	6000X	Parent Split	SU	Na_2O %	CaO %	Sc µg/g	Cr µg/g	FeO %	Co µg/g	Ni µg/g	Sr µg/g	Zr µg/g	Ba µg/g	La µg/g	Sm µg/g	Eu µg/g	Tb µg/g	Yb µg/g	Lu µg/g	Hf µg/g	Ta µg/g	Ir ng/g	Au ng/g	Th µg/g	U µg/g
*22.80	6	131	41	0.450	15.5	8.60	692	5.04	23.9	345	190	250	171	16.8	7.66	1.20	1.46	5.41	0.746	6.32	0.67	9.2	6.9	2.82	0.80
*23.60	6	129	41	0.443	16.0	8.24	668	4.57	20.0	275	155	120	128	11.4	5.36	1.14	1.04	3.69	0.508	3.87	0.47	10.1	4.7	1.85	0.47
*24.25	6	127	41	0.437	16.3	8.35	689	4.72	24.1	320	170	160	138	11.5	5.35	1.17	1.03	3.84	0.526	3.96	0.46	11.6	6.0	1.84	0.49
*24.75	6	125	41	0.439	16.2	8.37	709	4.70	21.7	290	195	150	124	11.5	5.40	1.14	1.04	3.78	0.537	3.99	0.47	9.5	5.7	1.87	0.49
*25.25	6	123	41	0.434	15.5	8.65	647	4.84	31.7	640	145	135	129	11.6	5.51	1.15	1.06	3.81	0.531	3.93	0.45	18.6	8.2	1.96	0.46
*25.75	6	122	41	0.453	15.7	8.61	700	5.02	27.1	375	175	200	138	12.3	5.70	1.17	1.06	4.04	0.561	4.32	0.52	12.6	8.4	2.03	0.57
*26.25	6	120	41	0.438	15.8	8.69	708	5.11	30.0	425	155	180	126	11.6	5.49	1.15	1.06	3.83	0.547	4.03	0.50	15.2	8.0	1.96	0.52
*26.75	6	118	41	0.447	16.2	8.73	726	4.93	22.0	290	185	180	139	12.8	5.98	1.17	1.17	4.20	0.584	4.58	0.54	9.3	4.6	2.18	0.57
*27.25	6	116	41	0.433	15.7	8.12	679	4.74	25.8	345	145	170	121	11.2	5.22	1.12	1.00	3.72	0.498	3.98	0.44	13.1	7.7	1.85	0.43
*27.75	6	115	41	0.451	16.1	12.05	864	5.76	24.5	350	175	430	201	31.9	14.53	1.36	2.68	8.86	1.202	10.30	1.03	9.6	7.2	4.26	1.21
*28.25	6	113	41	0.455	16.5	8.75	723	5.29	37.3	515	170	145	141	11.6	5.45	1.13	1.02	3.88	0.520	4.14	0.51	17.1	11.0	1.94	0.51
*28.75	6	111	41	0.451	15.5	8.71	708	4.95	24.3	340	180	150	145	12.0	5.58	1.17	1.09	3.88	0.545	4.22	0.50	11.0	5.7	2.01	0.47
*29.25	6	109	41	0.462	16.5	8.55	751	4.85	23.3	330	180	155	127	11.7	5.45	1.23	1.05	3.82	0.526	4.02	0.48	10.5	6.5	1.92	0.53
*29.75	6	107	41	0.447	15.7	8.86	715	4.96	23.5	345	155	250	151	12.2	5.77	1.18	1.09	4.03	0.545	4.77	0.50	12.5	5.3	2.00	0.65
*30.25	6	105	41	0.452	16.0	8.60	681	5.80	54.4	710	220	150	132	11.8	5.57	1.17	1.09	3.90	0.539	3.96	0.48	24.6	21.0	2.02	0.58
*30.75	6	103	41	0.443	16.1	8.84	719	5.18	31.4	465	200	185	138	12.0	5.65	1.18	1.05	3.93	0.556	4.08	0.49	16.4	9.2	2.06	0.46
*31.25	6	101	41	0.448	15.7	8.68	720	5.11	29.1	415	160	170	131	12.1	5.67	1.17	1.04	3.95	0.527	4.13	0.48	12.9	6.9	2.07	0.61
*31.75	6	99	41	0.448	16.1	8.64	706	4.85	22.4	305	190	210	127	11.4	5.33	1.16	1.03	3.76	0.509	4.00	0.44	10.3	4.8	1.83	0.68
*32.25	6	97	41	0.445	15.1	9.04	747	5.15	27.0	340	180	200	132	12.6	5.91	1.18	1.11	4.05	0.559	4.49	0.52	11.5	5.1	2.11	0.47
*32.75	6	95	41	0.458	15.4	9.14	752	5.47	33.5	500	180	195	140	13.0	6.06	1.20	1.15	4.25	0.570	4.57	0.49	15.1	9.5	2.17	0.57
*33.25	6	93	41	0.454	15.5	9.03	733	5.14	26.5	370	180	180	134	12.3	5.78	1.18	1.08	4.08	0.562	4.30	0.48	13.0	7.4	2.05	0.55
*33.85	6	91	41	0.443	16.2	9.00	728	5.27	31.7	420	195	180	123	12.3	5.80	1.18	1.10	4.04	0.559	4.24	0.49	15.8	9.1	2.16	0.55
*34.35	6	89	40	0.431	15.4	8.60	743	11.08	222.	3290	240	200	125	12.2	5.67	1.13	1.07	3.97	0.555	4.15	0.46	204.	65.	2.21	0.44
*34.75	6	87	40	0.434	16.4	8.81	717	5.17	30.2	395	180	190	148	11.8	5.57	1.15	1.07	3.90	0.556	4.17	0.47	14.5	7.3	1.99	0.48
*35.25	6	85	40	0.452	15.3	8.87	724	6.11	58.9	850	165	220	130	13.6	6.29	1.20	1.17	4.32	0.595	4.76	0.50	22.2	17.0	2.40	0.44
*35.75	6	83	40	0.451	15.6	11.07	893	6.15	26.5	375	170	240	144	14.5	6.90	1.24	1.32	4.84	0.667	5.09	0.62	8.5	6.8	2.41	0.62
*36.20	6	81	40	0.454	16.1	9.21	775	5.43	34.9	500	195	220	146	13.8	6.47	1.22	1.21	4.52	0.622	4.63	0.54	14.2	9.7	2.37	0.62
*36.70	6	79	40	0.449	15.5	9.26	759	5.21	26.8	370	190	185	131	12.3	5.82	1.19	1.08	4.12	0.558	4.36	0.46	11.2	6.3	2.02	0.68
*37.25	6	77	40	0.438	15.5	8.97	745	5.07	23.2	335	170	200	138	12.3	5.81	1.16	1.09	4.04	0.554	4.32	0.47	9.3	5.5	2.10	0.54
*37.75	6	75	40	0.442	16.1	8.87	725	4.93	22.8	355	190	160	123	11.9	5.58	1.16	1.05	3.90	0.545	4.24	0.48	10.7	4.6	1.98	0.55
*38.25	6	73	40	0.446	15.4	8.89	737	5.68	44.1	740	160	170	123	12.6	5.91	1.15	1.06	4.13	0.560	4.40	0.40	20.0	12.1	2.35	0.61
*38.75	6	71	40	0.456	15.1	9.34	778	5.38	27.3	410	210	190	153	14.1	6.59	1.22	1.21	4.68	0.631	4.91	0.54	10.6	7.4	2.45	0.54
*39.25	6	69	40	0.432	16.1	8.52	691	5.77	48.3	660	200	175	122	11.5	5.41	1.16	1.01	3.73	0.524	3.90	0.44	22.1	13.2	1.87	0.52
*39.75	6	67	40	0.440	15.5	8.89	726	4.98	23.4	295	205	185	128	11.9	5.61	1.16	1.05	3.97	0.551	4.25	0.49	10.7	5.1	1.96	0.53
*40.25	6	65	40	0.443	16.1	8.91	740	5.30	32.7	485	170	160	141	12.6	5.81	1.19	1.06	4.10	0.568	4.32	0.50	15.9	10.0	2.07	0.54
*40.75	6	63	40	0.446	15.6	8.96	726	5.49	38.7	560	195	205	136	12.7	5.92	1.18	1.09	4.04	0.560	4.45	0.51	17.7	10.2	2.18	0.68
*41.25	6	61	40	0.447	15.4	8.94	741	5.02	23.5	310	155	210	138	12.3	5.70	1.19	1.07	4.02	0.551	4.34	0.52	9.1	6.2	2.03	0.51
*41.75	6	59	40	0.444	15.9	8.88	762	5.00	22.6	320	185	160	144	13.4	6.23	1.20	1.18	4.36	0.599	4.39	0.55	11.4	5.9	2.16	0.52
*42.20	6	58	40	0.448	15.4	9.18	741	5.42	34.1	480	185	205	146	13.0	6.16	1.20	1.14	4.30	0.570	4.55	0.52	14.0	9.7	2.16	0.62
*42.70	6	56	39	0.443	15.2	8.97	727	5.04	23.7	345	175	180	127	12.4	5.70	1.18	1.07	4.00	0.537	4.37	0.48	10.4	5.6	2.03	0.47
*43.25	6	54	39	0.446	15.9	8.82	735	5.03	23.5	295	175	190	130	12.0	5.60	1.16	1.06	3.89	0.541	4.18	0.47	9.5	6.2	1.96	0.46
*43.75	6	52	39	0.446	16.3	8.68	693	5.50	45.5	650	220	170	139	11.4	5.35	1.17	0.99	3.79	0.519	4.04	0.50	21.3	14.3	1.92	0.46
*44.25	6	50	39	0.449	15.8	8.84	694	4.98	24.5	400	200	190	140	12.6	5.94	1.19	1.12	4.11	0.572	4.49	0.50	9.9	6.1	2.07	0.62
*44.75	6	48	39	0.450	15.7	8.71	705	5.14	33.0	470	180	145	132	11.7	5.47	1.18	0.99	3.83	0.521	3.96	0.45	15.0	8.6	2.01	0.51
*45.25	6	46	39	0.437	16.4	8.31	674	4.65	21.6	320	185	195	127	11.0	5.19	1.13	0.99	3.64	0.510	4.09	0.45	10.2	4.9	1.82	0.46
*45.75	6	44	39	0.452	16.5	8.78	714	4.91	22.5	315	160	200	146	12.9	6.09	1.18	1.18	4.20	0.590	4.35	0.51	10.1	5.5	2.18	0.52
*46.25	6	42	39	0.457	15.9	8.35	686	4.71	22.4	325	180	175	130	11.6	5.50	1.16	1.03	3.73	0.509	4.00	0.46	12.9	4.9	1.87	0.45

TABLE A3. (continued).

Depth (cm)	6000X	Parent Split	SU	Na_2O %	CaO %	Sc µg/g	Cr µg/g	FeO %	Co µg/g	Ni µg/g	Sr µg/g	Zr µg/g	Ba µg/g	La µg/g	Sm µg/g	Eu µg/g	Tb µg/g	Yb µg/g	Lu µg/g	Hf µg/g	Ta µg/g	Ir ng/g	Au ng/g	Th µg/g	U µg/g
*46.75	6	40	39	0.448	15.6	8.05	664	4.58	22.2	290	180	150	138	10.8	5.08	1.15	0.96	3.59	0.483	3.76	0.42	8.0	5.2	1.78	0.42
*47.25	6	38	39	0.443	15.7	8.34	676	4.78	22.6	295	185	170	120	11.2	5.30	1.14	1.00	3.70	0.502	3.87	0.42	9.3	6.1	1.86	0.49
*47.75	6	36	39	0.440	16.3	7.95	661	4.54	22.1	300	165	155	125	11.2	5.23	1.15	0.99	3.68	0.506	3.85	0.46	9.2	5.3	1.85	0.57
*48.25	6	34	39	0.437	15.8	7.39	603	4.18	19.8	280	180	145	125	10.2	4.75	1.10	0.90	3.35	0.448	3.59	0.43	8.9	5.1	1.72	0.41
*48.75	6	32	39	0.451	16.2	8.76	674	4.89	22.9	300	175	315	117	18.6	8.69	1.22	1.62	5.46	0.733	7.06	0.57	9.6	5.8	2.45	0.51
*49.25	6	30	39	0.442	16.6	8.53	683	4.73	23.3	305	185	205	117	11.4	5.42	1.16	1.01	3.77	0.521	3.87	0.46	11.6	5.8	1.92	0.53
*49.75	6	28	39	0.447	15.7	8.65	696	4.64	19.5	255	195	175	127	11.3	5.39	1.15	1.02	3.73	0.521	4.11	0.46	8.1	4.8	1.84	0.44
*50.25	6	26	39	0.466	15.4	9.03	755	5.31	31.1	445	195	190	147	14.1	6.62	1.22	1.24	4.59	0.625	4.82	0.55	12.3	9.1	2.32	0.59
*50.75	6	24	39	0.454	15.5	8.46	703	4.78	19.9	250	170	210	156	13.4	6.28	1.18	1.20	4.22	0.562	4.28	0.48	8.8	3.3	2.17	0.76
*51.25	6	22	39	0.437	16.7	8.10	651	5.02	41.3	640	175	170	127	12.5	5.87	1.17	1.11	3.88	0.540	3.86	0.45	18.5	14.0	1.96	0.47
*51.75	6	20	39	0.449	16.0	8.37	680	4.69	21.0	290	165	200	126	11.2	5.29	1.15	0.99	3.70	0.512	3.97	0.46	8.7	5.0	1.79	0.51
*52.25	6	18	39	0.454	15.6	8.45	698	4.93	26.8	400	200	180	127	11.5	5.34	1.17	0.99	3.68	0.517	4.04	0.44	12.6	6.7	1.94	0.44
*52.85	6	16	39	0.446	16.7	8.33	680	4.75	25.3	325	180	165	132	11.5	5.37	1.16	1.00	3.78	0.529	3.90	0.45	10.5	7.2	1.86	0.52
*54.25	6	3	39	0.475	16.1	8.23	674	4.74	24.7	365	215	235	126	10.6	5.01	1.21	0.93	3.59	0.499	5.28	0.59	11.9	7.5	1.79	0.47
*73.65	5	51	38	0.454	15.4	9.70	782	5.31	24.3	340	170	145	139	12.7	6.04	1.20	1.13	4.21	0.589	4.51	0.51	9.6	5.0	2.21	0.60
*74.90	5	53	38	0.460	14.9	10.24	801	5.58	30.1	420	180	200	146	13.1	6.08	1.23	1.16	4.41	0.600	4.54	0.52	12.5	7.5	2.19	0.47
*75.90	5	55	38	0.466	15.3	9.88	808	5.42	22.8	290	160	165	147	13.1	6.14	1.20	1.18	4.38	0.588	4.64	0.50	9.8	5.9	2.25	0.65
*76.90	5	57	38	0.463	15.4	9.66	775	5.52	33.0	500	175	210	142	13.1	6.19	1.22	1.17	4.35	0.595	4.53	0.52	12.7	15.0	2.22	0.63
*77.90	5	59	38	0.452	16.1	10.01	754	5.88	45.3	580	160	215	145	12.4	5.83	1.15	1.08	4.18	0.578	4.34	0.51	15.2	12.6	2.14	0.55
*78.90	5	61	38	0.465	15.8	10.16	752	5.23	26.6	325	165	200	148	12.5	6.08	1.23	1.19	4.35	0.606	4.35	0.50	9.7	5.1	2.11	0.55
*79.90	5	63	38	0.458	15.5	9.96	804	5.74	38.2	580	180	210	130	12.7	6.00	1.21	1.16	4.21	0.587	4.52	0.57	17.1	10.1	2.16	0.64
*80.90	5	66	38	0.464	15.2	10.34	823	5.58	28.1	400	180	205	153	14.7	6.93	1.23	1.30	4.73	0.646	5.13	0.60	11.8	10.9	2.48	0.71
*81.90	5	68	38	0.463	14.3	10.02	801	6.06	56.5	740	215	210	156	12.9	6.11	1.18	1.13	4.23	0.590	4.50	0.53	10.3	5.7	2.30	0.76
*82.90	5	70	38	0.466	15.0	10.26	824	5.59	27.8	410	140	190	148	13.4	6.34	1.18	1.19	4.51	0.607	4.94	0.53	9.7	8.1	2.20	0.44
*83.90	5	72	38	0.472	15.2	10.60	844	5.67	25.3	350	190	235	136	14.2	6.66	1.24	1.35	4.68	0.654	5.27	0.56	11.1	5.7	2.37	0.74
*84.90	5	74	38	0.465	15.3	11.66	876	5.98	25.3	350	215	240	150	12.5	5.99	1.18	1.24	4.24	0.609	4.41	0.52	11.5	5.2	2.03	0.58
*85.90	5	76	38	0.463	14.7	10.60	864	5.88	30.8	420	185	205	182	15.2	7.09	1.24	1.42	4.87	0.671	5.02	0.59	11.6	12.0	2.51	0.61
*86.90	5	78	38	0.476	15.1	10.64	826	5.79	31.6	420	175	190	143	13.0	6.19	1.24	1.22	4.28	0.615	4.86	0.57	14.0	8.8	2.33	0.65
*87.90	5	80	38	0.464	15.3	10.54	805	5.60	25.9	355	150	180	150	12.5	5.97	1.21	1.21	4.10	0.590	4.50	0.64	10.6	5.4	2.14	0.59
*88.90	5	82	38	0.467	15.1	10.48	823	5.77	30.4	400	180	205	139	13.3	6.22	1.23	1.31	4.22	0.601	4.67	0.52	14.8	8.6	2.25	0.63
*89.90	5	84	38	0.473	14.8	10.66	860	5.79	28.0	380	155	200	155	13.6	6.39	1.22	1.30	4.46	0.631	4.86	0.59	12.5	6.3	2.32	0.70
*90.90	5	86	38	0.471	14.9	10.80	830	5.77	28.3	395	205	190	145	13.5	6.38	1.24	1.33	4.63	0.654	4.96	0.59	11.7	8.2	2.30	0.51
*91.90	5	88	38	0.470	15.0	10.44	850	5.61	24.1	315	215	210	145	13.6	6.39	1.23	1.30	4.31	0.632	4.91	0.62	10.6	4.2	2.22	0.49
*92.90	5	90	38	0.476	15.1	10.45	832	5.59	26.1	355	135	210	156	13.4	6.27	1.24	1.31	4.45	0.610	5.00	0.54	13.4	6.9	2.30	0.63
*93.90	5	92	38	0.474	15.0	10.14	807	5.61	29.5	385	175	210	138	13.0	6.11	1.20	1.27	4.34	0.611	5.00	0.53	13.3	7.8	2.26	0.56
103.20	4	344	37	0.463	15.0	10.46	838	5.67	27.1	370	180	205	145	14.0	6.57	1.23	1.34	4.49	0.625	4.96	0.57	11.9	5.7	2.55	0.60
103.75	4	342	37	0.465	14.9	10.19	845	5.71	29.3	390	190	245	160	13.5	6.33	1.22	1.30	4.47	0.625	4.92	0.57	12.7	6.3	2.45	0.66
104.25	4	339	37	0.484	15.0	10.09	816	5.67	29.5	410	150	230	139	12.8	6.00	1.22	1.22	4.23	0.585	4.56	0.52	12.9	6.5	2.18	0.59
104.75	4	337	37	0.458	15.0	10.05	837	5.62	29.4	440	170	200	142	13.6	6.41	1.20	1.31	4.60	0.626	4.85	0.53	15.8	7.5	2.36	0.74
105.25	4	334	37	0.461	14.8	10.17	836	5.69	30.0	380	200	230	145	14.1	6.65	1.23	1.38	4.66	0.638	4.74	0.56	12.6	7.2	2.32	0.69
105.75	4	332	37	0.463	15.4	10.41	849	5.99	36.3	490	220	230	150	13.5	6.34	1.22	1.28	4.55	0.622	4.68	0.58	21.5	8.8	2.34	0.66
106.25	4	330	37	0.464	14.5	10.23	838	5.70	28.9	440	190	210	154	13.6	6.40	1.22	1.30	4.43	0.613	4.79	0.59	14.0	6.6	2.35	0.68
106.75	4	328	36	0.470	15.5	10.34	834	5.73	28.3	395	165	220	167	13.3	6.20	1.23	1.25	4.44	0.607	4.61	0.58	15.8	6.4	2.26	0.62
107.25	4	325	36	0.464	15.3	10.04	814	5.67	31.4	485	170	230	150	13.3	6.20	1.19	1.26	4.49	0.632	5.16	0.55	15.6	7.8	2.29	0.59
107.75	4	323	36	0.457	15.1	11.00	854	5.99	30.8	470	205	205	147	13.2	6.23	1.21	1.30	4.32	0.609	4.82	0.56	14.8	8.3	2.26	0.47
108.25	4	320	36	0.457	15.2	10.40	845	6.18	44.3	670	195	230	146	13.4	6.28	1.19	1.29	4.50	0.634	4.85	0.57	25.5	13.1	2.30	0.59
108.75	4	318	36	0.451	14.7	10.19	845	6.29	44.7	640	185	200	144	12.9	6.09	1.19	1.23	4.20	0.591	4.58	0.56	24.4	11.7	2.25	0.63

TABLE A3. (continued).

Depth (cm)	6000X	Parent Split	SU	Na_2O %	CaO %	Sc µg/g	Cr µg/g	FeO %	Co µg/g	Ni µg/g	Sr µg/g	Zr µg/g	Ba µg/g	La µg/g	Sm µg/g	Eu µg/g	Tb µg/g	Yb µg/g	Lu µg/g	Hf µg/g	Ta µg/g	Ir ng/g	Au ng/g	Th µg/g	U µg/g
109.25	4	316	36	0.467	14.8	11.04	882	5.97	31.7	495	160	240	150	13.9	6.62	1.23	1.35	4.57	0.640	5.00	0.54	16.7	7.0	2.29	0.63
109.80	4	314	36	0.460	14.9	10.35	861	6.13	41.7	650	190	215	153	13.4	6.36	1.21	1.33	4.37	0.624	4.76	0.57	22.7	9.8	2.37	0.58
110.30	4	312	35	0.465	15.4	10.20	851	5.93	38.5	610	185	215	147	13.0	6.10	1.21	1.22	4.32	0.589	4.63	0.54	21.3	10.0	2.17	0.58
110.75	4	309	35	0.458	15.2	10.33	848	5.77	31.7	490	180	185	156	13.2	6.19	1.26	1.30	4.28	0.603	4.79	0.55	17.8	8.7	2.32	0.43
111.25	4	307	35	0.471	15.0	10.80	861	5.93	31.0	435	180	190	142	13.0	6.12	1.21	1.20	4.32	0.600	4.72	0.54	15.8	7.2	2.30	0.55
111.75	4	305	35	0.479	14.8	10.52	854	5.93	32.4	495	205	235	162	14.7	6.97	1.22	1.40	4.91	0.692	5.31	0.60	18.7	8.6	2.45	0.70
112.25	4	303	35	0.458	15.0	10.40	829	5.90	39.1	580	165	240	147	14.4	6.79	1.22	1.37	4.53	0.631	4.98	0.58	19.4	8.8	2.45	0.56
112.75	4	300	35	0.458	14.9	10.27	842	5.98	37.7	525	170	195	137	12.8	6.03	1.22	1.19	4.31	0.596	4.56	0.53	17.2	8.4	2.25	0.63
113.25	4	298	35	0.470	14.9	10.93	851	5.93	30.0	480	215	215	149	13.7	6.50	1.23	1.33	4.57	0.640	4.96	0.59	16.6	7.6	2.37	0.66
113.75	4	296	35	0.461	15.4	10.06	825	5.88	36.7	580	170	230	144	14.0	6.47	1.23	1.36	4.35	0.619	4.75	0.56	19.0	6.3	2.24	0.55
114.25	4	294	34	0.469	15.0	10.31	825	5.84	33.4	470	165	225	134	12.9	6.15	1.22	1.21	4.47	0.633	4.95	0.54	14.9	8.2	2.31	0.65
114.75	4	291	34	0.458	14.8	10.13	826	5.66	29.9	420	180	230	142	13.5	6.33	1.19	1.34	4.34	0.616	4.74	0.58	13.6	7.3	2.28	0.58
116.00	4	289	34	0.469	14.7	10.27	835	5.72	27.9	400	160	245	159	13.5	6.37	1.24	1.26	4.37	0.620	4.94	0.55	12.8	6.8	2.38	0.54
117.35	4	284	34	0.466	15.1	10.21	840	5.90	35.1	500	175	200	153	13.8	6.59	1.21	1.30	4.57	0.641	5.00	0.54	17.7	8.1	2.39	0.63
117.85	4	282	34	0.462	15.3	10.05	818	5.73	31.9	470	195	220	141	13.3	6.23	1.21	1.26	4.41	0.616	4.66	0.58	14.7	7.5	2.31	0.62
118.25	4	279	34	0.465	15.1	10.24	836	5.64	26.6	385	195	175	133	13.5	6.38	1.19	1.31	4.27	0.624	4.67	0.59	13.8	7.0	2.26	0.54
118.75	4	276	33	0.474	15.0	10.48	869	5.92	34.2	485	190	205	151	14.6	6.83	1.25	1.35	4.68	0.654	5.00	0.60	15.7	9.2	2.32	0.59
119.25	4	274	33	0.460	15.1	10.50	858	5.66	27.1	365	195	210	158	13.6	6.42	1.20	1.34	4.56	0.632	4.83	0.55	11.7	5.9	2.35	0.59
119.75	4	272	33	0.461	15.1	10.37	822	5.70	29.5	410	160	235	178	13.4	6.30	1.23	1.32	4.54	0.628	4.80	0.58	14.3	6.4	2.22	0.57
120.25	4	269	33	0.462	14.7	10.02	820	5.39	23.2	358	170	190	159	13.3	6.22	1.18	1.25	4.29	0.604	4.98	0.53	11.2	7.1	2.35	0.54
120.75	4	267	33	0.462	14.9	10.36	830	5.63	27.0	390	160	210	157	13.9	6.49	1.22	1.30	4.40	0.620	4.65	0.58	13.4	5.4	2.35	0.58
121.25	4	265	33	0.468	15.2	10.33	840	5.74	30.8	445	195	230	172	14.2	6.67	1.22	1.36	4.73	0.661	5.05	0.61	13.5	7.9	2.47	0.68
121.75	4	263	33	0.462	15.0	10.45	834	5.74	28.8	405	170	215	153	13.4	6.25	1.22	1.26	4.51	0.613	4.63	0.56	13.1	11.4	2.31	0.39
122.30	4	260	33	0.477	14.7	9.90	805	5.53	28.3	380	230	180	134	13.2	6.25	1.25	1.28	4.22	0.599	4.71	0.53	12.5	6.4	2.22	0.59
122.80	4	258	32	0.465	15.6	10.26	830	5.79	33.0	465	185	230	171	14.4	6.66	1.24	1.34	4.67	0.637	5.18	0.60	15.1	9.1	2.40	0.72
123.25	4	256	32	0.471	15.3	10.07	800	6.03	43.1	595	195	205	150	13.4	6.26	1.23	1.27	4.41	0.601	4.61	0.55	19.6	10.7	2.26	0.52
123.75	4	254	32	0.457	15.5	10.36	853	5.66	28.2	425	155	200	135	13.8	6.44	1.22	1.33	4.44	0.633	4.85	0.58	14.2	6.2	2.29	0.45
124.25	4	251	32	0.456	14.9	10.11	822	5.57	27.3	385	185	190	137	13.4	6.29	1.19	1.25	4.39	0.619	4.78	0.56	11.8	5.3	2.32	0.54
124.70	4	249	31	0.467	15.0	10.53	855	5.93	30.6	445	190	260	159	14.3	6.76	1.25	1.38	4.65	0.659	4.97	0.61	13.6	7.9	2.52	0.59
125.20	4	246	31	0.463	15.4	10.18	823	5.59	26.2	340	210	225	160	13.6	6.37	1.22	1.27	4.40	0.622	4.89	0.59	13.9	5.5	2.33	0.59
125.75	4	244	31	0.446	14.9	9.77	792	8.80	158.6	2540	210	175	131	12.8	6.03	1.17	1.21	4.19	0.595	4.29	0.54	75.5	57.6	2.30	0.64
126.25	4	242	31	0.471	15.3	10.38	841	5.68	26.9	360	160	220	152	13.6	6.44	1.24	1.30	4.39	0.617	5.18	0.56	13.3	6.3	2.36	0.67
126.80	4	239	31	0.462	15.1	10.17	817	5.62	27.7	405	150	290	146	13.3	6.25	1.21	1.28	4.57	0.636	7.04	0.55	15.9	6.3	2.29	0.68
127.30	4	237	30	0.455	14.5	10.28	818	5.62	27.1	390	180	205	155	13.2	6.28	1.20	1.27	4.34	0.602	4.90	0.56	15.3	4.7	2.32	0.70
127.75	4	234	30	0.461	15.0	10.40	873	5.77	31.3	440	160	220	153	14.0	6.55	1.21	1.34	4.67	0.646	5.04	0.54	15.3	6.8	2.34	0.61
128.25	4	232	30	0.457	15.2	10.24	838	5.59	25.8	360	155	215	153	13.6	6.37	1.22	1.29	4.46	0.640	4.86	0.56	12.5	7.7	2.22	0.53
128.75	4	229	30	0.464	14.8	10.25	832	5.58	25.8	315	180	210	148	13.6	6.31	1.23	1.29	4.48	0.601	4.70	0.56	14.2	7.5	2.32	0.60
129.25	4	227	30	0.453	15.7	10.25	812	5.67	29.3	380	210	185	144	13.5	6.44	1.23	1.26	4.42	0.623	4.72	0.58	13.0	6.4	2.29	0.48
129.75	4	225	30	0.465	15.4	10.84	919	5.79	28.1	405	180	200	169	13.9	6.65	1.28	1.36	4.56	0.636	5.34	0.82	13.3	5.8	2.45	0.72
130.25	4	223	30	0.458	15.4	10.32	795	6.99	46.8	625	185	165	137	13.7	6.52	1.20	1.35	4.46	0.629	4.80	0.59	26.6	15.0	2.36	0.70
130.75	4	220	30	0.474	15.3	10.69	841	5.85	34.2	480	155	200	151	14.1	6.65	1.26	1.33	4.78	0.645	4.93	0.53	15.9	7.7	2.45	0.65
131.25	4	218	30	0.471	15.2	10.34	804	5.68	28.4	400	215	170	142	13.7	6.58	1.21	1.30	4.46	0.638	4.84	0.57	12.9	6.7	2.32	0.62
131.75	4	216	30	0.470	14.5	10.06	835	5.66	31.1	435	190	205	141	13.9	6.51	1.23	1.23	4.59	0.619	5.21	0.56	15.4	6.7	2.31	0.45
132.25	4	214	29	0.455	15.5	18.31	929	7.40	27.1	320	150	250	179	15.6	8.22	1.32	1.70	6.00	0.850	5.97	0.69	10.8	6.0	2.82	0.68
132.75	4	211	29	0.439	14.7	10.53	807	5.73	31.2	435	155	195	136	13.3	6.25	1.19	1.21	4.41	0.627	4.85	0.54	17.5	8.5	2.24	0.54
133.25	4	209	29	0.465	15.8	10.12	801	5.56	28.2	395	190	175	147	13.2	6.25	1.21	1.23	4.38	0.595	4.68	0.53	13.7	8.5	2.31	0.54
133.75	4	207	29	0.476	15.7	10.36	829	5.78	30.1	380	180	170	152	13.4	6.24	1.25	1.23	4.42	0.604	4.80	0.56	14.8	7.8	2.28	0.59

TABLE A3. (continued).

Depth (cm)	6000X	Parent Split	SU	Na_2O %	CaO %	Sc µg/g	Cr µg/g	FeO %	Co µg/g	Ni µg/g	Sr µg/g	Zr µg/g	Ba µg/g	La µg/g	Sm µg/g	Eu µg/g	Tb µg/g	Yb µg/g	Lu µg/g	Hf µg/g	Ta µg/g	Ir ng/g	Au ng/g	Th µg/g	U µg/g
134.25	4	205	29	0.453	14.9	10.57	819	5.68	26.5	335	185	195	147	13.6	6.33	1.23	1.28	4.56	0.602	4.80	0.53	13.2	7.0	2.36	0.66
134.75	4	202	29	0.463	15.4	10.34	815	5.60	25.0	330	190	200	144	13.8	6.56	1.27	1.25	4.48	0.631	4.85	0.56	11.1	6.4	2.35	0.60
136.00	4	200	29	0.463	15.5	10.39	836	5.60	26.1	345	170	185	148	13.6	6.46	1.23	1.28	4.44	0.622	4.77	0.57	13.9	5.8	2.24	0.58
137.25	4	195	29	0.458	15.4	10.12	819	5.60	26.8	365	180	205	148	13.6	6.42	1.23	1.26	4.48	0.632	4.79	0.58	12.4	8.0	2.37	0.60
137.75	4	193	29	0.451	15.4	10.35	827	5.65	28.8	415	155	180	155	13.9	6.64	1.21	1.33	4.52	0.653	5.04	0.59	15.9	6.3	2.44	0.72
138.25	4	190	28	0.454	14.5	10.54	850	5.63	25.5	375	200	175	145	13.7	6.31	1.25	1.25	4.52	0.594	4.71	0.59	12.1	10.9	2.31	0.64
138.75	4	188	28	0.466	14.7	10.25	840	5.65	26.1	370	160	185	129	13.8	6.46	1.24	1.31	4.72	0.630	5.25	0.60	11.9	9.1	2.31	0.64
139.25	4	186	28	0.457	15.4	9.99	1238	5.96	37.3	630	195	180	161	14.3	6.77	1.22	1.40	4.55	0.633	4.92	0.52	16.2	8.0	2.38	0.63
139.70	4	184	28	0.447	15.7	10.26	806	5.66	33.0	580	190	175	144	12.9	6.17	1.22	1.21	4.25	0.609	4.47	0.54	16.4	10.0	2.18	0.51
140.80	3	195	28	0.474	14.9	10.18	908	5.71	33.6	480	180	190	140	13.5	6.36	1.25	1.23	4.48	0.604	4.80	0.54	14.7	10.8	2.32	0.68
141.35	3	193	28	0.461	14.6	10.13	803	5.73	34.6	465	155	195	158	13.7	6.37	1.22	1.31	4.60	0.620	4.94	0.58	15.3	13.5	2.36	0.61
141.85	3	190	28	0.447	15.1	10.14	812	5.65	30.1	365	175	185	153	13.4	6.28	1.19	1.22	4.40	0.604	4.88	0.57	13.5	9.0	2.19	0.47
143.10	3	205	28	0.473	14.6	9.60	783	5.44	30.8	360	155	230	145	12.4	5.84	1.22	1.17	4.38	0.590	5.89	0.51	15.7	6.1	2.12	0.59
144.25	3	204	28	0.466	16.0	10.35	833	5.72	28.5	450	175	160	139	13.1	6.35	1.18	1.25	4.40	0.627	4.70	0.53	12.8	7.6	2.25	0.60
144.60	3	202	28	0.469	14.4	10.34	842	5.60	24.3	305	150	205	127	13.5	6.37	1.21	1.25	4.53	0.609	4.70	0.57	11.6	7.1	2.38	0.55
145.00	3	180	27	0.459	15.7	10.13	797	5.57	28.1	385	180	160	137	12.7	6.02	1.20	1.24	4.18	0.596	4.40	0.55	15.2	6.3	2.10	0.60
145.45	3	176	27	0.458	14.9	10.33	821	5.64	27.1	395	165	170	144	13.2	6.18	1.22	1.23	4.50	0.599	4.77	0.54	11.8	7.9	2.24	0.54
145.90	3	174	27	0.469	15.2	10.78	854	5.90	30.9	410	155	180	152	13.4	6.35	1.22	1.29	4.59	0.624	5.17	0.58	14.2	8.0	2.28	0.57
146.45	3	170	27	0.465	16.0	10.57	823	5.67	27.3	415	155	170	154	14.1	6.56	1.26	1.30	4.60	0.654	4.82	0.57	13.5	5.6	2.48	0.57
146.80	3	168	27	0.468	15.1	10.45	808	5.97	37.8	485	135	160	152	13.3	6.34	1.24	1.22	4.36	0.623	4.61	0.55	18.4	10.4	2.38	0.60
146.90	3	166	27	0.461	15.8	9.94	789	5.45	24.4	320	160	190	140	12.7	6.10	1.19	1.27	4.26	0.604	4.60	0.56	12.5	7.0	2.19	0.60
147.40	3	164	26	0.462	15.3	10.26	817	5.49	23.6	340	150	180	156	13.2	6.30	1.22	1.29	4.33	0.612	4.78	0.56	12.5	6.9	2.24	0.60
147.95	3	162	26	0.474	15.1	10.60	865	5.85	30.2	425	185	185	147	14.1	6.57	1.20	1.32	4.64	0.637	5.00	0.57	13.1	8.1	2.35	0.67
148.45	3	160	26	0.468	15.1	10.95	862	5.84	27.0	380	175	215	147	15.2	7.21	1.27	1.45	4.91	0.692	5.16	0.62	12.8	7.0	2.52	0.70
148.95	3	158	26	0.455	15.3	10.63	824	5.62	24.8	315	195	185	154	13.5	6.47	1.22	1.31	4.40	0.634	4.71	0.56	13.8	4.2	2.21	0.60
149.45	3	156	25	0.455	15.3	11.20	832	5.84	28.9	390	200	205	158	13.7	6.47	1.22	1.24	4.66	0.647	5.20	0.55	11.9	6.9	2.47	0.66
150.00	3	154	25	0.454	15.5	10.12	802	5.57	27.7	375	180	165	149	13.0	6.20	1.18	1.27	4.22	0.600	4.55	0.55	13.7	5.6	2.20	0.62
150.60	3	151	25	0.458	15.1	11.08	903	5.91	28.9	385	190	175	152	14.0	6.73	1.24	1.35	4.65	0.654	4.99	0.58	15.2	6.4	2.39	0.69
151.20	3	149	24	0.468	15.2	10.31	835	5.87	33.7	490	140	200	161	13.8	6.50	1.22	1.34	4.55	0.617	4.79	0.60	16.0	8.8	2.34	0.61
151.80	3	147	24	0.465	14.7	10.68	852	5.79	28.8	420	210	175	148	13.3	6.29	1.23	1.23	4.55	0.611	4.74	0.57	13.4	7.9	2.30	0.60
152.35	3	145	24	0.482	15.1	10.50	860	5.67	27.3	360	195	200	140	13.2	6.17	1.25	1.21	4.44	0.585	4.64	0.56	15.1	7.0	2.24	0.67
152.85	3	143	24	0.461	15.1	10.64	843	5.78	30.9	430	160	190	146	13.1	6.23	1.23	1.29	4.41	0.596	4.52	0.54	13.7	6.8	2.28	0.61
153.35	3	140	24	0.474	15.3	10.33	842	5.83	34.9	460	180	150	146	13.2	6.22	1.24	1.16	4.45	0.589	4.52	0.52	17.0	9.8	2.30	0.59
153.90	3	138	23	0.472	14.8	10.61	892	5.96	35.4	510	195	205	147	13.1	6.22	1.23	1.24	4.36	0.612	4.71	0.56	16.9	34.5	2.33	0.59
154.30	3	136	23	0.469	15.4	10.41	831	6.52	55.1	800	185	170	140	13.7	6.63	1.21	1.27	4.34	0.604	4.55	0.56	23.0	23.2	2.31	0.64
154.50	3	134	23	0.472	15.5	10.37	852	5.64	27.5	355	140	195	139	12.9	6.04	1.22	1.24	4.30	0.601	4.55	0.55	12.4	14.0	2.22	0.51
154.95	3	130	23	0.457	15.8	10.67	852	5.63	24.5	340	145	180	149	13.3	6.35	1.20	1.29	4.50	0.632	5.03	0.55	11.0	7.1	2.25	0.68
155.35	3	128	23	0.468	14.7	10.93	907	6.14	36.4	530	195	190	166	14.3	6.80	1.26	1.34	4.80	0.623	5.06	0.62	15.9	8.8	2.39	0.53
155.85	3	126	23	0.465	14.8	10.48	829	5.50	23.1	330	195	150	134	13.2	6.19	1.24	1.23	4.49	0.594	4.96	0.51	11.1	5.2	2.25	0.50
156.35	3	124	23	0.456	15.6	10.23	824	5.49	23.1	305	170	185	140	13.4	6.32	1.22	1.25	4.38	0.616	4.86	0.53	10.1	9.1	2.26	0.60
156.70	3	122	23	0.464	14.6	10.35	869	5.89	35.5	510	195	175	141	13.4	6.27	1.22	1.24	4.50	0.607	4.55	0.52	19.2	18.9	2.37	0.63
156.95	3	120	23	0.471	14.5	10.30	836	5.99	39.4	610	190	185	146	13.8	6.56	1.23	1.26	4.62	0.620	4.80	0.56	17.8	23.1	2.43	0.66
157.25	3	118	23	0.467	14.8	10.29	850	5.60	25.2	315	195	170	142	13.3	6.15	1.25	1.19	4.37	0.584	4.59	0.49	11.8	6.1	2.22	0.56
157.65	3	116	22	0.465	14.7	10.27	840	5.57	27.2	355	165	195	152	13.6	6.34	1.24	1.32	4.57	0.614	4.92	0.55	12.6	5.2	2.28	0.52
158.15	3	114	22	0.460	15.2	10.43	846	6.24	45.3	615	195	235	140	13.9	6.54	1.24	1.28	4.55	0.646	5.00	0.58	23.1	12.2	2.41	0.69
158.60	3	112	22	0.458	15.5	10.52	839	6.21	46.0	690	175	235	157	13.4	6.32	1.23	1.26	4.34	0.623	4.80	0.53	19.3	13.2	2.36	0.63
159.10	3	109	22	0.475	14.7	10.44	819	5.54	25.2	330	195	170	142	13.0	6.05	1.25	1.20	4.40	0.594	4.60	0.53	9.9	5.2	2.33	0.53

TABLE A3. (continued).

Depth (cm)	6000X	Parent Split	SU	Na_2O %	CaO %	Sc µg/g	Cr µg/g	FeO %	Co µg/g	Ni µg/g	Sr µg/g	Zr µg/g	Ba µg/g	La µg/g	Sm µg/g	Eu µg/g	Tb µg/g	Yb µg/g	Lu µg/g	Hf µg/g	Ta µg/g	Ir ng/g	Au ng/g	Th µg/g	U µg/g
159.50	3	107	21	0.476	15.6	10.42	819	5.51	23.9	335	165	170	149	13.2	6.29	1.24	1.22	4.34	0.600	4.59	0.55	9.8	12.3	2.15	0.59
159.90	3	104	21	0.465	15.7	10.38	826	5.53	25.4	370	155	210	152	13.0	6.14	1.21	1.24	4.32	0.607	4.79	0.56	10.6	5.4	2.23	0.58
160.50	3	102	21	0.466	14.8	10.60	861	5.81	28.6	445	195	200	161	13.3	6.21	1.21	1.24	4.45	0.613	4.80	0.60	14.5	7.2	2.24	0.61
161.05	3	98	21	0.471	15.2	10.29	835	5.58	24.7	340	160	225	141	13.2	6.09	1.20	1.24	4.39	0.615	4.76	0.55	13.3	6.2	2.25	0.65
161.45	3	96	20	0.470	15.7	10.43	841	5.59	24.5	375	180	235	151	13.3	6.22	1.22	1.24	4.44	0.619	4.97	0.56	11.1	6.3	2.35	0.59
161.85	3	94	20	0.467	15.1	11.07	833	5.79	28.7	445	170	240	145	13.0	6.16	1.23	1.23	4.44	0.606	4.71	0.55	14.7	5.9	2.24	0.52
162.35	3	91	20	0.461	14.5	10.72	859	5.65	25.5	360	160	220	131	13.1	6.15	1.22	1.27	4.44	0.622	4.81	0.58	11.1	5.1	2.15	0.60
162.90	3	88	20	0.463	15	10.22	824	5.52	24.7	385	165	205	148	13.3	6.25	1.22	1.26	4.36	0.598	4.76	0.56	10.3	5.5	2.21	0.57
163.40	3	86	20	0.464	14.7	10.08	802	5.65	30.6	500	155	220	129	12.9	6.06	1.19	1.23	4.32	0.589	4.54	0.54	15.2	7.2	2.20	0.55
163.85	3	84	19	0.470	15.1	10.70	872	5.72	25.2	375	155	240	170	13.7	6.41	1.24	1.31	4.57	0.629	4.97	0.58	11.8	5.2	2.36	0.64
164.35	3	82	19	0.460	15.2	10.37	823	5.63	27.0	395	180	230	145	13.1	6.14	1.23	1.24	4.40	0.605	4.70	0.54	12.2	7.5	2.19	0.64
164.85	3	80	19	0.472	14.6	10.08	869	5.65	29.9	455	175	240	141	13.4	6.21	1.22	1.27	4.46	0.608	4.78	0.57	13.6	6.3	2.31	0.55
165.35	3	78	19	0.460	14.8	10.76	845	5.88	28.5	430	160	245	160	14.6	6.75	1.21	1.37	4.76	0.656	5.11	0.60	11.8	6.4	2.44	0.60
165.85	3	75	19	0.481	14.7	10.22	815	5.55	24.8	390	200	235	140	13.5	6.22	1.25	1.26	4.49	0.614	4.80	0.56	10.7	4.7	2.39	0.62
166.35	3	73	19	0.463	15.1	10.41	845	5.71	27.7	410	190	235	138	13.2	6.20	1.23	1.25	4.42	0.618	4.86	0.58	12.2	8.3	2.19	0.44
166.85	3	71	19	0.461	15.4	10.48	828	5.64	24.1	385	170	265	143	14.0	6.55	1.23	1.32	4.60	0.642	4.98	0.58	11.7	4.6	2.38	0.64
167.35	3	69	18	0.462	15.3	10.57	836	5.97	35.9	555	180	235	131	13.4	6.27	1.20	1.26	4.49	0.626	4.74	0.55	17.6	8.9	2.26	0.58
167.85	3	67	18	0.465	15.4	10.35	804	5.53	25.6	390	160	240	143	12.9	6.09	1.22	1.24	4.25	0.592	4.66	0.55	12.0	5.5	2.16	0.58
168.35	3	62	18	0.456	15.2	10.31	834	5.63	27.8	390	175	215	153	13.2	6.17	1.20	1.27	4.34	0.602	4.65	0.56	12.1	5.6	2.21	0.68
168.85	3	60	18	0.470	15.2	10.40	826	5.60	24.7	345	185	250	143	13.1	6.13	1.22	1.26	4.35	0.614	4.84	0.56	11.3	4.7	2.19	0.67
169.35	3	58	17	0.469	14.8	10.53	851	5.76	26.1	385	150	230	146	13.8	6.39	1.22	1.29	4.61	0.649	5.06	0.57	11.6	5.9	2.45	0.61
169.85	3	56	17	0.464	15.4	10.45	817	5.79	30.6	455	160	250	147	13.9	6.51	1.22	1.31	4.51	0.632	4.90	0.60	12.5	7.3	2.37	0.63
170.35	3	54	17	0.480	14.8	11.31	847	6.04	31.3	460	180	255	172	14.1	6.62	1.23	1.34	4.82	0.659	4.91	0.57	16.0	6.3	2.56	0.78
170.70	3	52	17	0.474	15.2	10.28	821	5.74	28.9	440	175	230	149	13.5	6.33	1.23	1.29	4.43	0.621	4.87	0.54	13.9	9.0	2.26	0.65
170.95	3	50	16	0.469	14.8	10.19	822	5.63	30.3	475	170	220	135	12.8	6.02	1.18	1.22	4.38	0.609	4.64	0.53	15.5	6.8	2.14	0.59
171.35	3	48	16	0.468	15	10.31	827	5.74	28.6	450	175	245	145	13.5	6.25	1.22	1.27	4.51	0.636	4.99	0.60	13.2	105.	2.29	0.53
171.85	3	45	16	0.469	15	10.44	835	5.82	30.6	490	170	235	151	13.4	6.33	1.20	1.29	4.55	0.636	4.76	0.59	15.9	9.3	2.40	0.65
173.10	3	41	16	0.478	15.2	10.38	850	5.75	27.1	420	185	240	158	14.4	6.62	1.23	1.36	4.82	0.645	5.28	0.61	14.6	11.9	2.42	0.60
174.25	3	39	16	0.471	14.8	10.13	830	5.77	30.8	485	190	215	160	13.3	6.24	1.21	1.29	4.43	0.611	4.84	0.56	15.6	7.6	2.24	0.57
174.50	3	37	15	0.475	14.9	10.67	888	5.93	29.4	450	155	195	143	14.0	6.53	1.26	1.31	4.68	0.643	4.93	0.58	14.3	6.6	2.32	0.60
174.70	3	35	15	0.486	15.1	10.68	840	5.93	33.0	485	170	235	157	14.3	6.62	1.24	1.35	4.77	0.652	4.94	0.57	14.0	9.0	2.35	0.59
175.20	3	32	15	0.467	14.9	10.29	825	5.85	33.3	510	175	260	155	14.0	6.51	1.23	1.30	4.59	0.631	4.94	0.58	15.4	9.2	2.39	0.53
175.80	3	30	15	0.489	15.6	10.23	819	5.73	29.1	465	175	255	158	14.2	6.43	1.24	1.33	4.56	0.630	5.03	0.55	15.8	6.7	2.30	0.58
176.35	3	28	15	0.471	14.8	10.46	858	5.86	30.0	455	160	255	150	13.4	6.26	1.22	1.27	4.55	0.625	5.09	0.56	14.7	6.1	2.21	0.56
176.85	3	26	15	0.476	14.7	10.31	861	5.98	34.1	550	160	255	151	13.9	6.52	1.19	1.33	4.71	0.645	5.13	0.59	15.9	28.3	2.41	0.57
177.35	3	24	14	0.478	14.9	10.13	837	6.04	39.8	680	185	235	147	13.3	6.20	1.22	1.27	4.41	0.619	4.66	0.57	19.2	10.7	2.24	0.54
177.85	3	21	14	0.471	14.9	10.55	873	6.00	32.8	585	185	245	153	14.0	6.54	1.19	1.33	4.70	0.659	5.09	0.60	15.7	191.	2.43	0.57
178.40	3	19	14	0.477	14.7	10.31	844	5.95	35.2	530	185	215	149	13.2	6.17	1.21	1.22	4.44	0.613	4.73	0.59	14.9	8.9	2.22	0.53
179.05	3	16	14	0.472	14.6	10.01	853	6.88	66.5	1180	180	235	151	13.7	6.36	1.19	1.31	4.55	0.628	4.88	0.57	39.4	16.1	2.30	0.62
180.20	2	21	13	0.469	15.6	10.30	854	6.19	41.3	710	170	240	144	13.3	6.26	1.20	1.30	4.41	0.613	4.78	0.57	20.8	12.0	2.18	0.56
180.65	2	23	13	0.467	14.3	10.42	874	6.31	40.8	700	165	255	156	14.0	6.37	1.23	1.27	4.60	0.623	5.26	0.59	23.5	9.3	2.28	0.53
181.15	2	25	13	0.467	15.4	10.02	856	6.27	45.6	790	200	205	158	13.2	6.19	1.20	1.26	4.37	0.617	4.63	0.55	22.3	11.7	2.18	0.59
181.65	2	27	13	0.471	15.1	10.18	867	6.29	43.7	820	185	205	145	12.8	6.01	1.18	1.19	4.22	0.593	4.55	0.54	23.9	10.3	2.29	0.46
182.15	2	29	13	0.471	15.6	10.86	915	7.76	87.4	1480	175	240	144	13.7	6.38	1.21	1.30	4.58	0.641	4.89	0.56	32.9	24.3	2.15	0.58
182.65	2	31	13	0.465	15.1	10.00	861	6.72	55.6	1090	220	255	138	13.3	6.20	1.18	1.28	4.43	0.620	5.01	0.56	28.6	14.4	2.23	0.60
183.15	2	34	13	0.465	15.3	10.30	899	6.71	51.7	1000	185	240	135	12.6	5.95	1.18	1.23	4.19	0.590	4.57	0.53	32.8	11.7	2.14	0.55
183.65	2	36	13	0.474	15.5	10.29	910	6.58	48.4	900	200	200	151	13.0	6.01	1.23	1.21	4.30	0.589	4.57	0.52	28.6	12.7	2.28	0.53

TABLE A3. (continued).

Depth (cm)	6000X	Parent Split	SU	Na_2O %	CaO %	Sc µg/g	Cr µg/g	FeO %	Co µg/g	Ni µg/g	Sr µg/g	Zr µg/g	Ba µg/g	La µg/g	Sm µg/g	Eu µg/g	Tb µg/g	Yb µg/g	Lu µg/g	Hf µg/g	Ta µg/g	Ir ng/g	Au ng/g	Th µg/g	U µg/g
184.15	2	38	13	0.468	14.2	10.47	939	6.73	51.5	980	185	220	140	13.3	6.26	1.19	1.29	4.54	0.624	4.67	0.59	31.2	12.6	2.33	0.61
184.65	2	40	13	0.461	14.6	10.34	908	6.82	53.2	1030	180	220	150	13.5	6.22	1.20	1.25	4.52	0.630	4.90	0.57	32.3	11.9	2.42	0.53
185.15	2	43	13	0.480	14.2	10.30	885	6.59	49.4	920	190	215	161	14.2	6.56	1.22	1.32	4.63	0.642	4.78	0.59	28.1	11.9	2.31	0.57
185.60	2	45	13	0.462	15.0	10.35	876	6.67	52.6	960	195	220	153	13.1	6.11	1.20	1.25	4.41	0.613	4.61	0.54	27.7	12.8	2.30	0.51
185.95	2	51	13	0.466	14.5	10.14	874	6.56	49.5	960	190	200	134	13.2	6.11	1.18	1.28	4.31	0.608	4.56	0.55	29.0	11.7	2.26	0.51
186.35	2	53	13	0.476	14.8	10.38	877	6.65	50.1	910	175	230	164	13.5	6.19	1.20	1.25	4.50	0.624	5.02	0.61	30.2	10.6	2.32	0.55
186.45	2	56	13	0.474	14.6	10.33	860	6.18	39.4	720	175	230	149	13.7	6.31	1.22	1.31	4.53	0.629	4.96	0.57	18.6	7.4	2.45	0.64
186.95	2	58	12	0.489	14.7	10.18	835	5.90	33.1	570	165	255	153	13.4	6.22	1.22	1.27	4.45	0.603	5.07	0.60	17.6	9.3	2.42	0.66
187.25	2	61	12	0.502	14.2	10.46	862	6.12	34.9	550	170	320	183	15.2	7.07	1.22	1.43	4.97	0.688	6.36	0.72	15.5	10.0	2.78	0.67
187.50	2	63	12	0.497	15.2	10.36	855	5.90	29.4	450	165	245	162	15.6	7.08	1.24	1.41	5.00	0.687	5.51	0.65	13.0	6.7	2.65	0.65
187.75	2	65	12	0.501	14.9	10.39	856	5.64	23.9	335	170	400	171	16.3	7.42	1.25	1.49	5.31	0.733	7.55	0.68	9.9	15.3	2.58	0.65
188.20	2	69	12	0.504	14.0	10.34	834	5.62	25.1	325	190	300	165	15.4	7.15	1.22	1.45	4.99	0.671	5.64	0.67	7.8	5.1	2.54	0.73
188.65	2	73	12	0.523	15.2	10.38	863	5.83	35.6	455	175	280	168	15.9	7.26	1.24	1.47	5.17	0.693	5.70	0.65	15.8	9.2	2.60	0.59
188.95	2	75	12	0.516	15.1	10.05	813	5.68	26.9	350	190	270	174	15.4	7.12	1.24	1.43	5.00	0.686	5.73	0.71	10.6	6.5	2.54	0.57
189.45	2	78	12	0.526	15.5	9.48	788	5.27	24.6	340	170	275	167	15.6	7.04	1.25	1.43	4.95	0.673	5.57	0.62	9.7	4.5	2.43	0.49
190.05	2	80	12	0.498	15.7	9.25	758	5.38	34.9	465	185	310	153	14.3	6.58	1.19	1.32	4.74	0.643	5.93	0.60	20.3	8.5	2.34	0.56
190.55	2	82	12	0.508	15.0	9.84	806	5.40	23.6	315	200	225	160	14.2	6.65	1.20	1.30	4.65	0.628	4.84	0.60	9.7	4.9	2.39	0.54
191.10	2	84	11	0.494	14.9	10.25	867	5.95	31.8	470	190	255	156	14.7	6.85	1.21	1.38	4.77	0.670	5.12	0.58	10.8	9.8	2.26	0.66
191.65	2	87	11	0.509	15.2	10.17	865	5.76	38.5	385	175	235	148	13.4	6.11	1.21	1.29	4.41	0.594	4.73	0.57	14.7	7.7	2.16	0.64
192.25	2	89	11	0.508	15.6	10.04	826	5.56	25.1	310	180	210	142	13.1	6.15	1.18	1.31	4.46	0.609	4.64	0.53	9.0	5.7	2.18	0.50
192.90	2	92	11	0.506	14.8	9.88	823	5.51	26.5	330	180	225	152	14.0	6.57	1.23	1.36	4.50	0.628	4.85	0.56	10.7	7.3	2.16	0.48
193.50	2	94	11	0.513	15.3	10.30	845	5.68	29.5	370	185	230	146	14.2	6.44	1.23	1.29	4.56	0.620	5.12	0.60	11.8	6.7	2.44	0.65
194.05	2	96	10	0.517	15.5	10.47	855	5.68	25.2	350	175	225	149	13.9	6.42	1.22	1.35	4.65	0.637	5.17	0.55	10.1	7.0	2.27	0.50
194.60	2	98	10	0.510	15.0	10.36	852	5.54	21.9	275	180	255	155	15.4	7.11	1.27	1.43	5.06	0.695	5.37	0.65	7.9	4.4	2.61	0.56
195.20	2	100	10	0.511	15.2	10.53	854	5.50	21.5	290	155	225	165	15.5	7.18	1.27	1.46	5.09	0.708	5.37	0.65	8.7	4.7	2.77	0.77
195.75	2	102	10	0.496	15.3	10.25	839	5.55	23.7	275	200	230	169	14.0	6.54	1.22	1.30	4.55	0.642	5.02	0.61	9.3	5.8	2.37	0.58
196.30	2	104	10	0.509	15.2	9.91	817	5.35	22.5	305	165	260	162	14.7	6.87	1.22	1.41	4.76	0.654	5.33	0.62	9.2	6.1	2.50	0.61
196.80	2	106	10	0.516	15.5	9.79	819	5.44	26.8	300	175	305	155	14.6	6.65	1.25	1.39	4.86	0.652	5.81	0.60	7.4	6.4	2.51	0.63
197.20	2	110	9	0.504	15.4	9.75	805	5.27	22.3	270	170	215	164	14.3	6.62	1.22	1.38	4.67	0.641	4.98	0.63	8.9	4.4	2.37	0.79
197.65	2	112	9	0.508	15.1	9.35	791	5.13	21.8	280	180	205	150	13.6	6.26	1.20	1.24	4.36	0.610	4.81	0.57	8.3	6.0	2.27	0.72
198.15	2	115	9	0.500	15.5	9.26	777	5.23	25.1	310	170	235	153	14.0	6.52	1.20	1.34	4.56	0.632	4.74	0.59	8.8	5.0	2.41	0.43
198.65	2	117	9	0.510	15.1	9.60	777	5.27	24.3	290	155	235	154	14.2	6.59	1.22	1.30	4.68	0.632	4.66	0.58	8.7	4.6	2.33	0.63
199.15	2	119	9	0.513	15.4	9.86	806	5.36	21.5	255	190	215	156	16.9	7.76	1.26	1.53	5.11	0.677	4.73	0.59	7.6	4.0	2.36	0.60
199.65	2	121	8	0.514	15.2	9.51	803	5.25	22.0	280	170	215	133	12.8	5.92	1.20	1.20	4.18	0.577	4.66	0.52	8.9	7.1	2.14	0.54
200.15	2	123	8	0.496	15.3	9.19	767	5.04	21.8	280	180	200	129	12.0	5.57	1.20	1.13	3.93	0.550	4.29	0.53	9.3	4.2	2.14	0.59
200.70	2	125	8	0.513	15.0	10.02	832	5.62	28.4	375	200	230	156	13.8	6.39	1.23	1.31	4.54	0.617	4.87	0.59	11.1	6.4	2.39	0.64
201.40	2	127	7	0.494	15.0	9.30	790	5.39	30.7	425	185	235	149	13.4	6.21	1.20	1.23	4.51	0.606	4.81	0.58	10.8	9.6	2.39	0.70
202.15	2	129	7	0.509	15.1	10.01	842	5.48	23.4	290	190	235	157	14.7	6.83	1.23	1.37	4.88	0.666	5.27	0.65	9.2	4.6	2.49	0.59
202.80	2	132	6	0.511	15.4	9.44	785	5.22	22.2	296	185	220	161	15.5	7.14	1.24	1.41	4.97	0.680	5.16	0.63	14.1	5.1	2.65	0.66
203.30	2	134	6	0.509	15.4	9.62	828	5.30	23.1	295	170	230	173	14.4	6.63	1.20	1.37	4.81	0.659	5.22	0.62	10.2	5.7	2.63	0.71
203.75	2	136	6	0.508	15.1	9.53	837	5.36	26.4	380	175	225	174	15.4	7.08	1.24	1.42	4.91	0.664	5.27	0.65	11.8	6.9	2.47	0.62
204.25	2	138	6	0.508	15.1	9.74	829	5.44	28.0	380	170	225	156	14.4	6.59	1.22	1.32	4.74	0.634	5.04	0.60	12.8	7.7	2.48	0.80
204.55	2	140	5	0.518	15.4	9.20	758	5.15	23.8	330	205	245	168	13.7	6.17	1.23	1.25	4.51	0.619	4.78	0.63	10.9	5.4	2.44	0.59
204.80	2	142	5	0.496	14.7	9.65	810	5.68	35.1	520	175	225	146	13.1	6.03	1.18	1.21	4.38	0.617	4.55	0.56	23.2	9.6	2.14	0.56
205.20	2	144	5	0.499	15.2	9.39	791	5.12	21.3	265	175	225	136	13.2	6.16	1.20	1.24	4.32	0.594	4.75	0.55	8.4	4.3	2.25	0.66
205.65	2	146	5	0.498	15.2	9.21	775	5.07	21.3	290	175	210	151	13.3	6.12	1.18	1.25	4.34	0.593	4.86	0.60	8.4	6.5	2.23	0.60
206.15	2	149	5	0.503	14.7	9.31	784	5.42	30.1	420	160	235	149	14.2	6.68	1.22	1.37	4.76	0.643	4.89	0.59	13.9	8.4	2.42	0.65

TABLE A3. (continued).

Depth (cm)	6000X	Parent Split	SU	Na_2O %	CaO %	Sc µg/g	Cr µg/g	FeO %	Co µg/g	Ni µg/g	Sr µg/g	Zr µg/g	Ba µg/g	La µg/g	Sm µg/g	Eu µg/g	Tb µg/g	Yb µg/g	Lu µg/g	Hf µg/g	Ta µg/g	Ir ng/g	Au ng/g	Th µg/g	U µg/g
206.70	2	151	5	0.507	15.2	9.67	801	5.22	22.3	290	165	295	174	14.5	6.75	1.21	1.40	4.84	0.652	5.46	0.62	9.6	4.9	2.49	0.75
207.25	2	153	4	0.511	14.9	9.50	791	5.28	24.2	305	180	235	165	14.2	6.58	1.23	1.39	4.71	0.641	5.15	0.60	9.5	7.0	2.39	0.62
207.70	2	155	4	0.502	15.5	9.29	791	5.10	21.2	280	190	240	163	14.0	6.51	1.22	1.35	4.68	0.629	5.01	0.58	9.7	5.1	2.37	0.59
208.15	2	157	3	0.506	15.1	9.36	778	5.14	23.3	315	190	235	162	13.9	6.48	1.22	1.29	4.53	0.624	5.07	0.59	8.8	5.4	2.28	0.48
208.65	2	159	3	0.514	15.2	9.96	833	5.43	24.2	295	185	240	172	15.3	7.09	1.26	1.39	5.04	0.681	5.40	0.64	10.0	4.5	2.70	0.63
209.15	2	161	3	0.507	15.2	9.57	780	5.20	22.1	305	185	230	158	14.7	6.74	1.22	1.33	4.82	0.652	5.12	0.64	9.1	5.2	2.54	0.62
209.65	2	163	3	0.508	15.2	9.88	793	5.30	20.3	250	185	250	179	14.7	6.80	1.24	1.43	4.98	0.666	5.41	0.63	7.1	3.9	2.53	0.54
210.20	2	165	3	0.526	15.4	9.94	795	5.52	28.0	375	170	485	167	14.7	6.73	1.24	1.34	5.21	0.727	9.16	0.67	12.5	6.5	2.68	0.76
210.85	2	167	3	0.525	15.5	9.97	808	5.33	21.8	270	195	250	159	15.1	6.94	1.25	1.37	4.95	0.668	5.08	0.64	8.1	8.1	2.52	0.64
211.40	2	169	3	0.504	15.8	9.75	783	5.20	19.8	235	175	240	142	14.0	6.45	1.22	1.31	4.74	0.641	4.98	0.59	16.5	4.5	2.39	0.74
211.95	2	171	3	0.502	14.9	9.58	785	5.39	29.0	380	205	225	157	13.8	6.44	1.18	1.30	4.48	0.606	4.73	0.57	9.9	8.8	2.36	0.58
212.50	2	174	2	0.490	15.4	9.82	821	5.99	47.8	660	200	240	163	13.8	6.33	1.19	1.24	4.46	0.614	4.90	0.56	25.4	12.9	2.34	0.61
213.00	2	176	2	0.483	15.4	9.43	774	5.24	24.5	360	175	225	142	12.4	5.74	1.17	1.15	4.06	0.558	4.62	0.53	9.5	7.3	1.96	0.51
213.85	2	180	2	0.494	15.2	9.65	796	5.16	21.2	255	170	245	152	12.5	5.89	1.18	1.19	4.12	0.559	4.31	0.50	9.7	5.2	2.10	0.55
215.20	2	5	2	0.490	15.4	9.78	798	5.21	21.1	290	160	190	130	11.8	5.53	1.16	1.09	3.97	0.554	4.14	0.52	8.6	4.7	1.98	0.54
215.65	2	3	2	0.493	15.5	9.97	838	5.41	22.6	308	180	225	143	12.5	5.77	1.22	1.20	4.17	0.566	4.49	0.51	9.9	6.1	2.00	0.59
216.55	1	28	1	0.544	14.9	10.72	760	5.63	23.3	290	185	340	310	21.8	9.10	1.37	1.89	7.59	1.030	7.20	0.94	11.4	5.9	4.75	1.23
217.05	1	26	1	0.474	14.7	9.97	816	6.35	41.7	638	190	200	130	12.5	5.68	1.20	1.16	4.10	0.558	4.28	0.49	19.7	9.3	2.15	0.56
217.55	1	24	1	0.475	15.1	9.49	797	5.74	45.5	690	210	170	123	10.9	5.18	1.14	1.07	3.66	0.503	3.79	0.48	21.5	15.9	1.82	0.48
218.05	1	22	1	0.478	14.9	10.00	847	5.81	30.4	460	175	320	203	18.7	8.67	1.29	1.75	5.98	0.806	6.76	0.75	12.2	5.7	3.25	0.87
218.55	1	20	1	0.480	14.8	9.06	767	5.28	29.8	385	195	235	157	15.4	7.16	1.19	1.40	4.78	0.646	4.61	0.56	15.5	9.0	2.74	0.77
219.05	1	18	1	0.481	14.6	9.37	846	5.44	28.9	355	180	250	162	15.2	7.02	1.22	1.43	4.96	0.677	5.28	0.65	10.9	7.5	2.52	0.68
219.55	1	16	1	0.492	15.7	9.74	849	5.54	31.9	460	185	300	153	14.7	6.75	1.24	1.41	4.97	0.686	6.08	0.59	14.4	8.6	2.45	0.78
220.05	1	14	1	0.494	15.2	9.97	830	5.61	30.3	355	185	225	164	14.4	6.58	1.28	1.38	4.80	0.663	4.83	0.60	9.4	6.7	2.34	0.66
Mean				0.465	15.4	9.71	790	5.50	30.4	439	177	205	144	13.2	6.16	1.20	1.22	4.34	0.599	4.71	0.54	14.4	9.0	2.23	0.57
Minimum				0.401	14.0	6.13	505	3.62	16.2	194	120	91	89	7.9	3.73	1.02	0.71	2.62	0.368	2.75	0.32	6.7	3.0	1.28	0.27
Maximum				0.544	17.5	18.31	1238	11.08	222.	3290	239	483	310	31.9	14.5	1.37	2.68	8.86	1.202	10.3	1.03	204.	191.	4.75	1.23
±				0.010	0.5	0.10	8	0.06	0.3	25	25	25	11	0.2	0.10	0.02	0.03	0.08	0.012	0.09	0.03	1.3	1.5	0.06	0.05

Depth = Depth below surface of center of sampling interval based on depth data of *Allton et al.* (1981). For 60005 and 60006 (*), the soils have been disturbed and mixed as a result of voids; the original stratigraphic position is unknown (see text, section 5.1.2 and Fig. 10). For 60005 and 60006, the listed depth values represent the location in the core tube where sample was found during core processing. SU = stratigraphic unit (SU) of *Duke and Nagle* (1976). "±" = estimate of analytical precision (one standard deviation).

TABLE A4. INAA results for particles removed from <1-mm samples of 60001-7.

Particle Number	Note	6000X	Parent Split	Lab ID	Mass mg	Na_2O %	CaO %	Sc μg/g	Cr μg/g	FeO %	Co μg/g	Ni μg/g	Sr μg/g	Zr μg/g	Ba μg/g
6.01	S	6	93	227.058	0.452	0.172	17.8	8.75	329	3.21	2.5	<50	223	150	143
5.01	S	5	90	223.220	0.210	0.466	15.3	7.53	675	4.03	13.5	<350	<400	<250	<250
4.01		4	282	223.219	13.35	0.302	17.4	1.20	312	1.40	6.3	50	180	<30	14
4.02		4	207	223.292	5.02	0.604	14.4	7.78	656	4.86	19.4	260	200	160	114
4.03		4	218	223.291	4.61	0.534	11.6	17.0	1340	8.74	28.0	350	170	400	360
3.01	S	3	143	223.289	0.309	0.121	15.3	6.92	740	5.35	29.2	240	140	<250	<200
3.02	S	3	120	223.290	0.613	0.605	16.4	7.52	681	3.78	15.1	260	330	<250	<80
2.35	S	2	174	227.020	0.058	0.267	16.5	2.46	156	1.54	18.9	360	130	90	<100
2.36	S	2	84	227.019	0.036	0.523	14.4	9.51	1020	7.05	52.8	360	180	370	180
2.37		2	180	227.023	2.267	0.523	21.7	1.16	58	0.55	7.2	21	211	11	14
2.38		2	21	227.021	2.243	0.643	15.8	6.65	483	3.94	10.0	64	214	84	98
2.39		2	3	227.022	7.989	0.225	15.7	9.72	782	5.28	18.7	173	144	43	46
1.01		1	22	227.016	13.92	0.481	16.2	7.46	602	4.23	17.5	215	161	101	95
1.02		1	14	227.014	3.015	0.480	15.8	7.99	645	4.25	15.0	161	190	123	87
1.03		1	26	227.017	4.961	0.327	14.9	8.06	541	4.56	15.4	57	140	40	44
1.04		1	14	227.013	2.515	0.496	15.7	10.1	761	5.52	30.7	415	184	180	128
1.05		1	16	227.015	4.957	0.520	14.3	10.4	866	6.20	37.0	490	162	379	273
1.06		1	28	227.018	4.087	0.510	12.2	11.6	1154	6.63	13.6	194	142	400	260

TABLE A4. (continued).

Particle Number	La μg/g	Ce μg/g	Sm μg/g	Eu μg/g	Tb μg/g	Yb μg/g	Lu μg/g	Hf mg/g	Ta μg/g	Ir ng/g	Au ng/g	Th μg/g	U μg/g
6.01	10.28	25.9	4.91	1.51	0.97	3.73	0.518	3.91	0.51	<10.	<20.	1.74	0.33
5.01	5.99	n.a.	2.89	1.23	0.56	2.17	0.29	2.82	0.30	<10.	<30.	1.04	<1.
4.01	0.168	n.a.	0.074	0.727	0.017	0.059	0.0077	<0.1	<0.02	1.5	1.0	<0.03	<0.0
4.02	8.72	n.a.	4.05	1.40	0.87	2.99	0.426	2.94	0.37	11.	3.1	1.50	0.47
4.03	41.2	n.a.	19.4	1.61	3.83	12.2	1.67	9.2	0.94	6.	7.	6.84	1.72
3.01	4.12	n.a.	1.94	0.99	0.42	1.60	0.220	1.76	0.17	<10.	<20.	0.75	<1.
3.02	0.92	n.a.	0.54	1.09	0.15	0.40	0.058	<0.5	<0.3	<10.	<30.	<0.4	<1.
2.35	2.62	5.0	0.68	0.82	0.14	0.45	0.072	1.72	<0.3	14.9	9.5	0.19	0.21
2.36	13.70	33.5	5.49	1.12	1.10	3.66	0.531	6.73	0.38	15.0	14.0	1.97	0.44
2.37	0.28	0.7	0.13	0.97	0.02	0.07	0.010	0.20	<0.03	<5.	0.9	0.03	<0.1
2.38	6.67	17.2	3.17	1.44	0.61	2.13	0.291	2.37	0.27	2.5	<3.	0.88	0.27
2.39	3.46	9.0	1.71	0.77	0.33	1.33	0.184	1.25	0.15	6.7	1.7	0.53	0.16
1.01	8.24	21.	3.82	1.08	0.74	2.69	0.380	2.73	0.34	6.6	3.2	1.55	0.44
1.02	8.15	21.	3.83	1.08	0.73	2.61	0.365	2.82	0.31	6.0	2.5	1.22	0.33
1.03	3.13	8.0	1.46	0.79	0.28	1.14	0.161	0.99	0.13	1.3	<2.	0.45	0.12
1.04	11.3	29.	5.40	1.18	1.02	3.73	0.524	4.34	0.50	14.2	7.0	1.80	0.48
1.05	28.5	73.	13.2	1.36	2.55	9.16	1.271	9.05	1.22	13.9	10.2	5.35	1.55
1.06	27.4	71.	13.0	1.53	2.47	8.39	1.183	9.31	1.14	<3.	3.5	4.22	1.06

Note: S = sphere; n.a. = not analyzed.

TABLE A5. INAA results for >1-mm particles allocated from 60002 arranged in order of increasing Sc concentration.

Particle Number	Note	Parent Split	Lab ID	Mass mg	Na_2O %	CaO %	Sc μg/g	Cr μg/g	FeO %	Co μg/g	Ni μg/g	Sr μg/g	Zr μg/g	Ba μg/g
2.25		147	240.032	21.044	0.396	18.4	0.371	15	0.269	0.39	<10	175	<20	7
2.13		137	240.013	3.381	0.991	18.1	0.760	16	0.468	0.53	<15	311	<60	56
2.31		95	240.038	4.639	1.108	17.3	0.805	26	1.26	1.30	7	372	<40	48
2.26		147	240.033	4.221	0.541	17.4	2.07	127	1.59	2.49	12	238	<40	21
2.11		137	240.011	3.432	0.451	18.7	2.74	139	0.687	2.11	30	166	15	60
2.04		126	240.004	13.971	0.372	19.2	4.31	202	1.08	1.55	7	156	<20	14
2.19A		139	240.019	14.879	0.421	17.3	4.33	388	2.39	5.87	40	180	17	21
2.19B		139	240.020	10.474	0.421	17.4	4.41	309	2.46	5.22	22	169	15	25
2.19C		139	240.021	11.833	0.449	17.7	4.63	338	2.40	5.66	28	168	23	24
2.19D		139	240.022	2.212	0.456	17.7	4.63	321	2.51	8.05	90	192	39	27
2.19E		139	240.023	4.075	0.453	17.3	4.80	350	2.63	10.8	82	160	33	26
2.19F		139	240.024	4.250	0.417	17.7	4.22	304	2.40	5.41	48	171	19	21
2.19G		139	240.025	6.301	0.422	17.6	4.41	310	2.40	5.69	30	172	19	28
2.19H		139	240.026	1.757	0.460	17.1	4.56	358	2.23	2.77	24	195	<50	39
2.19	M	139	240.M19	55.781	0.432	17.5	4.46	340	2.42	5.99	38	173	19	24
2.08		124	240.008	9.812	0.700	16.3	4.80	470	3.37	20.7	331	245	20	37
2.21		147	240.028	2.847	0.272	15.2	4.99	391	6.90	11.4	<50	135	<120	8
2.14		137	240.014	5.757	0.403	15.9	5.40	530	3.68	11.2	60	166	50	44
2.15	N	139	240.015	1.585	0.013	0.3	5.70	475	11.5	59.1	37	<50	<50	<20
2.18		139	240.018	6.007	0.321	17.0	5.92	388	3.26	7.70	<50	146	<40	27
2.34A		95	240.041	5.231	0.502	15.4	6.58	584	4.10	20.8	323	186	200	162
2.34B		95	240.042	3.361	0.467	16.6	4.97	410	3.21	15.1	251	177	90	86
2.34C		95	240.043	3.313	0.572	14.5	8.49	767	4.66	16.7	288	160	350	234
2.34D		95	240.044	6.308	0.516	15.3	6.68	588	4.47	26.4	453	149	190	166
2.34	M	95	240.M34	18.213	0.513	15.4	6.66	586	4.17	20.9	348	166	200	162
2.01	S	126	240.001	6.664	0.413	14.6	6.71	816	4.25	14.0	86	140	95	119
2.03		126	240.003	15.864	0.450	14.9	6.87	581	4.08	16.2	194	173	110	86
2.23		147	240.030	5.745	0.438	17.1	6.94	457	3.42	6.88	19	166	23	29
2.09		124	240.009	6.900	0.300	17.2	7.07	411	3.51	7.38	22	139	<50	11
2.22		147	240.029	4.159	0.301	16.9	7.10	471	4.20	8.62	21	152	24	13
2.17		139	240.017	5.015	0.409	16.5	7.20	545	4.26	16.0	198	175	32	41
2.30		95	240.037	3.388	0.675	15.7	7.46	593	4.10	19.8	247	213	120	105
2.10		124	240.010	4.031	0.488	15.7	7.49	604	4.19	17.7	228	172	140	124
2.05		126	240.005	3.830	0.687	14.8	7.84	459	6.44	15.5	27	187	38	53
2.12		137	240.012	1.614	0.482	15.5	8.78	744	5.17	28.0	426	161	200	153
2.33		95	240.040	7.264	0.550	15.1	9.23	734	5.10	20.2	269	194	190	147
2.06		126	240.006	7.060	0.494	13.6	9.34	1155	5.14	16.2	66	162	190	153
2.02		126	240.002	9.006	0.494	15.3	9.45	782	5.34	22.5	295	168	240	175
2.16		139	240.016	4.297	0.469	13.6	9.57	951	8.03	81.6	1550	188	240	158
2.20	S	147	240.027	7.965	0.390	15.1	9.61	771	5.33	20.4	168	177	280	177
2.07		126	240.007	3.198	0.559	14.5	9.80	844	5.52	19.9	258	168	310	202
2.27		147	240.034	7.852	0.491	14.0	9.83	1032	5.06	13.8	72	187	240	202
2.24		147	240.031	16.243	0.530	13.8	10.17	1056	7.07	48.0	743	159	360	258
2.28		147	240.035	7.693	0.541	13.4	10.40	1072	6.61	46.3	710	176	320	226
2.32		95	240.039	7.789	0.529	15.2	11.00	801	5.79	17.9	223	180	390	256
2.29		95	240.036	4.237	0.586	17.8	13.59	1086	3.03	7.36	39	182	110	195

TABLE A5. (continued).

Particle Number	La µg/g	Ce µg/g	Sm µg/g	Eu µg/g	Tb µg/g	Yb µg/g	Lu µg/g	Hf µg/g	Ta µg/g	Ir ng/g	Au ng/g	Th µg/g	U µg/g
2.25	0.145	0.34	0.051	0.827	0.0090	0.028	0.0040	0.050	0.006	<2	<1	0.009	<0.05
2.13	2.79	6.2	0.683	2.08	0.096	0.215	0.0237	0.172	0.015	<2	<2	0.048	<0.06
2.31	1.31	2.9	0.411	2.37	0.068	0.224	0.0293	0.115	0.026	<1	<2	0.043	0.02
2.26	0.557	1.4	0.237	1.30	0.045	0.201	0.0284	0.15 7	0.036	1.3	<2	0.033	<0.06
2.11	1.93	5.0	0.654	0.869	0.128	0.512	0.0650	0.48	0.103	<2	<3	0.38	0.16
2.04	0.552	1.41	0.250	0.737	0.054	0.222	0.0296	0. 121	0.009	<1	<1	0.020	<0.3
2.19A	1.23	3.2	0.573	0.897	0.135	0.504	0.072	0.44	0.064	1.6	2.5	0.18	0.05
2.19B	1.22	3.1	0.578	0.875	0.131	0.498	0.070	0.42	0.058	0.9	<2	0.17	0.04
2.19C	1.27	3.3	0.596	0.900	0.144	0.551	0.073	0.46	0.073	1.4	<2	0.20	0.06
2.19D	1.32	3.4	0.609	0.896	0.141	0.565	0.077	0.49	0.058	1.4	1.2	0.20	0.08
2.19E	1.47	3.9	0.652	0.903	0.150	0.606	0.087	0.54	0.074	7.9	1.5	0.23	0.08
2.19F	1.18	3.0	0.549	0.904	0.121	0.484	0.069	0.41	0.048	<2	<2	0.17	0.05
2.19G	1.27	3.2	0.586	0.869	0.134	0.517	0.071	0.42	0.070	<2	<2	0.18	0.05
2.19H	1.48	3.9	0.649	0.989	0.155	0.616	0.080	0.48	0.050	7.6	<2	0.33	0.07
2.19	1.27	3.3	0.588	0.894	0.137	0.526	0.073	0.45	0.064	1.8	1.0	0.19	0.05
2.08	2.04	5.2	0.891	1.39	0.179	0.661	0.092	0.63	0.094	15.0	5.3	0.24	0.05
2.21	0.230	0.62	0.103	0.622	0.026	0.163	0.024	0.073	<0.06	<3	0.9	<0.04	<0.1
2.14	2.22	5.6	0.914	0.897	0.212	0.98	0.140	0.94	0.135	2.3	<2	0.57	0.16
2.15	2.22	6.0	0.973	0.033	0.190	1.92	0.397	0.110	<0.08	<2	<2	0.25	0.08
2.18	1.03	2.7	0.475	0.756	0.110	0.452	0.063	0.42	0.055	1.6	0.9	0.12	<0.2
2.34A	12.3	31.	5.44	1.16	1.14	4.08	0.553	4.46	0.524	7.9	9.4	2.11	0.69
2.34B	6.90	17.7	3.08	1.05	0.634	2.27	0.315	2.40	0.287	5.8	6.1	1.07	0.38
2.34C	24.5	62.	10.90	1.30	2.20	7.59	1.002	7.97	0.910	6.6	8.9	3.80	1.14
2.34D	13.6	35.	6.01	1.15	1.23	4.48	0.595	4.60	0.578	7.3	15.5	2.23	0.67
2.34	14.0	36.	6.20	1.16	1.27	4.52	0.605	4.77	0.569	7.1	10.8	2.27	0.71
2.01	6.84	17.1	2.63	0.935	0.638	3.29	0.457	2.65	0.511	2.5	<1.6	2.53	0.78
2.03	7.35	19.0	3.18	1.02	0.671	2.43	0.341	2.57	0.318	5.7	2.6	1.25	0.38
2.23	2.08	5.4	1.03	0.946	0.247	0.90	0.124	0.75	0.105	1.4	<2	0.24	0.09
2.09	0.81	2.0	0.378	0.688	0.092	0.393	0.056	0.25	0.039	<3	<5	0.08	0.03
2.22	0.767	2.0	0.404	0.747	0.101	0.430	0.060	0.30	0.035	<4	<4	0.072	0.03
2.17	2.58	6.6	1.17	0.896	0.279	1.03	0.150	0.92	0.133	58.	2.1	0.43	0.16
2.30	8.76	22.0	3.71	1.58	0.792	2.75	0.377	2.90	0.346	8.2	4.7	1.29	0.38
2.10	9.86	26.1	4.31	1.10	0.935	3.22	0.447	3.37	0.440	8.6	4.2	1.69	0.47
2.05	3.21	8.3	1.67	1.27	0.371	1.30	0.180	1.22	0.204	<4	<3	0.38	0.10
2.12	13.0	34.	5.79	1.199	1.19	4.15	0.571	4.60	0.530	17.4	5.9	2.04	0.54
2.33	12.5	32.	5.43	1.35	1.18	4.22	0.565	4.51	0.543	8.4	3.4	2.14	0.46
2.06	12.5	32.	5.34	1.16	1.17	4.43	0.624	4.45	0.587	<5	<4	2.26	0.60
2.02	16.4	42.	7.11	1.26	1.48	5.27	0.713	5.71	0.676	7.6	4.7	2.85	0.81
2.16	15.6	40.	6.79	1.24	1.43	5.24	0.714	5.41	0.650	67.	15.4	3.78	1.04
2.20	18.7	48.	7.95	1.27	1.70	5.77	0.781	6.54	0.739	9.0	2.8	3.12	0.80
2.07	17.6	46.	7.71	1.28	1.60	5.86	0.814	7.46	0.720	7.3	4.3	3.16	0.97
2.27	16.9	43.	7.12	1.28	1.52	5.85	0.797	5.93	0.721	3.3	1.3	3.30	0.90
2.24	26.7	68.	11.22	1.41	2.39	8.28	1.118	8.95	1.003	15.9	15.2	4.36	1.17
2.28	20.3	52.	8.56	1.31	1.90	6.89	0.938	7.26	0.914	21.0	14.2	3.75	1.04
2.32	27.0	70.	11.67	1.42	2.42	7.99	1.103	9.42	1.009	5.9	3.3	4.14	1.08
2.29	11.4	29.	6.85	1.74	1.63	5.35	0.700	3.20	0.222	<3	<4	1.21	0.53

Note: M = mass-weighted mean of subsamples; S = sphere; N = Na_2O value corrected for $^{24}Mg(n,p)^{24}Na$.

TABLE A6. INAA results for replicate samples of <1-mm soil 60601 and comparison of sample standard deviations (s.d.) with those of samples from the top 13 cm of 60010, all 21 samples from 60005, and top 21 samples from 60004.

Lab ID	Mass mg	Na_2O %	CaO %	Sc µg/g	Cr µg/g	FeO %	Co µg/g	Ni µg/g	Sr µg/g	Zr µg/g	Ba µg/g	La µg/g	Sm µg/g	Eu µg/g	Tb µg/g	Yb µg/g	Lu µg/g	Hf µg/g	Ta µg/ g	Ir ng/g	Au ng/g	Th µg/g	U µg/g
218.060	50.6	0.443	15.8	9.14	739	5.02	23.2	320	174	167	140	12.6	5.80	1.172	1.11	4.14	0.573	4.40	0.512	11.5	6.5	2.09	0.50
218.130	52.5	0.455	16.2	9.44	771	5.35	26.9	373	187	184	143	12.9	6.04	1.217	1.13	4.32	0.592	4.56	0.510	11.9	7.2	2.19	0.62
223.210	47.6	0.456	15.0	9.20	763	5.30	28.6	397	178	190	139	13.0	6.05	1.195	1.23	4.16	0.586	4.52	0.544	13.2	9.2	2.24	0.59
223.280	48.1	0.454	15.4	9.37	765	5.32	26.8	374	171	165	146	12.7	5.89	1.198	1.16	4.13	0.573	4.44	0.539	13.1	7.1	2.18	0.54
230.360	44.1	0.452	15.4	9.46	778	5.50	32.2	475	167	194	154	12.2	5.68	1.181	1.16	4.05	0.564	4.34	0.532	23.4	8.1	2.14	0.55
230.430	48.9	0.456	15.2	9.50	794	5.45	28.8	434	181	221	145	13.0	6.01	1.188	1.21	4.30	0.595	4.62	0.560	14.7	12.5	2.16	0.57
Mean		0.453	15.5	9.35	768	5.32	27.7	395	176	186	144	12.8	5.91	1.192	1.17	4.18	0.581	4.48	0.533	14.6	8.4	2.17	0.56
s.d.		0.005	0.4	0.15	18	0.17	3.0	53	7	20	5	0.3	0.15	0.016	0.05	0.11	0.012	0.11	0.019	4.4	2.2	0.05	0.04
%s.d.																							
60601	(n = 6)	1.1	2.8	1.6	2.4	3.2	11.	14.	4.1	11.	3.7	2.3	2.5	1.3	4.0	2.5	2.1	2.4	3.6	30.	26.	2.3	7.4
60010	(n = 27)	2.4	2.0	2.7	2.7	2.9	15.	19.	n.a.	n.a.	8.6	4.7	4.3	2.3	5.0	3.7	4.4	6.4	8.2	26.	24.	8.5	14.8
60005	(n = 21)	1.4	2.5	4.3	4.1	3.6	26.	26.	2.7	10.	7.1	5.4	5.0	2.0	7.0	4.6	4.2	5.8	7.6	17.	37.	5.1	14.1
60004	(n = 21)	1.7	1.7	2.9	1.8	2.9	16.	18.	9.8	8.	5.0	3.8	4.0	1.3	4.6	3.7	3.9	4.1	3.9	23.	22.	4.0	11.9

TABLE A7. INAA results for 50-60 mg samples of some Apollo 16 surface soils.

Sample	Station %	Na_2O %	CaO µg/g	Sc µg/g	Cr %	FeO µg/g	Co µg/g	Ni µg/g	Sr µg/g	Zr µg/g	Cs µg/g	Ba
61221,12	1	0.508	15.9	7.46	563	4.20	16.2	221	176	129	0.12	99
63341,80	13	0.497	15.5	8.21	616	4.58	17.4	232	172	137	0.09	112
64501,11	4	0.451	16.0	7.48	581	4.14	20.9	311	167	129	0.10	124
64801,35	4	0.450	15.7	9.60	756	5.17	25.4	336	165	193	0.16	136
67481,63	11	0.474	16.2	7.25	515	3.84	11.6	148	189	77	0.06	72
67511,4	11	0.430	17.0	8.28	526	4.27	12.8	75	163	45	0.07	49
67601,15	11	0.509	16.1	7.01	568	4.23	27.9	363	193	79	0.07	84
67701,18	11	0.510	16.0	7.31	558	4.17	16.6	218	171	80	0.07	88
67941,68	11	0.538	15.4	8.00	684	4.57	18.2	241	180	144	0.13	118
68841,29	8	0.449	14.9	9.32	768	5.37	27.5	410	180	183	0.11	146
69941,25	9	0.450	15.4	9.94	802	5.52	26.3	382	164	177	0.16	158
±(%)*		1-2	3	1	1	1	1	7	8	12	18	5

TABLE A7. (continued).

Sample	La µg/g	Ce µg/g	Nd µg/g	Sm µg/g	Eu µg/g	Tb µg/g	Yb µg/g	Lu µg/g	Hf µg/g	Ta µg/g	Ir ng/g	Au ng/g	Th µg/g	U µg/g
61221	8.53	22.2	12.	4.05	1.12	0.79	2.86	0.387	3.00	0.357	4.4	4.0	1.33	0.36
63341	10.1	26.0	17.	4.61	1.21	0.94	3.45	0.470	3.27	0.404	7.0	6.2	1.64	0.46
64501	10.8	28.1	20.	5.06	1.11	0.98	3.51	0.471	3.65	0.439	8.8	13.9	1.76	0.54
64801	12.9	33.1	21.	6.00	1.17	1.18	4.32	0.591	4.59	0.558	10.3	15.6	2.09	0.56
67481	5.72	14.8	9.	2.75	1.11	0.57	2.02	0.273	1.95	0.245	4.1	2.0	0.95	0.27
67511	3.49	9.0	5.	1.68	1.01	0.34	1.33	0.184	1.18	0.162	2.0	1.0	0.49	0.14
67601	6.61	17.2	10.	3.12	1.23	0.62	2.30	0.317	2.17	0.278	10.1	6.8	1.08	0.28
67701	6.99	17.9	10.	3.28	1.23	0.66	2.39	0.329	2.29	0.300	7.4	5.0	1.15	0.31
67941	10.9	28.1	19.	5.05	1.27	1.02	3.63	0.489	3.60	0.441	7.3	6.0	1.75	0.61
68841	14.4	37.2	23.	6.65	1.20	1.30	4.62	0.626	4.89	0.580	12.2	6.4	2.35	0.56
69941	14.3	36.9	23.	6.66	1.21	1.30	4.68	0.633	4.87	0.574	11.4	6.8	2.42	0.65
±(%)*	1	2	15	2	1	3	2	2	2	4	12	12	3	10

* Estimate of analytical precision (one standard deviation, relative).